IJEST

ISSN: 0973-6255
Vol. 5 No. 1
January - June 2011

Indian Journal of Engineering, Science, and Technology

A Refereed Research Journal









Published by

BANNARI AMMAN INSTITUTE OF TECHNOLOGY
(Autonomous Institution Affiliated to Anna University of Technology, Coimbatore -
Approved by AICTE - Accredited by NBA and NAAC with "A" Grade)
Sathyamangalam - 638 401 Erode District Tamil Nadu India
Ph: 04295-226340 - 44 Fax: 04295-226666
www.bitsathy.ac.in E-mail: ijest@bitsathy.ac.in

BANNARI AMMAN INSTITUTE OF TECHNOLOGY
Stay Ahead

Indian Journal of Engineering, Science, and Technology

IJEST is a refereed research journal published half-yearly by Bannari Amman Institute of Technology. Responsibility for the contents rests upon the authors and not upon the IJEST. For copying or reprint permission, write to Copyright Department, IJEST, Bannari Amman Institute of Technology, Sathyamanagalam, Erode District - 638 401, Tamil Nadu, India.

Indian Journal of Engineering, Science, and Technology
ISSN: 0973-6255
Volume 5 Number 1 **January - June 2011**

CONTENTS

On the Thermoeconomic and Exergy Analysis of Refrigeration Systems

S.K. Kalla[1], J.A. Usmani[2] and V.K. Saini[3]
[1&2]Department of Mechanical Engineering, IMS Engineering College, Adhyatmik Nagar, Ghaziabad - 201 009
[3]Department of Mechanical Engineering, Jamia Millia Islamia, New Delhi -110 025
E-mail:skkalla@yahoo.com
(R)

Abstract

Thermoeconomic analysis of energy systems has been covering a primary role among the emerging disciplines in the field, due to the in-depth understanding it provides as concerns the interactions between components and with the environment. Several methodologies have been proposed, some of them being oriented to perform cost accounting (CA) of existing energy systems, i.e. to properly allocate the cost of the resources consumed on the intermediate and final products of the plant, others focusing on the Optimization problem, i.e. attempting to make the energy analyst capable to detect trade-off values for the main design variables.

This paper reviews the research work carried out from the spin-off from the exergy analysis to the development of the thermoeconomic approach. It reports on the exergy analysis research involving the exergy destruction in the various components of the refrigeration system surveying the influence of the various factors affecting the coefficient of performance and exergetic efficiency. The paper also highlights that the optimization consists in the best COP at the least cost.

Keywords: *COP, Exergy, Refrigeration,Thermoeconomics, Vapor compression*

1. INTRODUCTION

Exergoeconomics and thermoeconomics are exergy-based economic methods that have evolved over several decades. Exergy and microeconomics forms the basis of thermoeconomics, also called exergoeconomics and exergonomics. With thermoeconomics, exergy efficiencies are determined, while non-energy expenditures such as financial and labour costs are related to the technical parameters of the device under consideration. In thermoeconomic optimization, the optimal design point and operating conditions are determined by minimising the total economic cost under financial, technical, environmental and other constraints. Exergy accounting method measures the amount of exergy resources to produce a good. Costs must be properly formed to understand and evaluate exergy costs and resource degradation, as well as cost and irreversibility relations. Numerous applications are described of exergy cost accounting and thermoeconomics, explaining thermoeconomic costs, thermoeconomic analyses of complex systems and operation diagnosis and optimization [1].

2. PRINCIPLES OF EXERGOECONOMICS

Exergoeconomics applied to the design and synthesis of energy-conversion plants is based on two important principles that represent the fundamental connections between thermodynamics and economics. The first principle is common to all exergoeconomic approaches and applications, whereas the second principle refers only to applications in which new investment expenditures are needed. These principles are briefly discussed in the following.

2.1. Exergy Costing

This principle states that exergy is the only rational basis for assigning monetary values to the interactions an energy system experiences with its surroundings and to the thermodynamic inefficiencies within the system. Mass, energy or entropy should not be used for assigning the above mentioned monetary values because their exclusive use results in misleading conclusions.

According to the exergy-costing principle, the cost stream (C_j) associated with an exergy stream (E_j) is given by

$$C_j = c_j E_j \quad [1]$$

where c_j represents the average cost associated with providing each exergy unit of the stream E_j in the plant being considered. Equation (1) is applied to the exergy associated with streams of matter entering or exiting a system as well as to the exergy transfers associated with the transfer of work and heat. For the cost (C_k) associated with the exergy (E_k) contained within the k-th component of a system we write

$$C_k = c_k E_k \quad [2]$$

Here c_k is the average cost per unit of exergy supplied to the k-th component.

2.2. Exergy Destruction Reduces Investment Cost

The exergy destruction represents in thermodynamics a major inefficiency and a quantity to be minimized when the overall plant efficiency should be maximized. In the design of a new energy-conversion plant, however, exergy destruction within a component represents not only a thermodynamic inefficiency but also an opportunity to reduce the investment cost associated with the component being considered and, thus, with the overall plant.

Figure 1 refers to a component (subscript k) of the overall plant and shows that the cost rate Z_k^{CI} associated with capital investment (superscript CI) decreases with increasing exergy destruction rate ($E_{D,k}$) within the same component. Instead of a single curve, a shaded area is presented to denote that the investment cost could vary within a given range for each given value of the exergy destruction. The effect of component size is taken into consideration in Figure 1 by relating both Z_k^{CI} and ($E_{D,k}$) to the exergy rate of the product generated in this component ($E_{P,k}$).

The vast majority of components in energy-conversion plants exhibit qualitatively the behavior between Z_k^{CI} and $E_{D,k}$ shown in Figure 1. Should the investment cost

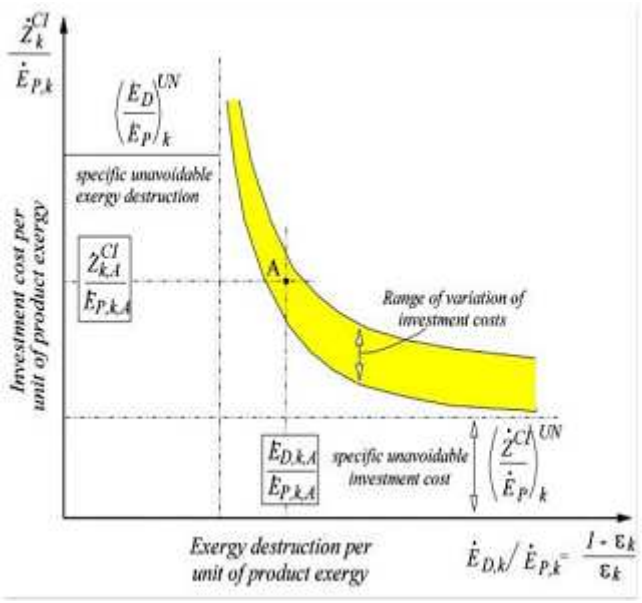

Fig.1 Expected relationship between investment cost and exergy destruction (or exergetic efficiency) for the k-th componenet of an energy conversion system

increase or remain constant with increasing exergy destruction, then the component being considered can be excluded from optimization considerations because in these cases we would always select for this component the design point that has the lowest investment cost and, at the same time, the lowest thermodynamic inefficiencies (i.e. the highest exergetic efficiency).

The curves and the shaded area shown in Figure 1 are usually not known. However, even then we can estimate the two asymptotic lines that determine the specific unavoidable exergy destruction

$$\{ E_{D,k} / E_{P,k} \}^{UN}$$

and the specific unavoidable investment cost

$$\{ Z^{CI} / E_P \}_k^{UN} \quad .$$

All design improvement efforts should focus only on the avoidable parts of exergy destruction and investment costs. These parts are calculated by subtracting the unavoidable value from the total value of the respective variable.

3. Application to Refrigeration

Exergy-based economic analyses have been undertaken for cooling, refrigeration and air conditioning. Akhilesh Arora and S.C.Kaushik [2] presented a detailed exergy analysis of an actual vapour compression refrigeration (VCR) cycle. A computational model was developed for computing coefficient of performance (COP), exergy destruction, exergetic efficiency and efficiency defects for R502, R404A and R507A. The results indicated that R507A is a better substitute to R502 than R404A. The efficiency defect in condenser was highest, and lowest in liquid vapour heat exchanger for the refrigerants considered.CE Vincent and MK Heun [3] explored and optimized the thermoeconomics of the refrigeration cycle for domestic refrigerators from an exergy perspective during steady state operation. They found that the Energy Efficiency Rating (EER) of the compressor has the most effect on system performance and economics, and, similar to previous studies, they found that the cost of refrigerating is driven by compressor costs. They also noted that future efforts to reduce compressor costs should be accompanied by a corresponding effort to improve compressor thermodynamic performance.

Arif Hepbasli [4] performed thermoeconomic analysis of household refrigerators for providing useful insights into the relations between thermodynamics and economics. In his analysis, the EXCEM method based on the quantities exergy, cost, energy and mass was applied to a household refrigerator using the refrigerant R134a. Thermodynamic loss rate-to-capital cost ratios for each components of the refrigerator were investigated. The ratios of exergy loss rates to capital cost values were obtained to vary from 2.949×10^{-4} to 3.468×10^{-4} kW US^{-1}. The exergy efficiency values were also found to range from 13.69 to 28.00% and 58.15 to 68.88% on the basis of net rational efficiency and product/fuel at the reference state temperatures considered, respectively.

B.B. Arora *et al.* [5] predicted the parametric investigations of actual Vapour Compression Refrigeration (VCR) cycle in terms of Coefficient of Performance (COP), Exergy Destruction (ED) and exergetic efficiency of refrigerants R-22, R-407C and R-410A with the help of a developed computational model. The investigation was carried out for evaporator and condenser temperatures in the range of -38^0 C to 7^0 C and 40^0 C to 60^0 C respectively. The results indicated that COP and exergetic efficiency for R-22 was higher in comparison to R-407C and R-410A. The optimum evaporator temperature for minimum ED ratio was evaluated at various condenser temperatures.

G.Q. Zhang *et al.* [6] observed that the application of thermoeconomic optimization design in an air-conditioning system was important in achieving economical life cycle cost. They introduced a new concept that exergy input into the system can be substituted for the sum of exergy destruction and exergy output from the system according to conservation of exergy. Optimization results indicated that thermodynamic optimization contributed to energy contribution reduction, but it unnecessarily lead to increase of life cycle cost; on the contrary, life cycle cost at thermoeconomic optimization was lower than that at thermodynamic optimization.

C. Aprea and A. Greco [7] dealt with the substitution of R22 in an experimental vapour compression plant with the most widely used drop-in substitute, i.e. the zeotropic mixture R407C. The overall exergetic performance of the plant working with R22 was consistently better than that of its candidate substitute. They concluded that in order to increase the overall performance of the vapour compression plant working with R407C, the evaporator and the compressor must be optimized and to improve the performance, the temperature difference must be decreased and the heat transfer coefficient must be increased. The first effect could be obtained by closely matching the refrigerant temperature profile with the secondary fluid temperature profile by adjusting the secondary fluid flow-rate. The second effect could be obtained by using a micro-fin tube.

Recep Yumruta *et al.* [8] presented computational model based on the exergy analysis for the investigation of the effects of the evaporating and condensing temperatures on the pressure losses, the exergy losses, the second law of efficiency, and the coefficient of performance (COP) of a vapor compression refrigeration cycle. The second law efficiency and the COP increases, and the total exergy loss decreases with decreasing temperature difference between the evaporator and refrigerated space and between the condenser and outside air.

C. Renno *et al.* [9] presented an exergetic analysis of a vapour compressor refrigeration plant when the refrigeration capacity was controlled by varying the compressor speed. When the inverter was used, the capacity of the refrigeration system was matched to the load, regulating the compressor motor speed. When the control of the compressor capacity was obtained by varying its speed there was energy saving with respect to the thermostatic control. The best results of the exergetic analysis were obtained using R22 followed by the non-azeotropic mixture designed as R407C that confirmed, among the fluid candidates R22 substitution a better performance, shown also at the compressor nominal speed.

C.O. Adegoke *et al.* [10] have shown that, the effect of imbalance between the major components of the refrigeration systems made the system to degrade the available energy. In the comparison of the two rigs used in their study, it was shown that rig a performed better than rig b because of the fact that the design model used was based on balanced points. Since energy in the running cost of mechanical refrigeration systems takes the largest share it was shown in their study that this running cost could be reduced by: basing the component design on balance points; not encourage superheating and limiting subcooling to between 3^{o} and 5^{o}C.

V.P.Venkataramanamurthy *et al.* [11] presented an experimental comparison of energy, exergy flow and second law efficiency of R22 and its substitute R436b, vapour compression refrigeration cycles. It was found that the evaporating temperatures have strong effects on the exergy flow losses and on the second law efficiency and COP of the cycle but little effects on the other components of the exergy losses. The second law efficiency and the COP increased, and the total exergy loss decreased with decreasing temperature difference between the evaporator and refrigerated space and between the condenser and outside air**.** The reasons for low exergy efficiency were due to large exergy destructions in the compressor and the condenser.

C. Aprea and C.Renno [12] experimentally studied the energetic and exergetic performances of a vapour compression refrigeration plant applied to a cold store, usually adopted for the preservation of foodstuff, using as working fluids R22 and its substitute R417A. It was experimentally observed that the best performances in terms of COP and exergetic efficiency were obtainable with R22 in comparison with the non-azeotropic mixture R417A. Moreover, the exergy destroyed in the plant components when R417A was used as working fluid was, on average, about 14% higher than the exergy destroyed with R22.

4. CONCLUSIONS

The use of conventional energy analysis based on the first law of thermodynamics cannot adequately evaluate the economic trade-offs between work and heat output. It is therefore more appropriate to analyze the efficiency of refrigeration system based on the second law concept of exergy. Better energy efficiency may or may not translate into lower operating costs for users and lesser environmental impact. So efficient refrigeration systems may or may not be economically optimized. The need of the hour is to investigate the efficiency coupled with economics for the refrigeration system. The studies are scant which takes into account, both thermodynamics and economics simultaneously. For example future efforts to reduce compressor costs should be accompanied by a corresponding effort to improve compressor thermodynamic performance. Techniques to assist engineers to feel easy in developing or operating simulation software and to well use the simulation results in product development processes are required and will be developed in the future. Such techniques include: general refrigeration system simulation platform based on graph theory, model-based intelligent simulation technique, and combination of knowledge engineering methodology with simulation. When electric cost increases greater investments, aimed at improving plant efficiency, become more and more advantageous. Thermodynamic optimization leads to initial investment increase. Although initial investment contributes to energy efficiency increase and energy conservation, too high investment is undesirable for consumers. At the same time, initial investment reduction leads to energy efficiency reduction and operating cost increase.

Thermoeconomic optimization design considering various factors is favourable. It will be interesting to study the effect of operating hours per year and interest rate on two optimizations. To improve the performance of the refrigeration system each component may be further studied from exergy usage and economics points of view. Eventually, a system exergy-economics optimization

study may be carried out to identify each component's relative importance with respect to operational conditions. Improvement in all economic features including the total cost of the system product, fuel (electricity) cost, capital investment and operating and maintenance cost, and the cost of exergy loss should be obtained even if it results in reduced exergetic efficiency of the optimized system.

REFERENCES

[1] M.A.Rosen, "A Concise Review of Exergy-based Economic Methods", In: 3rd IASME/WSEAS Int. Conf. on Energy & Environment, University of Cambridge, 2008, pp.136-144.

[2] A.Arora and S.C.Kaushik, "Theoretical Analysis of Vapour Compression Refrigeration System with R502, R404A and R507A", International Journal of Refrigeration, Vol.31, 2008, pp.998–1005.

[3] C.E.Vincent,M.K.Heun, "Thermoeconomic Analysis and Design of Domestic Refrigeration Systems", In: Domestic Use of Energy Conference, Calvin College,Grand Rapids, Michigan, USA,2006.

[4] A.Hepbasli, "Thermoeconomic Analysis of Household Refrigerators", International Journal of Energy Research, Vol.31, No.10, 2006, pp.947- 959.

[5] A.Arora, B.B. Arora, B.D. Pathak and H.L.Sachdev, "Exergy Analysis of a Vapour Compression Refrigeration System with R-22, R-407C and R-410A",International journal of Exergy, Vol.4, No.4, 2007, pp.441-454.

[6] G.Q.Zhang,L.Wang,L.Liu,Z.Wang, "Thermoeconomic Optimization of Small Size Central Air Conditioner", Applied Thermal Engineering , Vol.24, 2004, pp.471-485.

[7] C.Aprea,A.Greco, "An Exergetic Analysis of R22 Substitution", Applied Thermal Engineering, Vol.22, 2002, pp.1455-1469.

[8] R.Yumruta,M.Kunduz and M.Kanoglu, "Exergy Analysis of Vapor Compression Refrigeration Systems", Exergy, An International Journal, Vol.2, No.4, 2002, pp.266-272.

[9] C.Aprea, F.deRossi, A.Greco and C.Renno, "Exergy Analysis of Vapor Compression Refrigeration Systems" Exergy, An International Journal, Vol.2, No.4, 2003, pp.266-272.

[10] C.O.Adegoke, M.A.Akintunde, O.P. Fapetu, "Comparative Exergetic Analysis of Vapor Compression Refrigeration Systems in the Superheated and Subcooled Regions", Department of Mechanical Engineering, Federal University of Technology Akure, Nigeria AU J.T., Vol.10, No.4, 2007, pp.254-263.

[11] V.P.Venkataramanamurthy, P.S.Kumar, " Experimental Comparative Energy, Exergy Flow and Second Law Efficiency Analysis of R22, R436b Vapour Compression Refrigeration Cycles", International Journal of Engineering Science and Technology, Vol. 2, No.5, 2010, pp.1399-1412.

[12] C.Aprea and C.Renno,"Experimental Comparison of R22 with R417A Performance in a Vapour Compression Refrigeration Plant Subjected to a Cold Store", Energy Conversion and Management, Vol.45, 2004, pp.1807-1819.

Optimization of Wear Rate in Metal Matrix Composite Using - Taguchi Technique

T.R. Hemanth Kumar[1], R.P. Swamy[2] and T.K. Chandrashekar[3]

[1]Department of Industrial Engineering and Management, Sri Siddhartha Institute of Technology, Tumkur - 572 105, Karnataka

[2]Department of Mechanical Engineering. UBDT College of Engineering, Davangere - 577 004, Karnataka

[3]Department of Mechanical engineering, Sri Siddharthata Institute of Technology, Tumkur - 572 105, Karnataka

E-mail: hemantkumar.iem@gmail.com

(R)

Abstract

In the present study, Al-Cu-Mg Titanium Dioxide particle reinforced composite was synthesized using stir-casting method. Dry sliding wear behavior of Al alloy and its composite were tested using a pin-on-disc test rig. The experiments were conducted as per the Taguchi design of experiment and the wear parameters chosen were: Sliding speed, Load and sliding distance. This investigation was carried out to optimize the wear parameters, which, yields minimum wear rate of test samples. The analysis of variance was used to investigate the significant factors, which affect the dry sliding wear behavior of the composite. Based on Signal to Noise ratio analysis, the optimal settings of the process parameters have been determined. Confirmation test have also been performed to predict and verify the adequacy of the additive models.

Keywords: *Signal-to-noise ratio, Significant factor, Titanium dioxide, Quality characteristic.*

1. INTRODUCTION

In the 21st centaury, lightweight and energy efficient materials have been received extensive attention, since the problems of environment and energy become increasingly serious. Lightweight Aluminum alloys are desirable materials but their applications are restricted in engineering field because of their extremely poor wear resistance. The Aluminum Metal Matrix Composites (AMC) reinforced with hard ceramic particles, whiskers or fiber which can produce considerable alteration in the physical, Mechanical and Tribological properties of the base alloy [1]. The enhanced properties of the Aluminum metal matrix composites made them suitable for transport applications with a reduction of energy costs.

The Tribological behavior of materials depends on many factors, which are either extrinsic or intrinsic to the material undergoing surface interaction. Mechanical and physical factors such as, the effect of load, the sliding velocity, the sliding distance, the reinforcement orientation, the environment, temperature and surface finish are important extrinsic parameters, which effects wear behavior of AMCs. The material factors, which play prominent role in enhancing the Tribological properties are reinforcement type, reinforcement size and shape, reinforcement distribution and volume fraction. [2]

The alpas *et al.,* [3] studied the effect of normal load on the wear behavior of metal matrix composite and identified three different wear regimes. They identified three different wear regimes: at low load regime, the particles support the applied load. The wear resistance of composites is in an order of magnitude higher than unreinforced Aluminum alloy. In the intermediate load regime, the wear rate of metal matrix composites and Aluminum alloy are similar. At high load, the transition to severe wear occurs as the contact temperature exceeds a critical value. Shipway *et al.,* [4] studied the sliding wear behavior of Aluminum metal matrix composites and reported that, increasing the volume fraction of particles reduces the wear rate of MMCs. Similarly study was carried out by Ranganath *et.al.*,[5]

Miyajima *et al.,* [6] carried out dry sliding wear test on AMC reinforced with SiC - Whisker, Al2O3 - fiber and Sic - particles and reported that particle reinforcement are the most effective in improving the wear resistance of MMCs. Martin *et.al.*, [7] investigated

effect of temperature on the wear behavior of particulates reinforced Aluminum composites and the result analysis shows that, the specific wear rate is approximately constant with temperature up to a transition value which determines the limit between mild and severe wear.

Many Researcher's investigated the wear behavior of Aluminum Metal Matrix Composites against friction materials, has received particular attention because of the possibility of using theses materials for disc brakes, internal combustion engines and other engineering and automobile application. Components manufactured using Aluminum Metal Matrix Composites offers promising advantages, such as lowering density and higher stiffness and thermal conductivity [8-9]

Much research has been carried out to understand mechanical properties and wear behavior of composite materials. Meager information is available regarding the robust parameter design, which offers least wear rate of the metal matrix composite. In this light, this study is carried out to optimize the wear rate of Titanium Dioxide reinforced Aluminum Metal Matrix Composites using Taguchi's parameter design methodology.

1.1 Taguchi Methodology

Taguchi's parameter design methodology has proved to be an effective approach to producing high quality products at a relatively low cost. The optimization of the quality characteristics using Taguchi experiments has received limited attention among the engineering fraternity. Quality characteristic refers to performance characteristics that affect the final product quality, which, is very important to the end user [10]. Quality characteristic is measured by the deviation of a functional characteristic from its target value. The change in quality characteristic of a product under investigation in response to a factor introduced in the experimental design is the 'Signal' of the desired effect. The effect of the external factors (Uncontrollable factors) on the outcome of the quality characteristic under test is termed as 'the noise'.

The Signal-to-Noise ratio (SN ratio) measures the sensitivity of the quality characteristic being investigated in a controlled manner to those of external influencing factors (Noise factors) not under control. The SN ratio is a transformed figure of merit, created from the loss function. SN ratio combines both the parameters (the mean level of the quality and the variation around this mean) in a single metric. The aim in any experiment is always to determine the highest possible SN ratio for the result (wear rate) A high value of SN ratio implies that signal is much higher than the random effects of noise factors [11].

2. Experimental Procedure

2.1 Materials

Aluminum2618 alloy, which contains Copper and Magnesium as major constituent, was used as matrix material and its composition is shown in Table 1. Titanium dioxide of laboratory grade was used as a reinforcing material. 4wt % Titanium dioxide reinforced Al alloy composite was produced using stir-casting technique, which was used by researcher Mahindra et.al., [12]. Both

Table 1Composition of Al 2618 Alloy

Cu	Mg	Ni	Fe	Si	Ti	Mn	Al
2.18	1.43	1.1	0.93	0.16	0.04	0.028	Bal

Aluminum alloy and composite specimen were subjected to T-6 heat treatment standards.

2.2. Selection of Orthogonal Array

In the present study, the experiments were conducted as per the Standard orthogonal array. The wear parameters chosen for the experiment were: Sliding speed (S) in m/s, Load (L) in N and sliding distance (D) in m. Each parameter was assigned three levels, which are tabulated in Table 2. The experiment consists of 27 tests according to L 27 orthogonal array. The first column was assigned to sliding speed, second column was assigned to load and the fifth column was assigned to sliding distance. The remaining columns were assigned to their interactions. The response to be studied is the

Table 2 Process Parameters with their Different Levels

Factors	Code	Units	Level 1	Level 2	Level 3
Sliding Speed	S	m/s	1.256	2.090	3.056
Load	L	N	19.6	29.4	39.2
Sliding Distance	D	m	500	1000	1500

wear rate [weight loss] with the objective of 'Smaller is the Better' type of quality.

2.3 Experimental Set-up

In order to characterize the dry-sliding wear behavior of the specimens, wear tests were performed using a Pin-on-disc machine, which was similar to the machine described by C.S. Ramesh [13]. A Pin-on-disc is a classical method commonly used for wear experiments. During the experiment, the sliding between the pin and disc may result in wear on both contact surfaces of the pair. To facilitate measurement, the pin is generally the wearing member that has a lower hardness. Schematic diagram of wear test rig is shown in Figure 1. Circular pins of diameter eight mm and height 30 mm was used as a test specimen. The initial weight of the specimen was measured using an electronic balance which as a resolution of 0.001 gram. The test specimen was gripped in the wear testing machine to avoid rolling during the test. The wear test was conducted as per the orthogonal array of Taguchi as shown in Table 3. The wear rate of the specimen was studied as a function of the sliding velocity, applied load and sliding distance. Wear test were conducted as per procedure reported in the paper [14]. At the end of each experiment, the specimen was removed from the testing set-up, cleaned with acetone dried and weighed to determine the weight loss due to dry sliding wear. The difference in the weight measured before and after test gives the wear rate in gram. Each experiment was repeated twice and average response values were tabulated in Table 3.

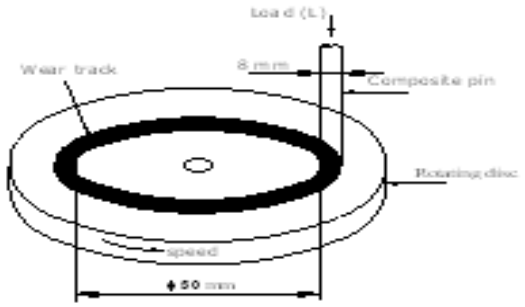

Fig.1. Schematic diagram of wear test rig.

3. Result Discussion

3.1 Wear Mechanism

Wear can be generally described as the removal of material from a surface in relative motion by mechanical or chemical processes. Titanium dioxide reinforced Al-Cu-Mg alloy metal matrix composite posse's superior wear resistance compared with unreinforced Al alloy. The wear mechanism in metal matrix composite is different from Al alloy and the test results shows that composite materials are more wear resistance than the matrix material as shown in Table 3. The enhanced wear mechanism in metal matrix composite is because of particulate reinforcement in matrix alloy. The mechanism of material removal during the wear process of the unreinforced alloy is by plastic deformation and gouging. In composite material the wear mechanism is by plastic deformation, gouging and fracture of reinforcing material (TiO2) leading to the formation of a thin layers at the interface, there by providing protection to the matrix material. This phenomenon is attributed to increase in the wear resistance of metal matrix composite [15].

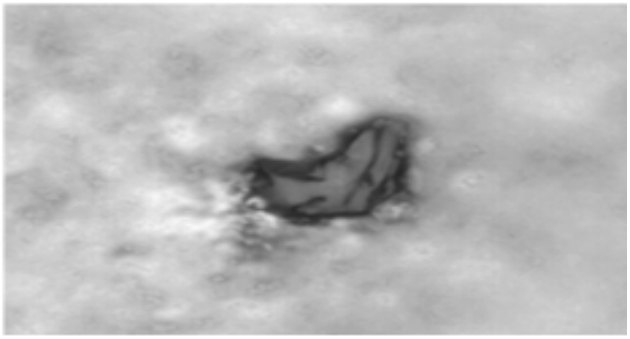

Fig.2 SEM photographs of TiO2 reinforcement in matrix material

Table 3 Orthogonal Array of Taguchi Matrix for Wear test & Test Results

Test	Sliding Speed (m/s)	Load (N)	Sliding Distance (m)	Wear rate of Al alloy (Gram)	Wear rate of Composite Material (Gram)	SN Ratio (db) of Al Alloy (X –1)	SN Ratio (db) of Composite Material (X –1)
1	1.256	19.6	500	0.007	0.006	43.0980	44.4370
2	1.256	19.6	1000	0.009	0.007	40.9151	43.0980
3	1.256	19.6	1500	0.014	0.011	37.0774	39.1721
4	1.256	29.4	500	0.007	0.006	43.0980	44.4370
5	1.256	29.4	1000	0.009	0.008	40.9151	41.9382
6	1.256	29.4	1500	0.016	0.015	35.9176	36.4782
7	1.256	39.2	500	0.010	0.008	40.0000	41.9382
8	1.256	39.2	1000	0.013	0.010	37.7211	40.0000
9	1.256	39.2	1500	0.017	0.015	35.3910	36.4782
10	2.090	19.6	500	0.007	0.006	43.0980	46.0206
11	2.090	19.6	1000	0.012	0.009	38.4164	40.9151
12	2.090	19.6	1500	0.015	0.013	36.4782	37.7211
13	2.090	29.4	500	0.006	0.007	44.4370	43.0980
14	2.090	29.4	1000	0.015	0.012	36.4782	38.4164
15	2.090	29.4	1500	0.014	0.016	36.4782	35.9176
16	2.090	39.2	500	0.012	0.010	38.4164	40.0000
17	2.090	39.2	1000	0.015	0.013	36.4782	37.7211
18	2.090	39.2	1500	0.016	0.014	35.9176	37.0774
19	3.056	19.6	500	0.007	0.006	43.0980	44.4370
20	3.056	19.6	1000	0.008	0.008	43.0980	41.9382
21	3.056	19.6	1500	0.007	0.009	43.0980	40.9151
22	3.056	29.4	500	0.008	0.004	41.9382	47.9588
23	3.056	29.4	1000	0.010	0.005	40.0000	46.0206
24	3.056	29.4	1500	0.011	0.006	39.1721	44.4370
25	3.056	39.2	500	0.011	0.009	39.1721	40.9151
26	3.056	39.2	1000	0.012	0.010	38.4164	40.0000
27	3.056	39.2	1500	0.014	0.011	37.0774	39.1727

Figure 2 shows the scanning electron microscopic view of Titanium dioxide reinforcement in Al alloy.

3.2 Analysis of Variance

The analysis of variance (ANOVA) establishes the relative significance of factors in terms of their percentage contribution to the response quality characteristic. ANOVA is also needed for estimating the error variance for the effects and variance of the prediction error. Based on ANOVA the optimal combinations of the process parameters are predicted. The analysis is carried out for the significance of 5 % (95% confidential level). The Table 4 and 5 shows analysis of variance for Aluminum alloy and composites.

From the results of ANOVA, it is found that distance factor has major influence on sliding wear characteristic (P = 43.34% for Aluminum alloy and P = 38.01 % for composite material). The second significant factor is

Table 4 ANOVA Test for SN Ratio for Al Alloy

Factors	DOF	SS	Adj SS	V	F	P	% Contribution
Sliding speed (S) M /Sec.	2	20.384	20.384	10.192	8.81	0.010	19.227
Load (L) N	2	59.520	59.520	29.760	25.72	0.000	25.05
Distance (D) M	2	102.144	102.144	51.072	44.13	0.000	43.34
S*L	4	9.180	9.180	2.295	1.98	0.190	3.44
S*D	4	24.988	24.988	6.247	5.40	0.021	23.831
L*D	4	7.504	7.504	1.876	1.62	0.260	2.72
Error	8	9.258	9.258	1.157			6.953
Total	26	232.979	232.979	-			

Table 5 ANOVA Test for SN Ratio for Composite Material

Factors	DOF	SS	Adj SS	V	F	P	% Contribution
Sliding speed (S) M /Sec.	2	53.552	53.552	26.776	26.39	0.000	20.49
Load (L) N	2	41.281	41.281	20.641	20.34	0.001	15.90
Distance (D) M	2	97.260	97.260	48.530	47.93	0.000	38.01
S*L	4	33.600	33.600	6.40	8.28	0.006	12.86
S*D	4	12.124	12.124	3.181	3.14	0.079	4.62
L*D	4	6.660	6.660	1.665	1.64	0.225	2.22
Error	8	8.116	8.116	1.015	-	-	5.610
Total	26	253.192	-				

3.3 Signal-to-Noise Ratio (SN ratio)

In the present investigation, the quality characteristic 'wear rate' is belong to 'Smaller is better' type of quality and the Signal-to-Noise ratio (SN ratio) for 'Smaller is better' type of quality response was calculated using the formula,

$$\eta = -10log_{10}\left\{\frac{1}{n}\sum_{i=1}^{n} y_i^2\right\} \qquad (1)$$

Where n = number of tests in a trial.
For the present study n = 2.
The objective of this study is to determine the highest possible Signal-to-Noise ratio for the quality characteristic being studied. The highest value of SN ratio implies that Signal is much higher than the random effects of Noise factors [11]. The SN ratio was computed using equation (1) for each of the 27 trial and the values are reported in Table 3. The average values of SN ratios of process parameters at three levels for both Aluminum alloy and composite material are plotted in Figure 3 and 4. It is evident from the figure that, Wear quality characteristic is minimum (high value of SN ratio) when the process parameters are at, 3rd level of parameter S, 1st level of parameter L and D. In both types of test specimens, least wear rate was observed with the same level of process parameters. At this parameter level the Noise factors are reduced to possible extent so that maximum Signal is reached. For the TiO2 reinforced composite material, the highest Signal-to-Noise ratio was obtained during the 22nd test run and for the Aluminum alloy, it was observed at 13th test run. Minimum wear rate was observed for the Composite materials when it is operated at higher levels of test parameters. The average wear rate of Aluminum alloy 0.0111gram, where as for the composite material it is 0.0096 gram. This shows that wear resistance of Titanium Dioxide reinforced Aluminum alloy is more than matrix material.

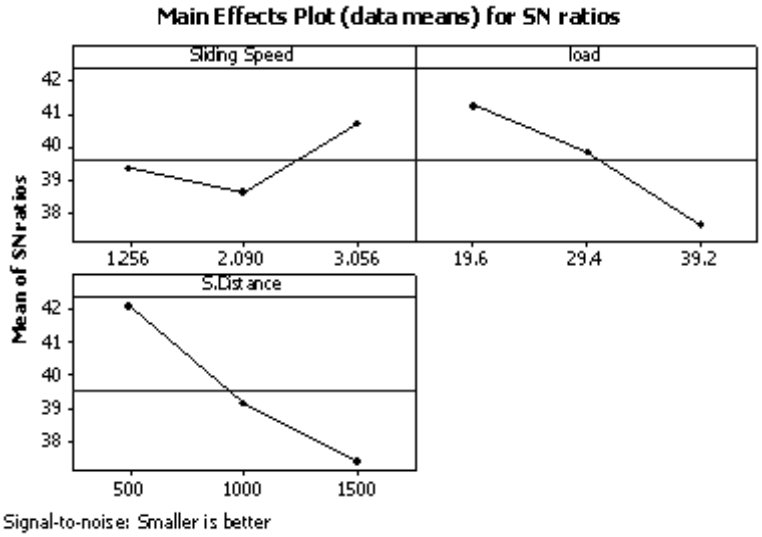

Fig. 3 SN ratio of A1 alloy composite

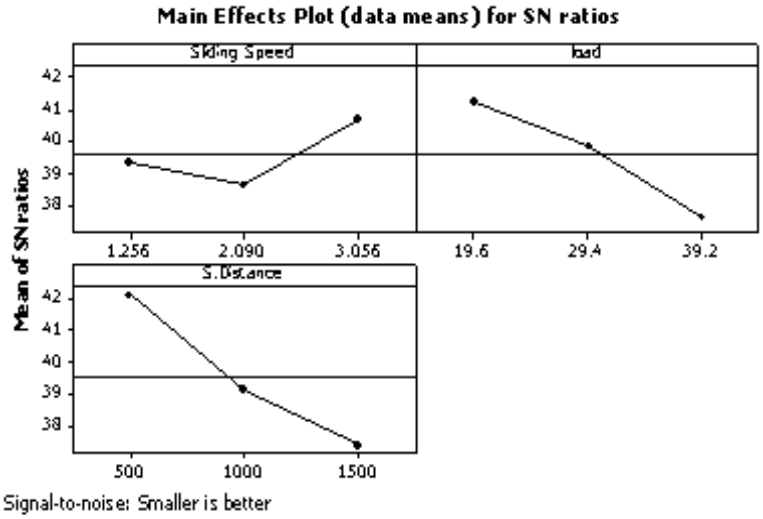

Fig. 4 SN ratio of titanium dioxide reinforced Al alloy composite

Load which as P = 25.05 % for Aluminum alloy and P = 15.90 % for composite material.

Hence, the optimum combinations of the factor levels have not been identical for Al alloy and for the composite material. This is because the wear mechanism induced in both types of test specimens is entirely different. Therefore, achieving both the optimal criteria simultaneously is impossible. Hence, further optimization process is adopted for Al composite material. The interaction effect is not being considered in estimating mean and confidence interval around the estimated mean due to poor additivity between parameters and interaction [16].

The estimated mean of response characteristic (Wear rate) can be computed as

$$\mu WR = \tilde{S}3 + \bar{L}\ 1 + \bar{D}\ 1 - 2\ \bar{T}\ WR. \qquad (2)$$

Where T wr is overall, mean wear rate of composite material is 0.0096 gram. S3, L1and D1 are Mean wear rate of composite material at the respective process parameters that yields highest SN Ratio. The value of m wr was computed and it was found to be 0.0046 gram. A confidence interval (C.I) for the predicted Mean on a confirmation run can be calculated using the following equation.

$$C.I. = \sqrt{\square} F\ \acute{a}\ (1, Fe)\ Ve\ [\frac{1}{neff} + \frac{1}{R}] \qquad (3)$$

Where n ef = $\frac{N}{1 + [Total\ DOF]}$

The other factors and their experimental results with appropriate description are tabulated below:

Symbol	Description	Experimental Values
α	Risk Factor	0.05
F_α	F-ratio Required for α	$F_{0.05}(1, 8)$ = 3.96
fe	Error Degrees of Freedom	8
V_e	Error Variance	0.0000193
n_{eff}	Effective Number of Replications	81 / (1+2) = 27
R	Repetitions for Confirmation Experiments	3

A confidence interval is calculated using the equation no (3) and it is found to be 3.94 X 10^{-3}. The predicted Mean wear rate is: μ_{wr} = 0.0046. The 95% confidential interval of the predicted optimal wear rate of the Composite material is:

$(\mu_{wr} - C.I) < \mu_{wr} (N) (\mu_{wr} + C.I)$
$0.00947 < 0.0046 < 0.00066$

4. Confirmation Experiment for Optimum Parameters

A confirmation experiment is the final step in design of experiment process. The confirmation experiment was performed, by conducting three tests using a specific combination of the factors and levels previously evaluated which yields highest SN ratio. The average value of wear rate was found to be 0.0051gram. This result was within the C.I. of the predicted optimal wear rate of the composite material.

5. CONCLUSION

Following conclusions were drawn from the present investigation.

i. Taguchi's robust parameter design method can be used to analyze and to optimize the wear problem of the metal matrix composites as described in this paper.

ii. Wear resistance of Titanium Dioxide reinforced Aluminum alloy composite is more than the Matrix material.

iii. Highest SN Ratio is obtained when the process parameters are at, third level of parameter S, first level of parameter L and D. In both types of test specimens, least wear rate was observed with the same level of process parameters

iv. The Mean wear rate of the composite material is 0.0096 grams and its Al alloy is 0.0111grams.

v. Optimum wear rate was observed for the Titanium Dioxide reinforced Al alloy composite material when the process parameters are at 3rd level of Sliding speed, 2nd level applied Load and 1st level of Sliding distance.

vi. Confidential interval of the predicted optimal wear rate of the TiO_2 reinforced Al alloy composite material is 3.94 X 10^{-3}.

vii. The confirmation tests showed that Wear rate was within the confidential interval values.

REFERENCES

[1] T.W. Clyne, "An Introductory Overview of MMC Systems, Types and Developments in Composites", Elsevier, Amsterdam, The Netherlands. Vol.3, 2000, pp.1-26.

[2] A.P. Sannio, H. J. Rack, "Dry Sliding Wear of Discontinuously Reinforced Al Composites: Review and Wear", Vol.189, 1995, pp.1-19.

[3] A.T.Alpas and J. Zhang, "Wear Rate Transitions in Cast Al-si Alloys Reinforced With Sic Particles", Scripta Metal Material, Vol.26, 1992, pp.505-509.

[4] P.H. Shipway, A.R. Kennedy and A.J. Wilkas, " Sliding Wear Behavior of Al Based Metal Matrix Composites Produced by a Novel Liquid Route", Wear, Vol.216, 1998, pp.160-171.

[5] G.Ranganath, S.C. Sharma and M. Krishna, "Dry Sliding Wear of Garnet Reinforced Zink / Al MMCs", Wear, Vol.251, 2001, pp.1408-1413.

[6] T. Miyajima and Y. Iwai, "Effects of Reinforcement on Sliding Wear Behavior of Aluminum Metal Matrix Composite", Wear, Vol.255, 2003, pp.606-616.

[7] A.Martin, J.Rodriguez and J. Llorea, " Temperature Effects on the Wear Behavior of Particulate Reinforced Al-Based Composite", Wear, 1999, pp.615-620.

[8] Mahagundappa M .Benal, H.K.Shivanand, "Effect of Reinforcements Content And Ageing Durations on Wear Characteristics of Al (6061) Based Hybrid Composites", Wear, Vol.262, 2007, pp.759 -763.

[9] M.L. Ted Guo and Chi.Y.A.Tsao, "Tribological Behavior of Al/SiC /Nickel-Coated Graphite Hybrid Composites", Materials Science and Engineering, A333, 2002, pp.s134-145.

[10] J.Antony, "Simultaneously Optimization of Multiple Quality Characteristics in Manufacturing Processes Using Taguchi's Quality Loss Function", Int. Journal of Advanced Manufacturing Technology, Vol.17, 2001, pp.134-138.

[11] Phillip. J. Ross, "Taguchi Techniques for Quality Engineering", Mc. Graw hill, New York, 2005, pp. 1-179.

[12] K.V. Mahindra and K. Radhakrishna, "Fabrication of Al – 4.5 % Cu Alloy with Fly Ash MMC and its Characterization", Material Science - Poland, Vol. 25, No.1, 2007, pp.57-67.

[13] C.S.Ramesh, R.Noor Ahmed, M.A. Mujeeb and M.Z.Abdullah, "Fabrication & Study on Tribological Characteristics of Cast Copper-TiO_2 - Boric Acid Hybrid Composite", Materials and Design, Vol.30, 2009, pp.1632-1637.

[14] R.K. Uyyuru, M.K. Surappa and S. Brusethaug, "Effect of Reinforcement Vol Fraction and Size Distribution on the Tribological Behavior of Al-Composite", Wear, Vol.260, 2006, pp.1248-1255.

[15] S.Chung and B.H. Hwang, "A Micro Structural Study of the Wear Behavior of SiC/Al Composites", Tribological International, Vol.27, 1994, pp.307-314.

[16] Taguchi G. Taguchi, "On Robust Technology Development Methods", New York, NY. ASME Press, 1993, pp.1-40.

Effects of Filler Wire and Current on the Joining Characteristics of Al - Li - Cu Alloy Using Tig Welding

A. Chennakesava Reddy
Department of Mechanical Engineering, JNTU College of Engineering, Kukatpally, Hyderabad - 500 085
E-mail: dr_acreddy@yahoo.com
(R)

Abstract

Weld beads of 3 mm thick Al-Li-Cu alloy sheets were prepared from filler wires of parent metal, Al-Mg and Al-Si alloys using TIG welding process. The welding was carried with different currents while voltage, gas flow rate and weld speed keeping constant. The weld beads were given post weld heat treatment. The welding efficiency of 91% was reported with filler wires made of parent metal and Al-Mg alloy and 60 Amperes of welding current.

Keywords: *Al-Li-Cu alloy, Filler wire, TIG welding, Welding current.*

1. INTRODUCTION

Aluminum-lithium-copper (Al-1.8Li-1.8Cu-1.0Mg-0.1Zr) alloy is a high strength lightweight alloy. It has 8.5% lower density, 10% higher stiffness and approximately equivalent mechanical properties to L73 (Al-4.3 Cu-0.6 Mg-0.8 Mn-0.7Si) alloy. Al-Li-Cu alloy is expected to replace L73 alloy on combat aircraft [1]. Lot of research was carried out on Al-Li-Cu alloy to study the various aspects viz: fabrication [2], corrosion and structure-property correlation [3]. It is necessary to study this alloy with respect to welding process for its optimum utilization.

This investigation was carried out to study the welding characteristics of Al-Li-Cu alloy using Tungsten Inert Gas (TIG) welding process. The chemical composition of work pieces is given in Table 1. The objectives of the work are:

i To study the effects of filler materials and welding current.
ii To study of penetration of weld beads.
iii To study the tensile properties and the microstructural characteristics of weld beads.

Table1 Chemical Composition of Work Pieces

% Weight	Li	Cu	Mg	Zr	Mn	Al
	1.8	1.8	1.0	0.1	0.001	Balance

2. EXPERIMENTAL PROCEDURE

The TIG welding was carried out on 5 mm Al-Li-Cu alloy plates, which were produced by rolling process. The chemical compositions of filler wires are given in Table 2. Systematic pre-welding surface preparation was carried out by degreasing, picking in 5% NaOH solvent followed by dipping in HNO_3 and rinsing in distilled water to avoid weld pore formation during TIG welding process.

Table 2 The Chemical Composition of Filler Wires

Filler Wire	Li	Cu	Mg	Zr	Si	Mn
Wire-1	1.8	1.8	1.0	0.15	-	-
Wire-2	1.0	2.0	1.5	0.10	-	-
Wire-3	-	4.3	0.6	-	0.7	0.8

Butt welds were made transverse to rolling direction with a gap of 1.0 mm. The welding characteristics were studied by varying the current, the composition of filler wire (1mm diameter), while the voltage (18V), Argon gas flow rate (10Ltrs/hr) and welding speed (200mm/min) were kept constant.

Flat tensile test specimens with gauge length of 25 mm and gauge width of 12 mm were prepared (Figure1). The specimens were tested using universal testing machine at a strain rate of 0.001 /s at room temperature. The weld beads were evaluated for joint efficiency after

subjecting them to post weld heat treatment (PWHT) (i.e. solution treatment at 525^{0}C and quenching in water and subsequently aging at 175^{0}C for 24 hrs). Small specimens for optical metallography were prepared using conventional mechanical polishing machine and etched using 2%HF solution and were revealed for microstructures using optical metallurgical microscope.

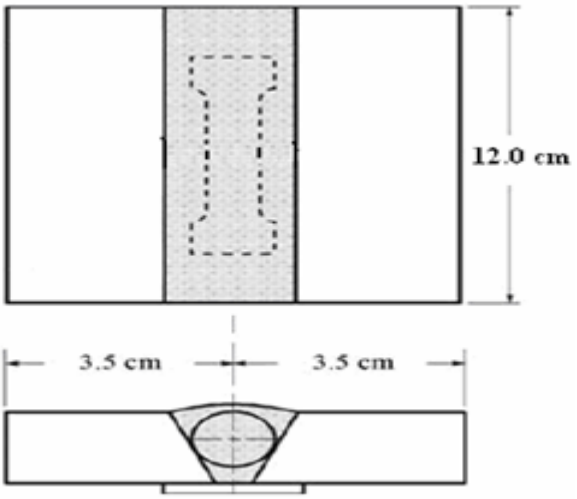

Fig.1 Preparation of tensile specimens

3. RESULTS AND DISCUSSION

Each experiment was repeated twice and each characteristic value is an average of two readings. Results are of experimental, optical and, microstructural observations.

3.1 Effect of Filler Material and Welding Current on the Mechanical Properties

The variation of tensile properties with the composition of filler wire and welding current are shown in Figure 2 and 3. It is observed that the ultimate strength and ductility decrease with increasing welding current. This is owing to high heat input resulted from high currents, which subsequently promote rapid solidification of weld pool. Rapid solidification promotes fine grain structure which can be attributed to the reduction of ductility. The tensile properties are maximum at welding current 60 amps. The chemical composition (which is near to that of plates) of wire-1 gives better tensile properties.

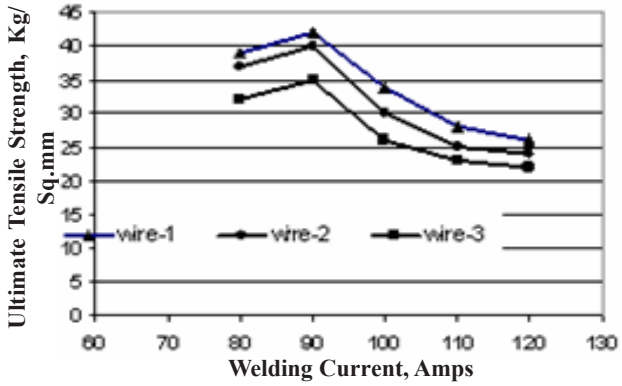

Fig.2 Effect of composition of filler wire and weld current on ultimate tensile strength

The low tensile properties in case of welds made of filler wire-2 and filler wire-3 might be due to the constitutional pollution of weld pools. The constitutional pollution is just because of the variation of filler wire composition with that of parent metal.

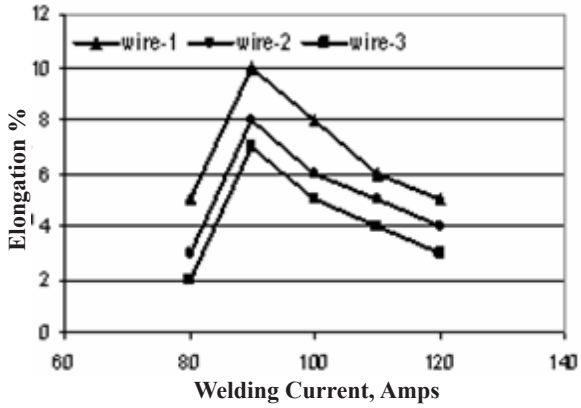

Fig.3 Variation of ductility with compositior of filler wire and welding current

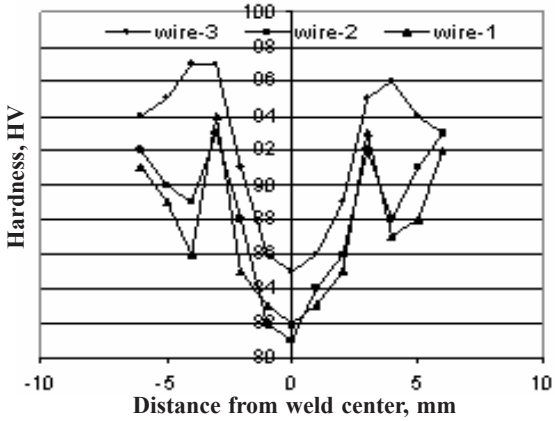

Fig.4 Effect of compositior of filler wire on hardness

The variation of hardness from the center of weld is shown in Figure 4. The aluminum alloy sheets which are cold rolled tend to have stronger mechanical properties of the produced due to increasing in the dislocation density. As the grains undergo re-crystallization and coarsening in the weld area, the strain induced dislocations will destroy resulting in decrease in the hardness of the weld. The softened regions noted throughout the weld can also be attributed to coarsening and dissolution of strengthening precipitates during the thermal cycle of the welding. The heat affectes zone (HAZ) is nearly at 3 mm from the center of weld.

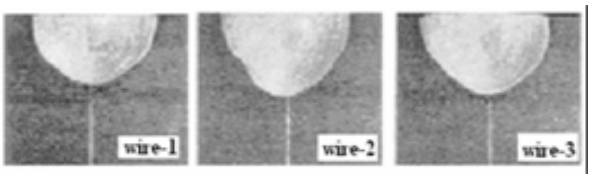

Fig.5 Weld bead profiles

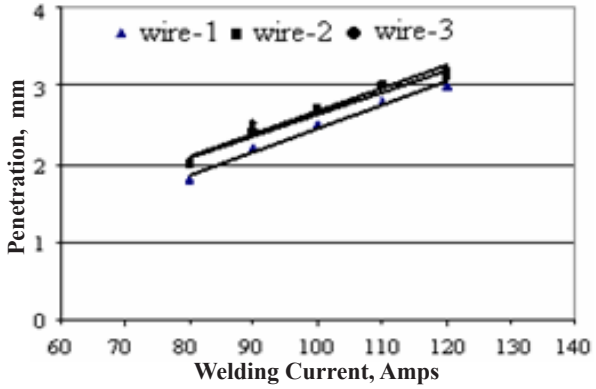

Fig.6 Effect of welding current on the depth of penetration

Weld bead profiles are shown in Figure 5. There is no clear variation in the weld bead profiles obtained with different wires. For welds produced at a fixed arc energy using argon shielding gas, a significant increase in the depth of weld penetration was observed without reduction in the weld bead width at the top face. The depth of penetration in case of wire-2 and wire-3 is nearly same, whereas it is shallow U profile for wire-1 (Figure 6).

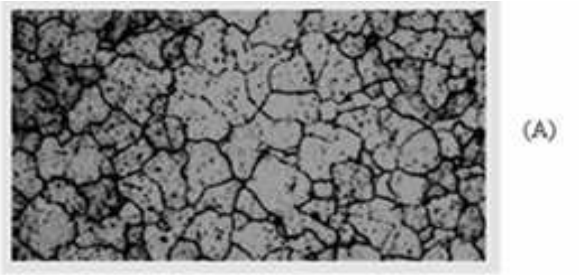

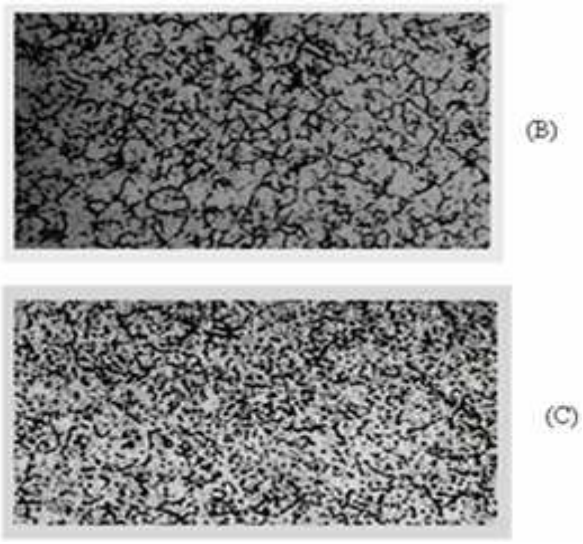

Fig.7 Microstructures of weld beads welded with different filler wires (10μM)

3.2 Microstructural Characteristics of Weld Beads

The microstructural characteristics of the weld beads are shown in Figure 7. The fusion zone of the weld bead prepared from the parent metal as filler wire as illustrated from the Figure 7(A) revealed the equiaxed grain structure. The microstructure of the fusion zone of the weld obtained by the filler wire-2 as shown in Figure 7(B) revealed the coarse cellular dendritic structure. Even though the filler wire-3 results fine grain structure as revealed from Figure 7(C), the tensile properties are contradictory. The reason could be the strengthening mechanisms induced on account of age hardening in the weld beads obtained by filler wire-1 and -2.

4. CONCLUSION

The ultimate strength and ductility decrease with increasing welding current. The welding current of 90 Amps gave maximum tensile properties of weld joints. The HAZ is neatly at 3mm from the center of weld joint. The strengthening mechanisms induced on account of age hardening in the weld beads obtained by filler wire-1 and -2 increase the tensile properties.

REFERENCES

[1] E.A. Starke, T.H. Sanders and I.G. Palmer, "New Approaches to Alloy Development in the AI-Li System", Journal of Metals, Vol.33, No.8, 1981, pp.536-866.

[2] W.E.Quist, M.Hyman and D.V.Badger, "Aluminium-Lithium Alloys", ASM International, 1987, pp.401-404.

[3] J. R. Davis, "ASM Specialty Handbook: Aluminum and Aluminum Alloys", Ohio: ASM International, Materials Park; 1994.

[4] S. Kou and Y. Le, "Nucleation Mechanism and Grain Refining of Weld Metal", Weld Journal, Vol.65, No.4, 1990, pp.65-70,

[5] C. F. Tseng and W. F. Savage, "The Effect of Arc Oscillation in Either Transverse or Longitudinal Direction has Beneficial Effect on the Fusion Zone Microstructure and Tends to Reduce Sensitivity in Hot Cracking", Weld Journal, Vol.50, No.5, 1971, pp.777-786.

[6] G. Madusudhan Reddy, A. A. Gokhale and K. Prasad Rao, "Weld Microstructure Refinement in a 1441 Grade Al–Lithium Alloy", Journal of Material Science, Vol.32, 1997, pp.4117-4121.

Adsorption of Fluoride from Aqueous Solution Using Emblica Officinalis Seeds as Adsorbent

G. Anusha[1], J.Raja Murugadoss[2] and P.Raju[3]

[1&2]Department of Civil Engineering, Bannari amman Institute of Technology, Sathyamangalam - 638 401, Erode District, Tamil Nadu

[3]Vetri Vinayaka College of Engineering and Technology, Trichy - 621 215

E-mail: anushanivasbit@gmail.com

(R)

Abstract

In recent years the problem of water contamination is drastically increasing due to the disposal of industrial wastewater containing Iron, Fluoride, Mercury, Lead, Cadmium, Phosphorous, Silver, Sulphur etc into water bodies. Due to which, the contamination leads to serious health disorders and in some worst cases it causes permanent disabilities or even causal losses. In the present work an attempt has been made to remove such contaminants particularly Fluoride and to study the efficiency on the removal of fluoride using a new material, Emblica officinalis which is commonly referred as gooseberry. Accordingly a set of experiments have been conducted using batch and column processes, with the help of activated carbon prepared from gooseberry. Experiments reveal that the adsorption capacity of gooseberry is significant as 68% to yield promising solutions.

Keywords: *Activated carbon, Batchstudy, Fluoride, Gooseberry.*

1. INTRODUCTION

Fluoride is a natural constituent of the Earth's crust and is present in varying concentrations in all ecosystems. It has drastically changed the biogeochemical cycles and in few cases it balances few class of metals [1-2]. The main anthropogenic sources of Fluoride are industrial sources viz. toothpowder manufacturing industries and groundwater. In addition it also induces adverse effects on the environment and human health and moreover they are highly toxic even at low concentration to human beings and other living beings.

The removal of fluoride from synthetic solution can be done by adsorption technique using powdered activated carbon. Though importance of this treatment is felt, its cost keeps the industrialists away from adopting the same. It is also a fact that till date no material proves to be a better adsorbent than commercial activated carbon [3]. Since the cost of activated carbon and its reactivation costs are high, this particular technology remains at an inaccessible distance and its application does not find a significant place in the field of environmental engineering [4]. Hence in this present work an effort has been made to introduce a new class of activated carbon, prepared from the Gooseberry seeds for the removal of such fluoride content from wastewater.

During adsorption, the atoms within the structure of the adsorbent are attracted in all directions relatively equally, whereas the atoms at the surface exhibit an imbalanced attractive force, which the adsorbate molecules help to satisfy. The significant parameter, which popularizes an adsorbent, is the presence of a great amount of surface area; normally via the wall area or slots, capillaries or pores permeating its structure, in a very small volume and unit weight.

2. MATERIALS AND METHODS

2.1 Adsorption with Activated Carbon: An Overview

Certain organic compounds in wastewater are resistant to biological degradation and many others are toxic or nuisance (odor, taste, color forming) even at low concentration. Low concentration materials are not readily removed by conventional treatment methods. Activated carbon has an affinity for organics and its use for organic contaminant removal from wastewater.

The larger surface area, a critical factor in the adsorption process, enhances the effectiveness of the activated carbon for the removal of organic compounds from wastewater by adsorption. The surface area of activated carbon typically ranges from 500-1400 m2/g

and the effect of chemical nature of the carbons surface is less significant than the surface area. This chemical nature or polarity varies with the type of carbon and can influence attractive force between molecules.

2.2 Experimental Methodology

2.2.1 Preparation of Adsorbent Using Gooseberry

The gooseberry seed is a material which is thrown out as a waste. These wastes were collected and their size were reduced by breaking it into small pieces. Then they were dried in an oven at a temperature of 170°C for 24hrs. It was then packed in an air tight in a cylindrical fluoride container with top completely sealed to prevent the entry of air during the process of charring. The sealed container was heated in a muffle furnace by slowly raising the temperature up to 600°C and subsequently it is maintained for duration of one hour. The activated carbon thus prepared was subsequently washed with distilled water and oven dried.

2.2.2 Batch Adsorption

Batch adsorption study was made by employing orbitary shakers. 150 ml of desired concentration were agitated continuously with known amount of the activated carbon powder by varying the dosage. Samples were taken and their residual fluoride were monitored at regular intervals. After a lapse of a prefixed contact time, 50 ml of sample was drawn from the samples and filtered using a whatman No.40 filter paper and was analyzed in spectrophotometer for its residual fluoride concentration. To assess the influence of optimum pH, optimum dosage, time interval and isotherm, four different set of experiments were carried out, viz. a) Bottles with different pH ranging from 1 to 12 were varied and conditions were analyzed for residual fluoride concentration. b) Bottles with increasing doses ranging from 0.5g to 5g of the adsorbent with fixed contact time were analyzed. c) Bottles with optimizes pH and sorbent dosage were agitated for varied timings ranging from 5 to 40 minutes with the interval of 5 minutes and then analyzed for residual fluoride concentration. d) Langmuir isotherm was plotted and the isotherm satisfies the equilibrium condition of the adsorbent.

3. RESULTS AND DISCUSSIONS

3.1 Optimum pH Studies

With reference to the discussion in section 2.2.2, nine experiments were conducted to study the influence of pH on the efficiency of fluoride removal. Accordingly the pH was varied with an interval of 2 for a range of 9 to 12.From the above experiments it is found that the hydrogen ion concentration plays a critical role on the adsorption capacity of gooseberry. It is found that for a pH of 5, the efficiency was found to be better. Further another set of 9 experiments were conducted to determine the influence of dosage on the removal efficiency. Dosage was varied from 0.025g to 0.6g with an interval of 0.025g and it has been found that the dosage variation gives a significant role in determining the removal efficiency. It is found that for the dosage of 1.5g, the removal efficiency has an appreciable increase. Similarly 8 set of experiments were conducted and the influence of time interval for fluoride removal was determined by varying the time interval from 5 mins to 40 mins with an interval of 5mins. It has been found that time also plays an important role in addition to pH and dosage.By varying the time interval, it was found that at the contact time of 20mins,the removal efficiency has an appreciable increase.

3.4 Langmuir Isotherm for the Adsorption Pattern

Irving Langmuir devised a simple model involving a thermodynamic equilibrium to predict the fraction of solid surface covered by an adsorbate as a function of its gas pressure. This was later extended to liquid systems, where the equilibrium involved concentrations in solution. The Langmuir model is discussed in most elementary texts on physical chemisry, and most reference books on adsorption will have an extensive treatment, including references to theoretical and experimental reports. In this model adsorbate and solvent molecules compete to adsorb on sites on the surface of the powder.

The essential characteristics of the Langmuir isotherms can be described by a separation factor RL
Value of RL

RL > 1 - unfavorable
RL = 1 - linear
0<RL<1 - favorable
RL =0 - irreversible
RL = 0.33

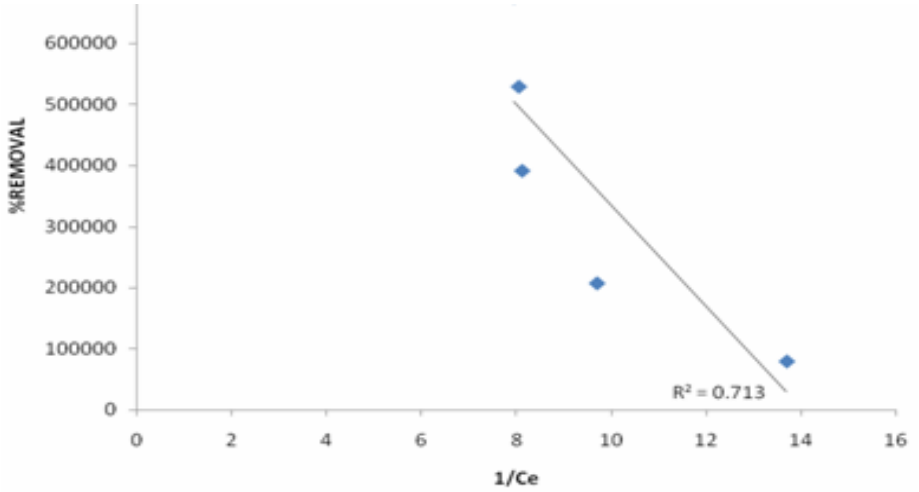

Fig.1 Langmuir isotherm test for synthetic solution

As the R L value lies between 0 and 1, it indicates favorable adsorption for fluoride uptake. The R2 value is less than 1 which also says that the adsorbent used is favorable for fluoride uptake.

3.5 Column Adsorption Studies

In the laboratory, the experiments were conducted with 45mm diameter and 300 mm length column setup. The studies were carried out for a fixed flow rate of 2 mL/min and for which the depths of carbon are taken as 2.5 and 5cm. The column was packed with adsorbents at various depths. The influent and effluent were adjusted to be 2mL/min. Samples were collected at regular interval of 15min and analyzed for residual concentration. The percentage removal was calculated till the carbon gets exhausted. The experiments were conducted for all the adsorbents and the results obtained were compared. The results were plotted taking volume treated in mL as abscissa and residual metal concentration in mg/L as ordinate.

4. CONCLUSION

The efficiency of a new variety of adsorbent prepared from the seeds of Emblica Officinalis has been successfully demonstrated through series of laboratory experiments by varying the values of pH, dosage and time for the synthetic solution.The experiments were carried out for fluoride removal and the results reveal that the seed of Emblica Officinalis has much potential for pH= 5,dosage =1.5g and contact time = 20 minutes.

REFERENCES

[1] S.T Ramesh, R. Gandhimathi and M.Vinoth, “Cement Kiln Dust Based Low Cost Adsorbents for COD Removal from Domestic Water”, Environmental Pollution Control Journal, Vol.1, No.4, 2008, pp.53-57.

[2] J.H.Verma and P.B Nagarnaik , “Control of Ground Contamination using Synthetic Media”, Environmental Pollution Control Journal, Vol.11, No.6, 2008, pp.56-59.

[3] A.H.Mahvi, K.Maleki, and A.Eslami,‘Potential of Rice Husk and Rice Husk Ash for Phenol Removal in Aqueous Systems’, American Journal of Applied Sciences, Vol.1, No.4, 2004, pp.321-326.

[4] Saifuddin.M.Nomanbhay and Kumaran Palanisamy,” Removal of Heavy Metal from Industrial Waste Water using Chitosan Coated Oil Palm Shell Charcoal”, Environmental Biotechnology, Vol.8, No.1, 2005.

[5] Saritha Sharma and Abha Agarual, “Effect of Heavy Metals (Zinc, Nickel, Cadmium) on Seed Germination, Total Chlorophyll content and Grain Yield of Mustrard (Brassica Juncea)”, Ecology Environment & Conservation, Vol.14, No.1, 2008, pp.111-114.

[6] D.S.Bhargava. and D.J Killedar., “Residual Concentration Model for Fluid Adsorption’, IE(1) Journal, Vol.89, pp 30-33..

Methanol-Jatropha Biodiesel-Diesel Tri-Compound Blends: Environment Friendly Oxygenated Biomass Fuel for Diesel Engines

E. Rajasekar[1] , K. Balamurugan[2] and A. Murugesan[3]
[1]Department of Automobile Engineering, [2]Department of Mechanical Engineering,
Institute of Road and Transport Technology, Erode - 638 316, India.
[3]Department of Mechatronics Engineering, K.S.Rangasamy College of Technology, Tiruchengode, India.
E-mail: rajasekarirtt@yahoo.co.in

(R)

Abstract

Biodiesel is gaining potential world over as a sustainable alternative fuel to diesel. The purpose of this study is to investigate the emission and performance characteristics of Jatropha Methyl Ester (JME) fuel and methanol-JME-diesel tri-compound fuel blends in a direct injection diesel engine, and to compare it with that of a conventional diesel fuel. There are many technical barriers to the direct use of alcohols in diesel engines. Hence methanol-JME-diesel tri-compound fuel blends were used. A slight increase in BTE at all loads, considerable reduction in NOx emissions at all loads and significant smoke reduction at full load was observed for the tri-compound fuel blends. Methanol can be blended up to 15% in diesel - biodiesel fuel blends to fuel existing CI engines without any hardware modifications to reduce engine out emissions, fuel crisis and global warming.

Keywords: *Alternative fuels, Global warming, NOx reduction, Jatropha methyl ester, Methanol, Tri-compound fuel blends.*

1. INTRODUCTION

Diesel vehicles are by far the most popular method of transporting goods and people world over. They are also the worst polluters of environment causing health risks. In recent years, the legislated maximum levels of emissions from engines are becoming more and more stringent. The test limits of EURO III are about 30-40% lower when compared to that of EURO II for diesel passenger cars and light commercial vehicles and there is a further drop of about 30% for EURO IV. Future regulations like EURO V and presumably VI will force diesel engine manufacturers to drastically reduce NO_x and particulate matter emissions. Among various developments to reduce emissions, the application of oxygenated fuels such as diesel-biodiesel fuel blends, and methanol-biodiesel-diesel tri-compound fuel blends for diesel engines is an effective way to reduce vehicular pollution.

1.1 Indian Scenario

Biodiesel and methanol are the renewable and viable fuel options for automobiles of countries like India with staggering reliance on imported petroleum fuels. It is only in recent years that systematic efforts have been made to utilize vegetable oils and alcohols as fuels in engines. Many literature reviews [1] show that European countries and the USA have mainly concentrated on saffola, rapeseed, linseed, sunflower, peanut, soybean oils, etc., as alternative fuels for diesel engines, which are essentially edible in nature. In the Indian context, only non-edible vegetable oils can be seriously considered as fuel for IC engines as the edible oils are in great demand and are far too expensive at present.

1.2 Global Warming

Climate change is one of the most difficult challenges facing the world today and preventing it will necessitate profound changes in the way energy is produced, distributed and consumed. Burning fossil fuels such as coal, oil and gas provide about three-quarters of the world's energy. However, when these fuels are burned, they emit greenhouse gases (GHGs) that are now recognized as being responsible for climate change. The primary greenhouse gas emitted through fuel combustion is CO_2. Land-use and land-use changes, notably

deforestation, also involve emissions of CO_2 [2]. From the increased pressure from international initiatives such as the conferences of Rio de Janeiro 1992, Berlin 1995, Geneva 1996, Kyoto Agreement 1997 and Copenhagen 2009 to reduce carbon emissions and the lobbying activities of environmental pressure groups, it is clear that governments have a tough challenge on their hands.

Global warming is the main reason why there is a need to avoid producing CO_2. Gases like CO_2 travel up into the upper atmosphere (the troposphere) where they act as a screen to sunlight. They allow the suns rays in but stop the heat radiation from re-emerging, much as it happens with the glass in greenhouse. The result is that the greenhouse, in this case the whole world, heats up. However, the vast tonnage of CO_2 gas released into the atmosphere seems likely to upset the natural balance. Latest observations suggest that global CO_2 concentrations in the atmosphere currently stand at 387 parts per million (ppm) and continue to grow at an annual rate of around 2 ppm [3].

Table 1.1 shows world CO_2 emissions in million metric ton (MMT) by region [2] and it is clear that the expected CO_2 production world wide would be 33284 Million Metric Tone (MMT) in 2015 and 36023 MMT in 2020. To tackle the twin challenges of energy supply and GHG emission reduction, oxygenated biomass fuels like alcohols, biodiesel and vegetable oils can be used.

3. MATERIALS AND METHODS

3.1 Oxygenated Biomass Fuels

The term biofuel is referred to as liquid or gaseous fuels for the transport sector that are produced from biomass. A variety of fuels can be produced from biomass resources including liquid fuels such as ethanol, methanol, biodiesel and gaseous fuels, such as hydrogen and methane. Liquid biofuels are primarily used to fuel vehicles, but can also fuel engines or fuel cells for electricity generation. Biofuels are easily available from common biomass resources. They have a considerable environmental friendly potential, are biodegradable and contribute to sustainability.

Producing and using biofuels for transportation offers alternatives to fossil fuels that can help provide solutions to many environmental problems. Biodiesel and methanol provide significant reductions in GHG emissions compared to gasoline and diesel fuel. Due to the low content of pollutants such as sulfur in biofuels, the emissions of biofuels are much lower than that of conventional fuels.

The dwindling fossil fuel sources and the increasing dependency of the developed countries on imported crude oil have led to a major interest in expanding the use of bioenergy. Figure 1 shows the share of alternative fuels compared to the total automotive fuel consumption in the world as a futuristic view [5]. Hydrogen is currently more expensive than conventional energy sources. There are several reasons for biofuels to be considered as relevant technologies by both developing and industrialized countries because of energy security, environmental concerns, and socioeconomic issues related to the rural sector.

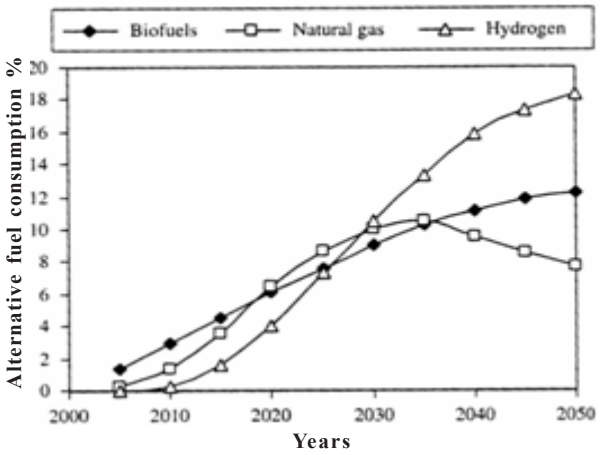

Fig. 1 Share of alternative fuels compared to the total automotive fuel consumption

3.1.1 Biodiesel

The National Biodiesel Board, USA, technically defined the biodiesel as "a fuel comprised of mono-alkyl esters of long chain fatty acids derived from vegetable oils or animal fats, designated B100, and meeting the requirements of ASTM D 6751". In addition to meeting engine performance and environmental criteria, biodiesel has to compete economically with diesel fuels in order to survive in the market [6]. One way of reducing the biodiesel production costs is to use the less expensive feed stocks containing fatty acids such as non-edible oils obtained from plant species like jatropha curcas, pungamia pinnata, mahua and neem.

3.1.2 Alcohol

Methanol and ethanol are two accepted alternative fuels which possess the potential to be produced from biomass sources. Neither of the fuels is well suited for use in diesel engines, and the use of high compression ratios, ignition improvers and ignition assistance devices is common [7]. Bio-methanol is made from cellulosic biomass unlike the traditional feedstock. The calorific value and cetane number of the diesel-methanol blends are lower than that of diesel fuel, requiring the use of cetane improving additives. In fact, diesel engines cannot operate normally on methanol-diesel blend without special additives.

3.1.3 Tri-compound Fuel Blends

As far as combustion is concerned, one of the best ways to utilize alcohol in a diesel fuel is to combine it with a vegetable oil to make the corresponding ester of the vegetable oil (biodiesel). Although biodiesel cannot entirely replace petroleum-based fuels, methanol-biodiesel-diesel tri-compound fuel blends can be used in existing engines to achieve both environmental and energy benefits. There are many technical barriers to the direct use of alcohol in diesel engines due to its low cetane number, lower calorific value, lower flash point, poor solubility in diesel fuel and reduced lubricity. Biodiesel fuels are good renewable sources that can be used as oxygenates to increase oxygen content of the methanol-diesel blends. Biodiesel fuels are the emulsifiers or surfactants that allow more methanol in the tri-compound fuel blend, improve blend tolerance for water, and keep the blend fuel stable. Blending biodiesel and alcohol with fossil diesel dramatically improved the solubility of alcohol in diesel fuel over a wide range of temperature. If the barriers of biodiesel and alcohol using on diesel engines are taken into account, it is a better way to blend methanol, biodiesel, and diesel together (tri-compound fuel blends) for application. The fuel properties tested for the tri-compound blends are depicted in the Table 2.

Table 1 World CO_2 Emissions in MMT by Region, 1990-2020

Region	1990	2002	2010	2015	2020
Mature Market Economies	10,465	11,877	13,080	13,745	14,392
North America	5769	6701	7674	8204	8759
Western Europe	3413	3549	3674	3761	3812
Mature Market Asia	1284	1627	1731	1780	1822
Transitional Economies	4894	3124	3643	3937	4151
Emerging Economies	6101	9408	13,478	15,602	17,480
Asia	3890	6205	9306	10,863	12,263
Middle East	845	1361	1761	1975	2163
Africa	655	854	1122	1283	1415
Central and South America	711	988	1289	1480	1639
Total world	21,460	24,409	30,201	33,284	36,023

Table 2 Fuel Properties Tested for Tri-compound Fuel Blends

	Diesel	M15J20	M15J40	M15J60	M15J80
Diesel (vol. %)	100	65	45	25	05
Methanol (vol. %)	0	15	15	15	15
JME (vol. %)	0	20	40	60	80
Density (g/cm^3)	0.820	0.832	0.836	0.843	0.851
Calorific value (MJ/kg)	42.50	38.55	38.11	37.78	37.46
Oxygen content (Wt. %)	0	7.67	9.52	11.64	13.82

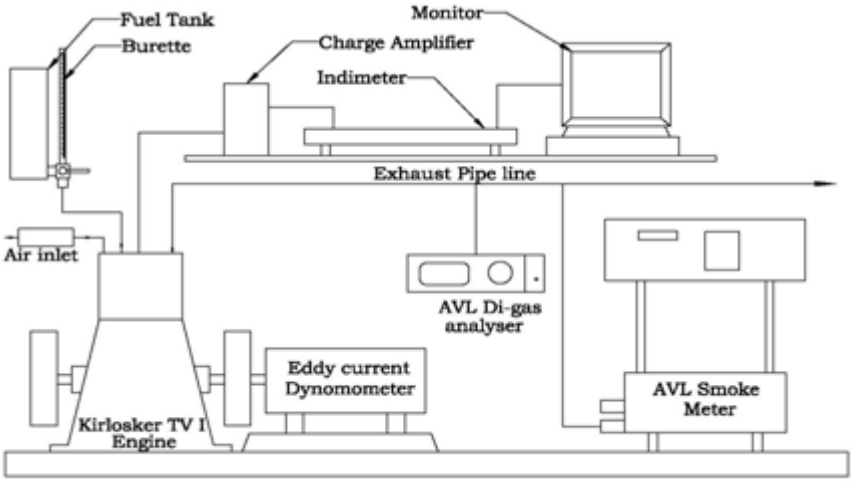

Fig.2 Schematic of engine test rig

4. Experimental Setup

Experiments were conducted in a four-stroke single cylinder direct-injection water-cooled CI engine. Transient exhaust smoke was measured using the AVL 444 standard smoke meter. Oxygen and NO_x concentration in exhaust were measured by electrochemical method using the AVL Digas 4000 analyzer. Exhaust HC, CO and CO_2 concentrations were measured by non destructive infra red (NDIR) method with the same analyzer. An eddy current dynamometer with an electronic control panel was used to load the engine. The detailed layout of the experimental setup is shown in the Figure 2 and photographic view is given in Appendix I.

Appendix I Photographic view of the experimental facility

5. Results and Discussion

Figure 3 depicts the effect of brake power on brake thermal efficiency (BTE). BTE of diesel fuel and pure JME were 29.77 % and 30.76% respectively. The BTE of the tri-compound fuel blend M15J20 was 31.28% at full load condition. To obtain the same engine power (torque and speed), the fuel consumption must be increased when JME and methanol contents is increased in the blends, owing to its lower heating value.

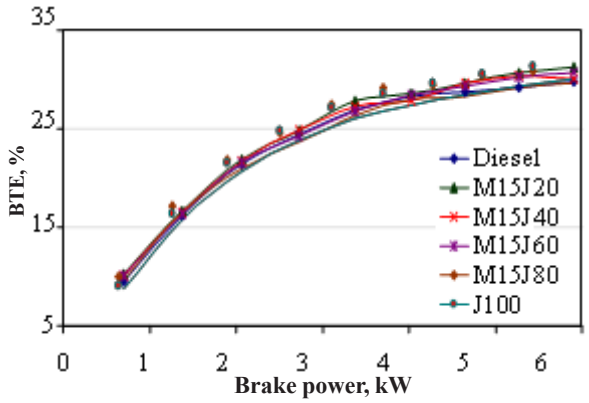

Fig.3 Effect of brake power on brake thermal efficiency

Figure 4 shows the variation of BSEC with brake power for methanol-JME-diesel tri-compound fuel. At lower loads for fixed methanol content of 15%, if the JME content is increased in the fuel, then the BSEC values increased. This may be due to the high latent heat of evaporation of methanol which reduces the cylinder temperature and affect the fuel volatility. At higher loads fuel oxidation promoted by high cylinder temperature and hence BSEC values of tri-compound fuel blends are very close to that of diesel fuel.

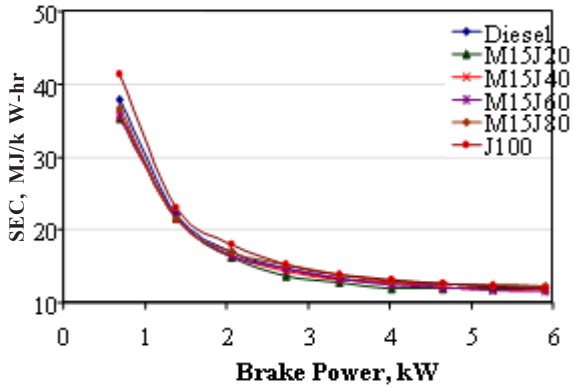

Fig.4 Effect of brake power on brake specific energy consumption

The effects of brake power on HC and CO emissions for all fuels tested are shown in Figure 5 and 6 respectively. When 100% JME is used, the dissolved oxygen in the fuel may promote a more complete combustion and effectively reduce the formation of unburned HC and CO emissions. For pure JME fuel about 50% reduction in HC emission was observed. Biodiesel is a low carbon fuel and has a lower elemental carbon to hydrogen ratio than diesel fuel. Methanol in JME-diesel fuel blend reduces the CO and HC emissions. The reason for low HC and CO emissions of tri-compound fuel blends is the dissolved oxygen content in methanol and JME.

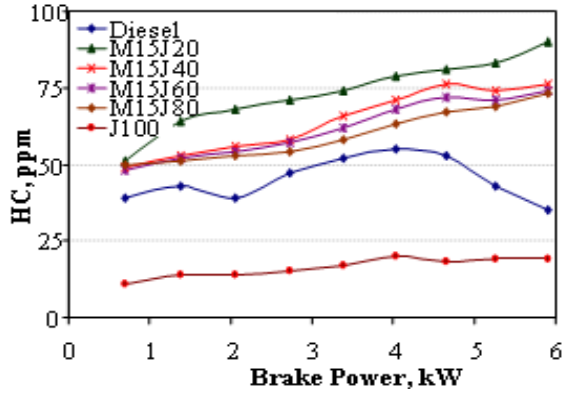

Fig. 5 Effect of brake power on hydrocarbon emission

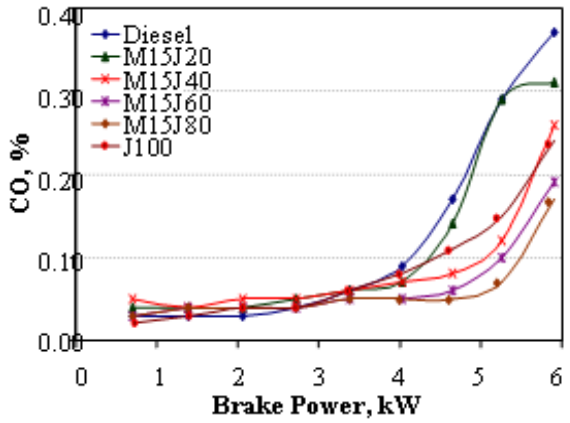

Fig. 6 Effect of brake power on carbon monoxide emission

The effect of brake power on CO_2 is depicted in Figure 7. The CO_2 emission was less for all tri-compound fuel blends at all loads and for pure JME fuel it was considerably reduced. In its simplest form, the carbon cycle of vegetable oil consists of the fixation of carbon and the release of oxygen by plants through the process of photosynthesis and then combining the oxygen and carbon to form CO_2 through processes of combustion. It is appropriate to mention here that the CO_2 released by petroleum diesel was fixed from the atmosphere during the formative years of the earth; whereas the CO_2 released by biodiesel gets continuously fixed by plants and may be recycled by the next generation of crops. The carbon cycle time for fixation of CO_2 and its release after combustion of biodiesel is quite small as compared to the cycle time of petroleum based fuels.

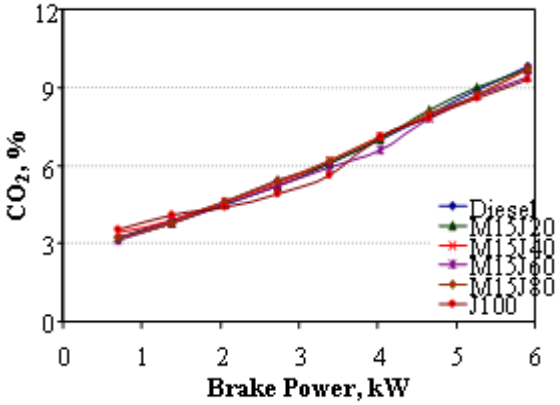

Fig. 7 Effect of brake power on carbon dioxide emission

The effect of brake power on NOx emissions is shown in Figure 8. Considerable reduction in NOx emissions for methanol-JME-diesel tri-compound fuel blends at low and medium load conditions and 75-100 ppm increase for sole JME operation in all loads was observed. Higher cetane number and dissolved oxygen content of the JME fuel promote the combustion process and results in high cycle temperature and hence high NOx emissions [6]. When methanol was blended up to 15 % in diesel-JME fuel blends, NOx was considerably (100 to 200 ppm) reduced in low and medium loads. The latent heat of vaporization of methanol is much higher than diesel fuel which can reduce the NOx emissions produced.

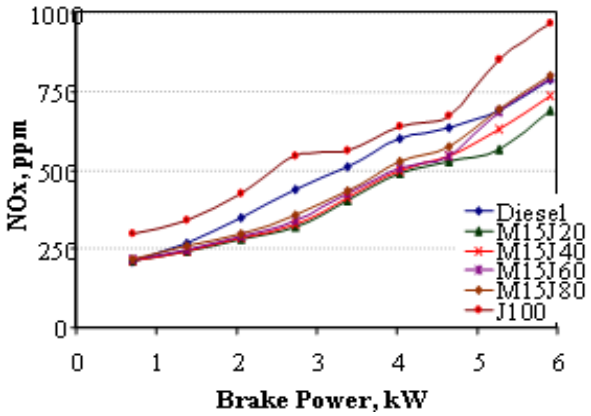

Fig. 8 Effect of brake power on oxides of nitrogen

Figure 9 depicts the effect of brake power on smoke. In part load conditions the smoke value increased considerably for all methanol-JME-diesel tri-compound fuel blends than that of fossil diesel. This was due to the higher viscosity of JME at low temperatures which reduced the rate of spray atomization. The latent heat of vaporization of methanol is much higher than that of diesel fuel which results in delayed evaporation and poor mixture formation of tri-compound fuel blends. Hence increased smoke emission by 10 to 15 HSU was observed at lower loads. At low starting temperatures fuel evaporation was more difficult. These lead to worse fuel/air mixing and thus to more intense soot formation. At full load conditions for all tri-compound fuel blends significant smoke emission was observed. This could be attributed to the increased abundance of oxygen from methanol and JME, which creates favorable combustion conditions for the fuel droplets. As reported in several publications [6,7], the reduction of smoke with the use of biodiesel is justified by the presence of molecular oxygen, which acts as an internal oxygen supply and by the absence of aromatic components that are considered as soot precursors.

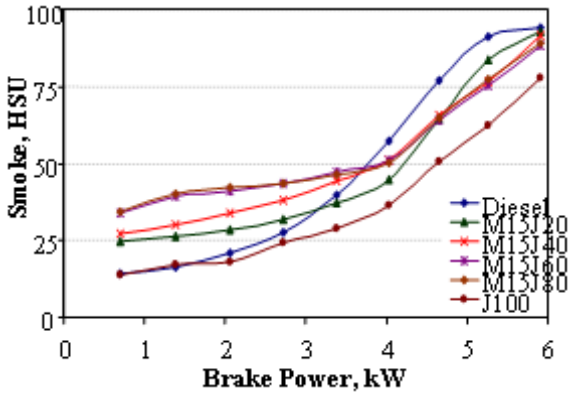

Fig. 9. Effect of brake power on smoke emission

6. CONCLUSIONS

The following are the main conclusions based on the present experimental investigation:

- 20% JME can be used to have lubricity benefits and to reduce engine emissions. 100% JME provides both the benefits and also provides complete replacement of fossil diesel, if the biodiesel could be supplied in sufficient amounts at an affordable cost.
- Biodiesel alone will not solve our dependence on imported oil within any practical time frame, use of this and other alternative energy sources like alcohols could contribute to a more stable supply of energy.
- The blend of M15J20 ie., 15:20:65 of methanol-JME-diesel tri-compound fuel gives the highest BTE (31.28%) which is higher than that of fossil diesel.
- A reduction of 100-200 ppm in NOx emissions at all loads and 10-15% reduction of smoke at full load was observed for the tri-compound fuel blends.
- Oxygenated biomass fuels like JME and methanol can be used in CI engines to reduce engine emissions, global warming and dependency on imported oils with out major engine modifications.
- Based on the present investigation, it is strongly recommended that the blending of biodiesel, methanol and diesel fuel can be considered as a promising alternative fuel for diesel to fuel existing CI engines.

REFERENCES

[1] S. Fernando and M. Hanna "Development of A Novel Biofuel Blend Using Ethanol Biodiesel Diesel Micro Emulsions: EB-Diesel", Energy and Fuels, Vol.18, 2004, pp.1695-1703.

[2] Ibrahim Yuksel, "Global Warming and Renewable Energy Sources for Sustainable Development in Turkey", Renewable Energy, Vol.33, 2008, pp.802-812.

[3] National Oceanic, Atmospheric Administration, "Mauna Loa CO_2 Annual Mean Data", Boulder. / http://www.esrl.noaa.gov/gmd/ccgg/ trends/S, 2009.

[4] Ayhan Demirbas, "Biofuels Sources, Biofuel Policy, Biofuel Economy and Global Biofuel Projections" Energy Conversion Management, Vol.49, 2008, pp. 2106-2116.

[5] R.L. McCornick, S.Michael, Graboski, L. Teresa, Alleman and Andrew, "Impact of Biodiesel Source Material and Chemical Structure on Emissions From a Heavy-duty Diesel Engine", Environmental Science and Technology, Vol.35, 2001, pp.1742-1747.

[6] E.Rajasekar, A.Murugesan and N.Nedunchezhian, "Review of NO_x reduction Technologies in CI Engines Fuelled with Oxygenated Biomass Fuels", International Journal of Renewable and Sustainable Energy Reviews, Elsevier, Vol.14, 2010, pp.2113-2121.

[7] Shailendra Sinha and Avinash Kumar Agarwal, "Performance Evaluation of a Biodiesel (Rice bran oil methyl ester) Fuelled Transport Diesel Engines", SAE, No.2005-01-1730, 2005, pp.1-9.

Application of Artificial Neural Network in Optimization of SMAW Hardfacing Electrode Composition

S. Selvi[1], E. Rajasekar[2] and G. Baskar[3]

[1]Department of Mechanical Engineering, Institute of Road and Transport Technology, Erode-638 316, Tamil Nadu

[2]Department of Automobile Engineering, Institute of Road and Transport Technology, Erode-638 316, Tamil Nadu

[3]Department of Civil Engineering, Institute of Road and Transport Technology, Erode-638 316, Tamil Nadu

Email: selvimech@yahoo.com

(R)

Abstract

In this work an attempt has been made for the optimization of electrode composition of Shielded Metal Arc Welding [SMAW] hardfacing using Artificial Neural Networks (ANN's). Hardfacing process variables and suitable electrode composition play a very significant role in determining the required hardness, life of the component with minimum wear and corrosion rate in any welding reclamation process employed today. A feed forward neural network was adopted here to model the hardfacing electrode. ANN was selected for the optimization of the formulated electrode chemical composition. To train the network, the compositions of nine elements viz., C, Cr, Co, Mg, Mo, Ni, P, S and Si were considered as input variables, while hardness and wear rate were considered as output variables. Results obtained from ANN were validated by statistical methods (Chi-Square and t- Test) and found that they were within the permissible limit of ± 5%. The composition of the electrode was optimized using the ANN model with reasonable accuracy.

Keywords: *Artificial Neural Network, Back-Propagation,Electrode Composition, Hardfacing,Optimization*

1. INTRODUCTION TO ANN

Artificial neural networks have been defined as "massively parallel interconnected networks of simple (usually adaptive) elements and their hierarchical organizations which are intended to interact with the objects of the real world in the same way as biological nervous system do1. Experimental investigation of the composition of various electrode elements is complex, time consuming and costly, especially for studies which use many different metals and operating conditions. Therefore, a mathematical model can be used to predict the composition of hardfacing electrodes. But the resulting accuracies may not always be satisfactory. One alternative to the mathematical model is the experiment-based approach, such as ANNs. They are recently developed techniques which are invariably used in obtaining accurate correlations which involves non-linear data. ANN can learn from examples and achieve what conventional mathematical techniques cannot. Modern neural networks can be trained to solve problems that seem impossible for conventional computers or human beings2. Neural networks attempt to achieve good performance via dense mesh of computing nodes and connections3.

2. MODELING OF HARDFACING ELECTRODE

Shielded Metal Arc Welding hardfacing electrode composition can be optimized by using ANN with the given input. The test results obtained in the experimental study of hardfacing of valve seat ring have been used to train and test the ANN. In the training stage, the ANN was presented with pairs of several input and corresponding desired output data4. The network was trained till the error between the actual and computed was minimized for all pattern pairs. In the testing stage, a new input pattern was presented and the output of the ANN was computed, which when compared with the actual or target value, should provide an exact replica with minimum prediction error5.

2.1 Input-Output Mapping

One need not have any idea of the functional relationship that exists between input and output. The only requirement to create and train an ANN is the knowledge of known sets of inputs and corresponding outputs. Other than optimization, their applications include

classification, prediction, pattern recognition & identification, assessment, forecasting, and monitoring & control. The major advantage of ANN over statistical models lies in its ability to model a multivariate problem without making complex dependency assumptions among input and output variables6,7.

2.2 Feed Forward Back Propagation Network

Several ANN topologies have been developed for different applications, the most popular being the Feed Forward Back Propagation Network. It is a gradient descent error-correcting algorithm, which updates the weights in such a way that network output error is minimized. The back propagation algorithm performs two phases of data flow. First, the input pattern is propagated from the input layer to the output layer and, as a result of this forward flow of data, it produces an output. Then the error signals resulting from the difference between the computed and the actual are back propagated from the output layer to the previous layers for them to update their weights8. The process is then repeated as many cycles as needed until the error is within a prescribed tolerance.

3. STAGES IN ANN

The operation of ANN consists of four stages namely:

- Data Presentation – The input parameters used to train the ANN.
- Data Normalization - The input and output data are normalized between their minimum and maximum values to obtain values within the range from 0 to1.
- Training – In the training stage the ANN is
- presented with pairs of several input and corresponding desired output data. The network is trained till the error between the actual and computed is minimized for all pattern pairs.
- Testing – In the testing stage, a new input pattern is presented and the output of the ANN is computed, which when compared with the actual or target output, should provide an exact replica with minimum forecast error.

3.1 Data Presentation

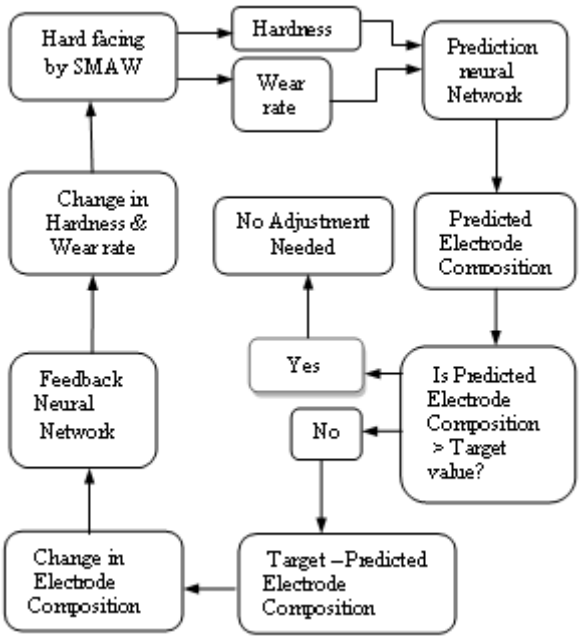

Fig. 1 Flow chart of ANN for electrode composition optimization

The flow chart and the proposed network used for optimization of electrode composition are given in Fig. 1. The main objective of this model is to maximize the hardness and minimize the wear rate on the valve seat ring by optimizing the elements of hardfacing electrode. The following elements of the hardfacing electrode to be developed are considered as input parameters and hardness and wear rate are considered to be the output parameters:

- Carbon
- Chromium
- Copper
- Manganese
- Nickel
- Sulphur
- Silicon
- Molybdenum
- Phosphorous

3.2 Data Normalization

The input and output data patterns were normalized between the values of zero and unity, using the following relationship so as to avoid the clustering of the training data in the boundary of the activation/transfer function.

$$Z_{norm} = 0.1 + \frac{Z - Z_{min}}{1.25\,(Z_{max} - Z_{min})} \qquad [1]$$

where

Z_{norm} = Normalized data (range between 0 to 1)
Z_{min} = Minimum value of the data range
Z_{max} = Maximum value of the data range and
Z = Data value to be normalized.

3.3 Training

For ANNs, two data sets are needed: one for training the network and the second for testing the same network. The usual approach is to prepare a single data-set, and differentiate it by a random selection. An important stage when accommodating a neural network is the training step, in which an input is introduced to the network together with the desired outputs, the weight and bias values are initially chosen randomly and the weights are adjusted, so that the network attempts to produce the desired output. The goal of any training algorithm is to minimize the global error level, such as the Mean Percentage Error (MPE), Root-Mean-Square Error (RMSE), and absolute fraction of variance or coefficient of efficiency (R2). The computer code solving the back-propagation algorithm and to train and test ANN was implemented under the MATLAB environment. The following network parameters were adopted for the purpose of training the network:

Network Algorithm	: Resilient Back Propagation Algorithm (RP)
Transfer Function	: Log Sigmoid
Maximum Epochs	: 15,000
Error Goal	: 0.00001 (Mean Square Error)
Time	: Maximum time to train in seconds (unlimited time)
Leaning Rate	: 3
Increment to weight change	: 1.2
Decrement to weight change	: 0.5
Initial weight change	: 0.07
Maximum weight change	: 50.0
Number of hidden layers	: 1 and 2

3.4 Log Sigmoid Transfer Function

The sigmoid transfer function shown below takes the input, which may have any value between plus and minus infinity, and squashes the output into range 0 to1. This transfer function is commonly used in Back propagation networks, in part because it is differentiable.

3.5 Testing

For the purpose of testing the model performance, randomly selected data from the total database were presented to the network. The following model performance estimators were computed to test the prediction capability of the ANN model.

1. Mean Percentage Error (MPE) $= \frac{\sum \left(\frac{X_i - F_i}{X_i}\right) \times 100}{n}$ [2]

2. Mean Absolute Percentage Error (MAPE)
$= \frac{\sum \mathrm{mod}\left(\frac{X_i - F_i}{X_i}\right)}{n} \times 100$ [3]

3. Mean Error (ME) $= \frac{\sum (X_i - F_i) \times 100}{n}$ [4]

4. Mean Absolute Error $= \left[\frac{\sum \mathrm{mod}\,(X_i - F_i)}{n}\right]$ [5]

5. Root Mean Square Error (RMSE)
$= \left[\frac{\sum (X_i - F_i)^2 \times 100}{n}\right]^{1/2}$ [6]

6. Coefficient of Correlation (R)
$= \left[\frac{\sum (X_m - X_i) \times (F_m - F_i)}{\sum (X_m - X_i)^2 \times (F_m - F_i)^2}\right]^{1/2}$ [7]

7. Coefficient of Efficiency (R^2)

where, X_i and F_i are observed and computed values of the variables and X_m and F_m are the mean of the observed and computed values of the variables.

4. RESULTS AND DISCUSSIONS

The network was initially trained with input and output patterns with different number of neurons in the first hidden layer and the above model performances were estimated. It has been found that, even though the correlation coefficient (R) and the coefficient of efficiency (R2) were good to accept the model. The initial results obtained both for training and testing with single hidden layer and goal of 0.001 were not up to the accepted level. Some of the other estimator's values were out of the acceptable limit for few output values due to the noisiness in the data. Hence the error detection technique was adopted for better prediction of the model and the errors of the model were reduced considerably.

In order to establish the relationship between the input and output variables with neural network, finite discrete samples of experimental data were used to train the network. During the training process, various

configurations were analyzed and some of them with 9-50-2, 9-20-2, 9-15-2, 9-10-2, 9-5-2 etc., were presented. The training error and the goal achieved for various networks trained are given in Table 1.

Table 1 Training Error of the Various Neural Networks

Configuration	No. of Iterations	Training Error	Goal
9-50-2	6254	0.0014125	0.001
9-20-2	11475	0.0011654	0.001
9-15-2	14879	0.0013850	0.001
9-10-2	19654	0.0012765	0.001
9-5-2	22546	0.001000	0.001

After many trials, the result indicates the training error and goal achieved is the same value of 0.001 for the network 9-5-2. The network 9-5-2 i.e, 9 input parameters, 5 neurons in the hidden layer and 2 output parameters gives the maximum value of R^2 which is clearly shown in Table 2.

The R^2 values for various elements range from 0.8 to 0.99 for the network 9-5-2. The best network is the network with the faster convergence speed. Interestingly the training error of the model was reduced considerably for this network which as depicted in Table 1. One should not forget that too small neurons in the hidden layers may lead to under training and too many neurons may lead to over training of the network9,10.

Table 2 R^2 Values of Single Hidden Layer Neural Networks

Elements/ Network	*C*	*Mn*	*Mo*	*Ni*	*Si*	*Cr*	*S*	*P*	*Cu*
9-50-2	0.2075	0.1928	0.3239	0.5804	0.4262	0.4599	0.6329	0.5841	0.4897
9-20-2	0.6393	0.6531	0.6419	0.7294	0.7447	0.8065	0.7637	0.8080	0.8150
9-15-2	0.7298	0.6049	0.6938	0.9143	0.7189	0.6212	0.7899	0.6599	0.8082
9-10-2	0.7712	0.6598	0.8103	0.7339	0.8083	0.7392	0.8219	0.8089	0.8738
9-5-2	0.9970	0.9970	0.9598	0.8186	0.8222	0.9621	0.9986	0.8945	0.9992

Table 3 Optimized Chemical Composition of the Formulated Electrode

Elements	C	Cr	Mn	Cu	Mo	Ni	P	Si	S	Fe
Chemical Composition	0.13	17.73	0.82	0.05	0.16	0.27	0.028	0.22	0.02	Rest

Thus the network 9-5-2 provides satisfactory prediction of composition of electrode. The actual and predicted values of few elements composition obtained for test data by simulation of the network 9-5-2 are shown in Figures 2 to 7. Most of the predicted values fall with in ±5% deviation from the observed values. The optimization was carried out using MATLAB as a tool in order to map the weight % relationship between the nine elements (C, Cr, Cu, Mg, Mo, Ni, P, S and Si) mainly to achieve higher hardness and lower wear rate. The optimized chemical composition of the formulated electrode obtained is given in Table 3. A significant result has been achieved and hence it was found that neural networks are excellent tools for solving complex problems that are not well understood in terms of the relationships between the different variables.

5. VALIDATION OF THE MODEL

5.1 Chi-square (÷²) Test

A test of goodness of fit establishes whether or not an observed frequency distribution differs from a theoretical distribution. The goodness of fit for the given data set was confirmed with the help of Chi-square test by using 26 data sets as follows:

The level of significance, á = 0.05
No. of Sample data taken, n = 26
Degrees of Freedom, n-1 = 25
Chi-Square table value = 37.652

The Chi-square statistics is calculated by finding the difference between each observed and theoretical frequency for each possible outcome, squaring them, dividing each by the theoretical frequency, and taking the sum of the results as given:

$$\div^2 = \frac{(O_1-E_1)^2}{E_1} + \frac{(O_2-E_2)^2}{E_2} + \frac{(O_3-E_3)^2}{E_3} + \frac{(O_n-E_n)^2}{E_n} \quad [7]$$

where O1, O2, ….On = Observed data and
$E_1, E_2, \ldots E_n$ = Predicted data

Using the Equation [7], $\div^2$ value calculated from the 26 data set is equal to 36.933. Since the calculated value is less than the table value the goodness of fit of data is confirmed.

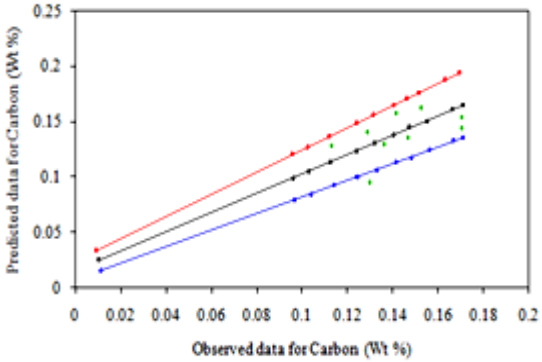

Fig. 2 Prediction network test data - Observed data Vs Predicted data for Carbon

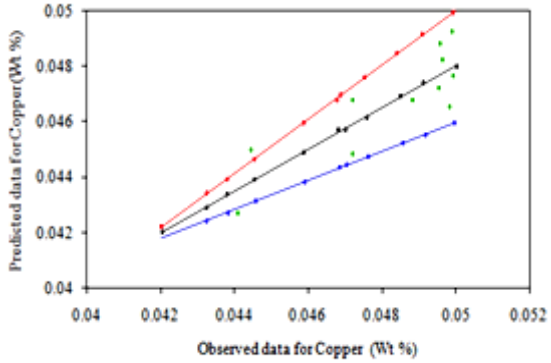

Fig. 3 Prediction network test data - Observed data Vs Predicted data for Copper

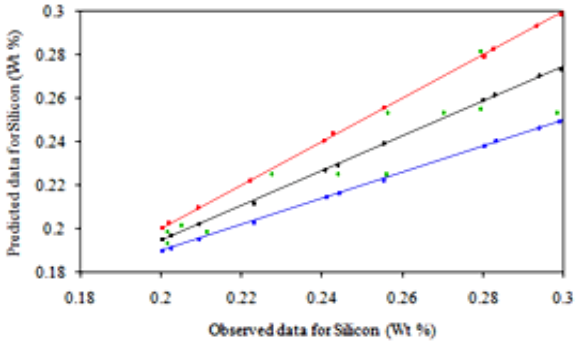

Fig. 4 Prediction network test data - Observed data Vs Predicted data for Silicon

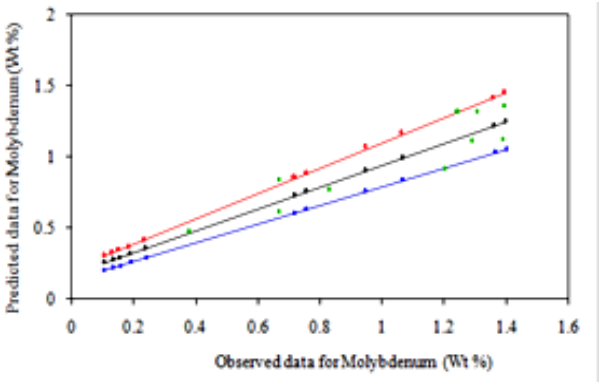

Fig. 5 Prediction network test data - Observed data Vs Predicted data for Molybdenum

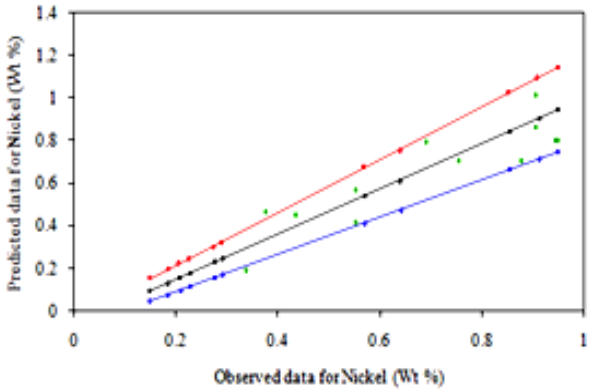

Fig. 6 Prediction network test data - Observed data Vs Predicted data for Nickel

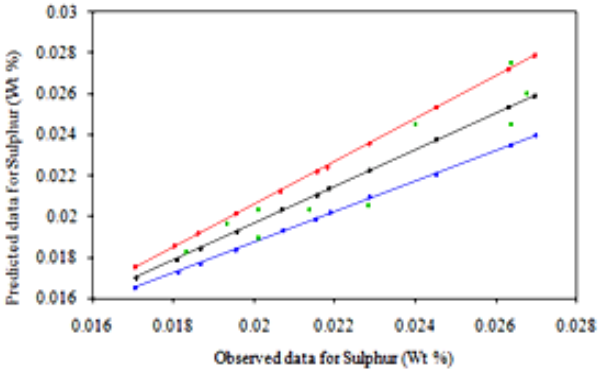

Fig. 7 Prediction network test data - Observed data Vs Predicted data for Sulphur

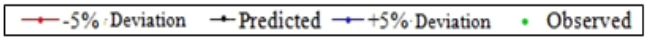

5.2 t – Test

The t-distribution can be used to compare the mean of a sampled population to some fixed, known value. This statistical test of hypothesis is referred to as a "one-sample t-test."

This statistic can evaluate whether or not there are significant differences in the means of two independently sampled populations. In addition to the assumption of independence, it is assumed that within each population the variable of interest is normally distributed with equal variances.

The level of significance (á)	= 0.05
Calculated t value	= tc
No. of sample data taken for test (n)	= 19
Degrees of Freedom (n-1)	= 18
Corresponding t-table value (tt)	= 2.10

The following equations were used to calculate the tc value:

$\bar{x}$ = Sample mean = $\frac{x_1+x_2+\cdots+x_n}{n}$ [9]

μ = Population mean [10]

$s = \sqrt{\frac{\sum(x-\bar{x})^2}{n-1}}$ [11]

$tc = \frac{(\bar{x}-\mu)}{s/\sqrt{n}}$ [12]

From Equation [12], tc was calculated and observed that all the tc values were less than the t-table value tt. For example, tc value for chromium is 0.601787 and t-table value tt for chromium is 2.10. Since the calculated value tc is less than the t-table value tt, it is confirmed that the mean value for chromium have very minimum deviation. In the similar way the mean values for all the other elements have checked to have minimum deviation.

6. CONCLUSIONS

- The network 9-5-2 provides satisfactory prediction of composition of hardfacing electrode.
- Coefficient of efficiency (R2) of the test data for all nine parameters is above 0.8 to 0.999.
- The predicted values of composition of hardfacing electrode obtained for test data by the simulation of the network 9-5-2 are with in ±5% deviation from the observed values of the parameters.
- The results were validated by statistical methods (Chi-Square and t- Test) and found that they were within the permissible limit of ± 5%.
- The network results obtained have shown that the ANN model can be used for optimizing the composition of Shielded Metal Arc Welding hardfacing electrode with reasonable accuracy.
- Consequently, with the use of ANNs, composition of any hardfacing electrode can be determined by performing only a limited number of tests instead of a detailed experimental study, thus saving both engineering effort and funds.

REFERENCES

[1] T. Kohonen, "An Introduction to Neural Computing", Neural Networks, Vol.1, 1988, pp.4-8,

[2] D.D. Massie, "Neural-network Fundamentals for Scientists and Engineers", ECOS'01, 4-6 July 2001, Istanbul, Turkey, pp.123.

[3] G.A. Carpenter and S.Grosspery, "A Massively Parallel Architecture for a Self- Organizing Neural Pattern Recognition Machine", Computer Vision, Graphics and Image Processing, Vol. 37, 1983, pp. 54-110.

[4] Kristin Andersen, G.E. Cook, G. Karsai and Kumar Ramaswamy, "Artificial Neural Networks Applied to Arc Welding Process Modeling and Control", IEEE Transactions on Industry Application, Vol.26, No.5, 1990, pp.824-830.

[5] R.P.Lippmann, "An Introduction to Computing with Neural Nets", IEEE ASSP Mag., April 1987, pp.4-22.

[6] D.T. Pham, and X.Liu, "Neural Networks for Identification, Prediction and Control", London: Springer Verlag, 1995.

[7] D.W. Coit and A.E. Smith, "Using Designed Experiments to Produce Robust Neural Network Models of Manufacturing Processes", Proceedings of 4th Industrial Engineering Research Conference, 1995, pp. 229-238.

[8] G. Baskar, "Strategic Appraisal of Human Resource Functions of State Transport Undertakings for Profitability using Artificial Neural Network", Ph.D., Thesis, 2004.

[9] Saikishan Suryanarayanan, Vijay Manikandan Janikiraman, Jayanath sekar, Lakshmi and Narayana Rao, "Prediction of Cetane Number of a Biodiesel Based on Physical Properties and Study of their Influence on Cetane Number", SAE 2007, 2007-01-0077, pp.1-6.

[10] Mustafa Canakci, Ahmet Erdil, Erol Arcaklioglu, "Performance and Exhaust Emissions of a Biodiesel Engine", Applied Energy 2006, Vol.83, pp.594-605.

A Grand Unification of Six Sigma, Quality Function Deployment and TRIZ

M. Shanmugaraja[1], M. Nataraj[2] and N. Gunasekaran[3]
[1&2]Department of Mechanical Engineering, Government College of Technology, Coimbatore - 641 013, Tamil Nadu
[3]Angel College of Engineering and Technology, Tirupur - 641 665, Tamil Nadu
Email: raja8011@yahoo.co.in, m_natanuragct.yahoo.com, guna_kct_cbe_tn_in.yahoo.com
(R)

Abstract

Today organisations have a sound pursuit and passionate to understand the ins and outs of performance excellence for creating and delivering products or service in an increasingly better, faster and on cheaper basis. Performance excellence is holistic phenomenon that can be achieved through an integrated framework of strategy, improvement and innovation. This paper proposes a performance excellence framework which progresses in a lockstep, as the output of one piece become the inputs for the next, driven by change oriented strategic and organisational improvement. A grand unification of methodologies like Six Sigma, Quality Function Deployment and TRIZ is used in this framework to optimize the interplay of strategy, improvement and innovation. The proposed conceptual model serves as a gate-way to amplify a high value concept of business to offer maximum outcome within the minimal constraints of the business.

Keywords: *Improvement, Innovation, Organization, Performance excellence, QFD, Strategy, Six Sigma, TRIZ.*

1. INTRODUCTION

A study on influences of business over the last 50 years and longer revealed a list of names like Shewart, Ford, Deming, Drucker, Ono, Gates, Hamel, Womack, Harry, Welch, Walton and many others [1]. Each one holds a key to some important aspect of business performance improvement-some aspect of how an organization creates and delivers value on an increasingly better, faster, and cheaper basis. And some hold the keys to how a business innovate itself periodically to bring on new and different value propositions, which are then relentlessly improved until the cycle needs to repeat itself again [2]. But today's global scenario routed the business improvement through performance excellence which needs holistic thinking and holistic action. It is known that to achieve performance excellence, very best companies have an integrated framework within which they entwine the activities of strategy, improvement, and innovation on an ongoing basis [3]. In other words, if the goal of an organization is to do what it does better, faster, and cheaper, they can achieve that goal by optimizing the interplay of strategy, improvement, and innovation [4]. This is where we look at combining the elements of performance excellence into a holistic model by integrating all parts as tightly and consistently as possible.

This article proposes a Performance Excellence Model (PEM) that progresses in a lockstep, as the outputs of one piece become the inputs for the next piece. This model is underpinned with performance improvement methods like Six Sigma, Quality Function Deployment and TRIZ.

2. UNDERPINNING OF PEM MODEL

PEM is developed by adopting the grand unification approach to enable organizations to plan and execute it in a synergistic fashion. The elements of PEM build progressively, balanced, coordinated, and integrated with effective change leadership based on strategic priorities. PEM is conceptualized in such way that among the domains of performance excellence, strategy and innovation have a lot to learn from the domain of improvement, particularly when it comes to making strategy and innovation more methodological, deployable, measurable, predictable, and controllable. The groundwork closely follows classical Axiomatic Design (Figure 1) but with a change.

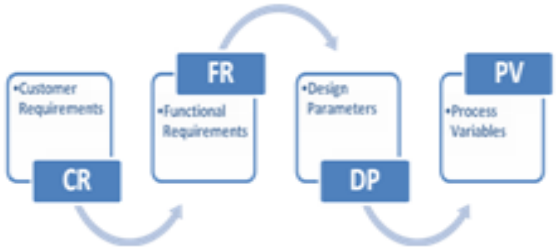

Fig. 1 Classic axiomatic design domains

The classical axiomatic design model doesn't really address the strategic components of performance excellence, because it's deliberately focused on operations [5]. An additional domain "societal need" (SN) is added to the existing axiomatic design domains to develop PEM approach as shown in Figure 2. The reason is that societal need is the absolute root of business, as all corporations exist to meet the one penultimate objective of fulfilling human needs. Hence the PEM approach doesn't make "watches"; it enables people to know the "time".

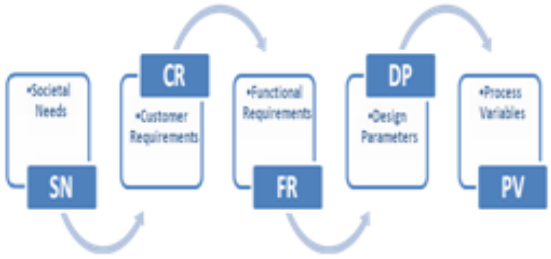

Fig. 2 Performance excellence model

As shown in Figure 3, TRIZ approach is designed to filter the societal requirements (SN) from which Customer Requirements (CR) are identified using Quality Function Deployment (QFD). On the customer requirement end, Six Sigma covers the gamut of all other domains. Function Modelling from TRIZ can also employ in defining functional requirements [6]. So each of these domains enables the next in progressive fashion, and this gives glimpse into a more sequential approach to the networked reality of performance excellence variables.

SN	CR	FR	DP	PV
		Six Sigma	Six Sigma	Six Sigma
	QFD	QFD		
TRIZ		TRIZ	TRIZ	TRIZ

Fig. 3 Applications of Six Sigma, QFD and TRIZ to the various domains of PEM

3. PEM EXCELLENCES

Performance Excellence Model development (Figure 4) starts with strategic thinking through TRIZ and entails envisioning the fuzzy edge of latent societal and customer needs. With a balanced picture of how the organization can preserve its current position, while also evolving into something different, it can derive great value from strategic planning methods with QFD, which connect strategy and execution as inseparable parts of a seamless whole. Key outcomes of strategic thinking and strategic planning are focused vision, meaningful missions, prioritized goals, aligned objectives, rational metrics, optimized tactics and systematic review cycles.

In the language of PEM, these elements serve to preserve a company's position and success, because they enable an organization to optimize its current offerings, capabilities, technologies and processes. Key outcomes of Six Sigma are operational stability, measurement integrity, reduced waste, minimized inventory, reduced variation, higher margins, increased capacity, reduced cycle time, lower costs, and other benefits, not the least of which is a culture of people relentlessly committed to improvement.

Fig.4 Performance excellence model

4. PEM CONSTITUENTS

Practically, all of business is the drive to accomplish the mission of the organization better, faster, and cheaper. To make products better, faster, and cheaper. And to operate processes better, faster, and cheaper. From a colloquial perspective, that's what all the various management tools do: They play some role in improving quality (better), redesigning processes (better still), spawning reinvention and growth (a lot better), minimizing waste and inventory (faster), reconfiguring operations (faster again), and, of course, cutting costs (cheaper) as a by-product of all this and a direct result of such targeted initiatives as corporate reorganizations, mergers, and technology implementations. In the PEM funnel (Figure5), the business mission is realized by mixing the strategic initiatives Six Sigma, QFD and TRIZ in an appropriate proportion to assure better quality product or process at cheaper in a fastest time frame.

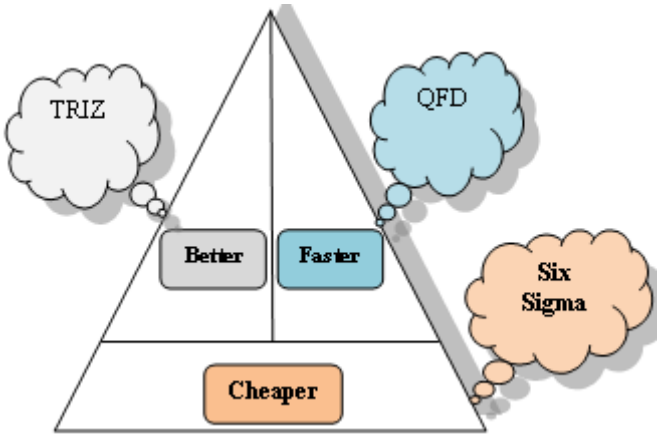

Fig.5 PEM constituents

4.1 Six Sigma

4.1.1 Definition

From a statistical perspective, Six Sigma is a metric of process measurement symbolized by the Greek letter ó that represents the amount of variation with a normal data distribution [7]. Fundamentally, Six Sigma quality level relates to 3.4 defects per million opportunities (DPMO).

4.1.2 Methodology

There are two major improvement methodologies in Six Sigma [8]. The first methodology, DMAIC, is used to improve already existing processes and can be divided into five phases; define measure, analyze, improve and control. Several studies have shown successful cases of DMAIC application in a variety of contexts such as healthcare, thermal power plants, retailing, financial services and manufacturing process [9], [10]. In contrast, the second methodology, design for Six Sigma (DFSS), is used for new processes or when the existing processes are unable to achieve business objectives such as customer satisfaction [11].

4.1.3 Benefits

Six Sigma benefits are related to various areas such as reduction in process variability, reduction in in-process defect levels, reduction in maintenance inspection time, improving capacity cycle time, improving inventory on-time delivery, increasing savings in capital expenditures, increase in profitability, reduction of operational costs, reduction in the cost of poor quality (COPQ), increase in productivity, reduction of cycle time, reduction of customer complaints, improved sales and reduced inspection [10]. Six Sigma benefits for service organizations may involve improved accuracy of resources allocation, improving accuracy of reporting, reduced documentary defects, improving timely and accurate claims reimbursement, streamlining the process of service delivery, reduced inventory of equipment, reduced service preparation times, improved customer satisfaction, reduced defect rate in service processes, reduced variability of key service processes, transformation of organizational culture from fire-fighting mode to fire-prevention mode with the attitude of continuous improvement of service process performance, reduced process cycle time and hence achieve faster service delivery, reduced service operational costs, increased market share, leading to greater job satisfaction for employees, improved consistency level of service through systematic reduction of process variability and effective management decisions due to reliance on data and facts rather than assumptions and gut-feelings [12], [13].

4.1.4 Tools and Techniques

Six Sigma tool has a specific role and is often narrow in focus, where as Six Sigma technique has a wider application and requires specific skills, creativity and training [14]. Examples of Six Sigma tools include Pareto analysis, root cause analysis, process mapping or process

flow chart, Gantt chart, affinity diagrams, run charts, histograms, quality function deployment (QFD), Kano model, brainstorming, etc. Moreover, Six Sigma technique utilizes various other tools; for example, statistical process control (SPC) [11].

4.2 Quality Function Deployment (QFD)

QFD is a powerful tool that addresses strategic and operational decisions in businesses [15]. It provides a means of translating customer requirements into appropriate technical requirements for each stage of product development and production. A typical approach to QFD is the four-phase process by the American Supplier Institute (ASI) in the USA, which is admired, and widespread [2]. Four phases to be considered can be briefly described as below.

Phase I: Qualitative customer requirements are translated into design-independent, measurable, and quality characteristics of the product.

Phase II: Examination of the relationship between the quality characteristics and the various components or parts of the design. The result of phase II is a prioritization of the component parts of the design in terms of their ability to meet the desired quality characteristic performance level.

Phase III: Prioritization of manufacturing processes and specifications for key process parameters that are deployed to the fourth and final phase.

Phase IV: The key manufacturing processes and associated parameters are translated into work instructions, control and reaction plans, and training requirements necessary to ensure that the quality of key parts and processes is maintained.

4.3 TRIZ

Theory of Inventive Problem Solving (TRIZ) is a problem-solving, analysis and forecasting tool derived from the study of patterns of invention in the global patent literature [1].

To develop inventive solutions to problems, TRIZ methodology utilizes the following thinking tools [1];

i. Inventive principles for business and management problems
ii. Separation principles for resolving organizational contradictions and conflicts
iii. Substance-field analysis for visualizing highly complex systems
iv. Anticipatory failure recognition for prediction and evaluation of risks
v. Utilizing system resources for effective cost- saving decisions
vi. Pattern of evaluation of technical systems to support systematic and multidimensional thinking
vii. Innovation Situation Questionnaire for problem identification and CTQ identification
viii. Contradiction matrix to resolve physical and technical conflicts
ix. Standard solutions to inventive problems
x. ARIZ algorithm to eliminate contradictions which causes the problem

Besides the above said tools, TRIZ also employs certain more tools like Level of Innovation, Laws of System Evolution, Ideal Final Result, Ideality degree, Functional analysis, Mind Mapping, Physical, Chemical and geographical effect to develop or produce innovative products with high quality and profit with an Anticipatory future failure protection to increase market share of the organization.

5. IMPLEMENTING PEM

Maybe organizations should be training PEM champions and practitioners in addition to training black belts, Kaizen event facilitators, TRIZ experts, risk managers, and so on. Yes, as known, the initial resistance is, “Oh no, not more people to train!” But the reality is that corporate skill sets have to-must-keep up with an evolving world. And in this evolving world, the force of leadership will have to make tangible steps toward performance excellence integration. Therefore, it’s wise for an organization to implement the parts of PEM that it can, with the vision of the whole in mind.

6. PRACTICALLY SPEAKING

The adoption of a Performance Excellence Model (PEM) can be quite daunting, as it involves the entire organization. The organization typically must assess all of its current initiatives, and it engages in prioritization

sessions to decommission activities that do not support the strategic plan-or activities that could interfere with the PEM deployment. Of course the input to these sessions is the strategic plan. If this body or work is missing or incomplete, it must be produced, and it must contain a vision, a service mission, an economic mission, strategies, goals and objectives, a scorecard, and an operational review cycle. The inherent consequences of variation teach us that implementing a PEM model is better than implementing each contained initiative by itself in a sequenced manner. Once again, there is nothing wrong with bringing the pieces of a PEM model together over time in a sequential, coordinated way-especially if each is introduced as part of a bigger picture from the outset. Simply put, taking a PEM approach is more efficient and effective and, if done right, will yield a more impressive ROI over a certain defined midterm time frame, such as five years. The net return is more sizeable in all the important areas of corporate performance, not just certain ones. The idea of an organization creates an event in the marketplace some might call "blazing growth" when all the performance indicators are buzzing. At its essence, this growth is a function of bringing new forms and solutions to customers, who buy them and keep buying them because the competition can keep up on only one of the two critical fronts of business success-preservation or evolution-but not both. In other words, no company grows and sustains its growth if it is good at only innovation or improvement.

7. CONCLUSION

If all the gears and wheels of performance success are defined into an overarching model, an organization will know better how to sequence and direct its portfolio of interventions over time. As one initiative gains momentum and makes an impact, others are planned, because the effect of one program will dwindle as it bumps up against challenges it's not equipped to handle. Of course running a successful enterprise is a much larger task than any one program or initiative can handle. There has been enormous movement toward holism and consolidation in managerial know-how over the past 100 years, and this will continue by sheer force of evolution. It seems inevitable that the domains of strategy, improvement, and innovation will come together even more over time as their methods connect and blend. And in the context of Performance Excellence Model, the core force of your vision, missions, and goals determines the impact of the many methods you implement to achieve them. TRIZ can fuel the development of robust strategic thinking. Then QFD determines adequate strategic plan to accomplish customer needs. The rest of performance excellence is taken care by Six Sigma in some rational configuration, magnify that intent into reality.

REFERENCES

[1] D. Silverstein, N.DeCarlo and M. Slocum, "Insourcing Innovation How to Achieve Competitive Excellence Using TRIZ", Auerbach Publications, Tylor & Francis Group, New York London 2008.

[2] M.S. Slocum and E. Domb, "The Integration of Comprehensive QFD, TRIZ, and Six Sigma in An Axiomatically Driven Total Product/Process Development System", Proceedings of TRIZCON2004, 6th Annual Altshuller Institute for TRIZ Studies International Conference, Seattle, WA, USA 2004.

[3] M.S. Slocum, "Total Product/Process Development System Where Six Sigma Meets TRIZ and QFD", Proceeding of ETRIA World Conference: TRIZ Future 2003, Aachen, Germany 2003.

[4] Gavetti, Giovanni and J. Rivkin, "How Strategists Really Think: Tapping the Power of Analogy," Harvard Business Review, April 2005, pp.54.

[5] X. Zhao, "Integrated TRIZ and Six Sigma Theories for Service/Process Innovation", Proceedings of ICSSSM '05, 2005 International Conference on Services Systems and Services Management, Vol. 1, No.13-15, 2005, pp.529-532.

[6] J. Hipple, "The Integration of TRIZ with Other Ideation Tools and Processes as Well as With Psychological Assessment Tools", Creativity and Innovation Management, Vol.14, No.1, 2005, pp.22-33.

[7] E.A. Averboukh, "Six Sigma Trends: Six Sigma in Financial Services", TRIZ Journal, April 2006.

[8] R. Schroeder, K. Linderman, C. Liedtke and A. Choo, "Six Sigma Definition and Underlying Theory", Journal of Operations Management, Vol. 26, No.4, 2008, pp.536-54.

[9] U. D. Kumar, D. Nowicki, J. E. Ramirez-Marquez, and D. Verma, "On the Optimal Selection of Process Alternatives in a Six Sigma

Implementation", International Journal of Production Economics, Vol.11, No.1, 2008, pp.456-467.

[10] G. S. Roger, K. Linderman, C. Liedtke and A.S. Choo, "Six Sigma: Definition and Underlying Theory", Journal of Operations Management, Vol. 26, 2008, pp.536-554.

[11] P.Nonthaleerak and L.Hendry, "Six Sigma: Literature Review and Key Future Research Areas", International Journal of Six Sigma and Competitive Advantage, Vol.2, No.2, 2006, pp.105-61.

[12] A. Chakrabarty and K. Tan, "The Current State of Six Sigma Application in Services", Managing Service Quality, Vol.17, No.2, 2007, pp.194-208.

[13] L.R. Smith, "Six Sigma and the Evolution of Quality in Product Development", Six Sigma Forum Magazine, Vol.1, No.1, 2001, pp.28-35.

[14] J. Antony, "Can Six Sigma be Effectively Implemented in SMEs?", International Journal of Productivity and Performance Management, Vol. 57, No.5, 2008, pp. 420-423.

[15] G. Mazur, "QFD 2000: Integrating Supporting Methodologies into Quality Function Deployment", Proceedings of the 12th Symposium on Quality Function Deployment, Novi, MI, USA: QFD Institute, 2000.

Triangular Matching Based Fingerprint Authentication with Hamming Distance

S. Valarmathy
Department of Electronics and Communcation Engineering, Bannari Amman Institute of Technology,
Sathyamangalam - 638 401, Erode District, Tamil Nadu
E-mail: atrmathy@rediffmail.com
(R)

Abstract

A fingerprint matching system based on triangular matching and hamming distance is proposed which offers improved results especially for very low quality and deformed fingerprints images. An inquiry fingerprint image must validate the identity of the human by means of test image acquired in real time by minutiae matching. The verification system consists of feature extraction and verification blocks. The feature extraction block is used to extract the real minutiae from reference images and the verification block performs the matching online. The features are extracted from the inquiry images with suitable filtering and minutiae extraction procedures. Triangular Matching is employed to overcome the relative non-linear deformation present in the fingerprint image pairs. The deformation angle chosen in this paper is between 0^o-16^o to the verification system. The hamming distance metric is used for the matching validation for which 0.15 is set as the threshold value. If the distance value is less than or equal to 0.15, then the reference image and test image is perfectly matched. If the distance value is slightly greater than 0.15 with a maximum tolerance level of 16% even then the reference image and test image is matched. But if the given test image is not a part of the database, and then the matching action is denied.

Keywords: *Fingerprint, Hamming distance, Minutiae,Triangular matching,Verification.*

1. INTRODUCTION

A fingerprint is the pattern of ridges and valleys on the surface of the human finger. The uniqueness of a fingerprint can be determined by the pattern of ridges and furrows as well as the minutiae points. Minutiae points are local ridge characteristics that occur at either a ridge bifurcation or a ridge ending. Even identical twins are said to have different fingerprints.

Most classical fingerprint recognition algorithms take the minutiae and the singular points, including their coordinates and direction, as the distinctive features to represent the fingerprint in the matching process. There are two major methods of fingerprint matching: Minutiae matching and global pattern matching. The first approach analyses ridge bifurcations and endings. The second method represents a more macroscopic approach which considers the flow of ridges in terms of arches, loops and whorls. As the equal-error-rate is low, then fingerprint recognition is very accurate. The strength of fingerprint identification is that it can be deployed in a varied range of environments. It is a proven core technology among all the biometrics and, the ability of enrolling multiple fingers can increase the system accuracy and the flexibility dramatically.

The major points addressed in automatic verification systems are: fingerprint acquisition, verification, identification, and classification. The fingerprint images are acquired by a commercial scanner with a 150 dpi resolution in useful format. Fingerprint identity verification requires some knowledge of the individual to be identified. The system is asked to accept or reject the hypothesis of matching between a stored fingerprint image and the test image. Consequently, the system must match the person's characteristics directly against those stored as reference information.

The system presented in this paper verifies the identity, rather than recognizing the person and is based on minutiae matching.

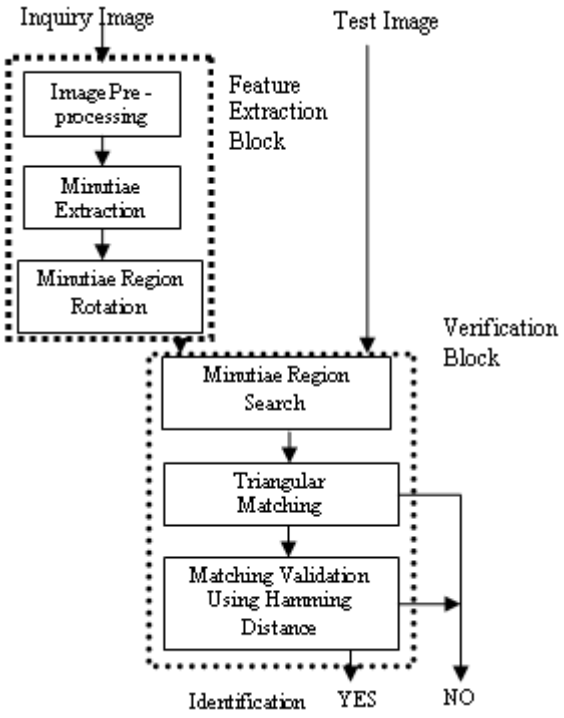

Fig.1 Block diagram of the proposed system.

2. IDENTIFICATION SYSTEM

Figure 1 shows the block diagram of the proposed system. The system compares two fingerprint images: an inquiry image and a test image. It is assumed that a inquiry image is available for the person to be identified and that it may be processed offline. The test image is acquired and used in real-time. The operation sequence applied to the reference image is shown in the Feature Extraction Block and the effectual fingerprint matching carried out on each test image is shown in the Authentication Block. The reference image is carefully filtered using a nonlinear filter to reduce noise and to use the extensive gray-scale dynamics. The minutia coordinates are extracted for each detected minutiae. The test image is acquired and filtered by the same device and filter as applied to the reference image. The filtered test image is scanned by a moving window technique [10] searching for possible correspondences between the reference minutiae regions and the test image. If some correspondences are found, a triangular matching is applied and a possible fingerprint matching is defined. Finally, this uncertain matching has to be verified by hamming distance to overcome the strong local deformations.

2.1 Feature Extraction Block

The procedures of this block are applied to the reference image only. The main outcome of this process is the real minutiae set of fingerprint, minimizing the false minutiae and maximizing the true ones.

2.1.1 Image Pre processing

The image preprocessing stage includes filtering, use of extensive gray scale dynamics, binarization and thinning processes. The median filter is used to reduce the noise as much as possible to facilitate the subsequent minutiae extraction operations. In order to enhance the contrast of the fingerprint image histogram equalization is adopted. This stretches the contrast for most of the image pixels; the transformation improves the detectability of many image features.

Fingerprint image binarization is to transform the 8-bit gray scale fingerprint image to a 1-bit image with 0-value for ridges and 1-value for valleys. A locally adaptive binarization method is performed to binarize the fingerprint image. Each pixel is assigned a new value (1 or 0) according to the intensity mean in a local neighborhood (8x8 pixels), as follows

$$\mu_{mn} = \frac{1}{AB} \sum_{j=nB}^{(n+1)B-1} \sum_{i=mA}^{(m+1)A-1} G_s(i,j) \qquad (1)$$

μ_{mn} - mean of region (m x n)th sub-image of size (AxB)

$G_s(i,j)$ - original image

The pixelwise binarized image is given by

$$I_{new}(n1,n2) = \begin{cases} 1 \text{ if } I_{old}(n1,n2) \geq \mu_{mn} \\ 0 \quad \text{otherwise} \end{cases} \qquad (2)$$

Thinning algorithms reduce connected patterns to a width of a single pixel while maintaining their topology. A good thinning algorithm is also resistant to contour noise and produces a skeleton that falls approximately on the medial axis of the patterns. Modified Zhang-Suen Algorithm is used in our work. The algorithm alternates two passes, each selecting points for deletion based on different criteria.

2.1.2 Minutiae Extraction

The minutiae considered in the identification system are ridge bifurcations and ridge terminations. The aim of this procedure is to extract the real minutiae of a fingerprint image from the well-filtered, skeletonized, and binarized images. Besides classical methodologies for removing close minutiae, new approaches are used for deleting spurious minutiae by ridge repair, short ridge elimination, and island filtering.

2.1.3. Minutiae Region Rotation

Identification of minutiae in the test image is based on a comparison between regions surrounding the minutiae in the reference image and each point in the test image. A 16*16 square area is extracted around each minutia in the reference image and it is matched against an area in the test image having the same shape and size. It has to take into account three effects, even if the test image represents the same fingerprint as the reference image: it may have different contrast, it may be distorted, and it may be rotated. Image distortion is well cared by defining a suitable threshold while computing the similarity of regions using the L1 vector norm. The relative rotation of the images has to be investigated more closely in order to evaluate its effect in the similarity computation. One hundred minutiae regions were extracted randomly from different images and matched against several rotated versions of the same images, computing the difference between corresponding image pairs.

The values are normalized by dividing the computed difference by the maximum possible difference between two images, a white and a black image. As one may expect, the difference is zero for 0 and 360 degrees, while it is maximum for 180 degrees. This latter behavior is due to the smallest overlap of corresponding ridges and valleys in bifurcations and terminations.

2.2 Matching Block

The operations of this block form the real verification procedure. The test image is compared to the reference image using the information already extracted by the Feature Extraction Block (FEB). The test image is presented to the authentication block and the minutiae regions of the reference image are moved around the test image searching for possible correspondence. The possible correspondences are validated by hamming distance.

2.2.1 Minutiae Region Search

Each minutia in the reference image associates a set of rotated regions around the minutiae itself. The test image is scanned point by point and the similarity between each rotated version of the area surrounding the reference minutiae and the region around the current test image point is computed. The best similarity between each rotated version is considered and if the similarity is above the threshold, the current pixel is a possible candidate in the test image. For each reference minutiae, a small cluster of neighboring pixels results on the test image for each candidate region. The mass center of the cluster is the candidate minutiae point. This thresholding operation is very important because it is impossible to define a universal threshold for a very large number of images. If the threshold is too low too many points will become possible candidates, whereas if it is too high, some corresponding images will never associate with feature points. The ranking ensures that the correspondence will be possible in nearly all images and the number of correspondences will be controlled.

The reference image is shown as Figure 2a. A small square is drawn around the current minutiae to be matched. Figure 2c is a zoom on this region where a bifurcation point may be observed. A corresponding region should be sought in the test image. This searching procedure is based on the similarity computation between two gray-scale regions of the same size.

In particular, the region around each pixel of the test image is compared to the minutiae region of the reference image and a possible correspondence is accepted according to the similarity of the sub images.

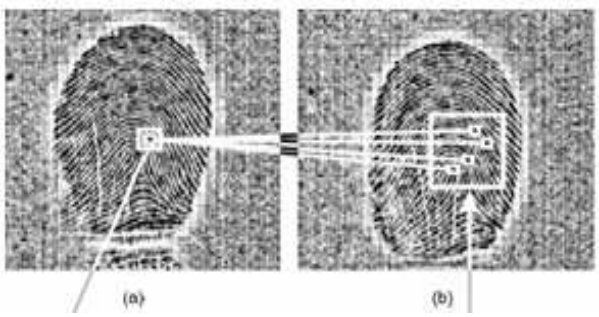

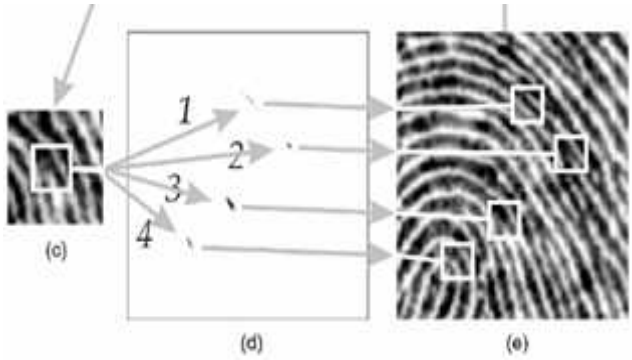

Fig. 2 Minutiae region search (a) Reference image with minutiae to search for (b) Test image candidate regions (c) Zoom on the reference minutiae (d) Similarity map drawn on test image and (e) Zoom on test image with the corresponding regions

2.2.2 Triangular Matching

In order to define an effective matching technique, a deformation model must be identified. When looking at different images containing the same fingerprint, a strong global deformation of the images can be observed. This distortion is due to static friction on a sensor surface, or paper, or rolling of the finger during ink-based registration techniques. However, small portions of the images do not take into account to exhibit manifest distortion. The idea of how to take into account small local variations, which may lead to huge global distortion, is discussed as follows.

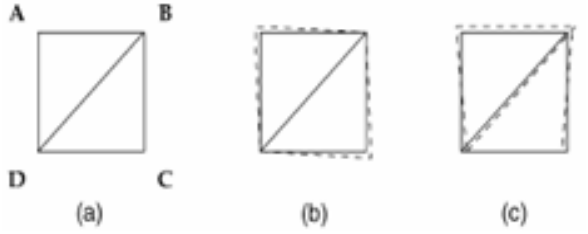

Fig. 3 Triangular matching (a) Two triangles forming a square, (b) and (c) Distortion of the triangles

Figure 3 Triangular Matching (a) Two triangles forming a square, (b) and (c) distortion of the triangles, where each edge is shortened or extended by less than 10% of its original length.

A pair of triangles forming a square is shown in Figure3, in particular in Figure3a. By shortening or extending some of the edges by less than 10% of their original length, the two images shown in Figure 3b or Figure 3c may be obtained. This small distortion makes the original form easily recognizable and may be comparable with the local distortion of a fingerprint image. In particular, the area around minutiae may be slightly distorted due to static friction caused by the fingertip touching a hard surface. By replicating the square of Figure 3 several times, it is possible to create a big image. A complete fingerprint image may be considered to consist of several small pieces, some of them representing minutiae. Figure 4 on the left shows a cross formed from the squares of Figure 3. On the right, the same cross is shown where the edges of the squares were shortened or extended by less than 10% of the original length. Such a small local distortion produces a 6% shortening of edge AB and a 45% extension of edge GH.

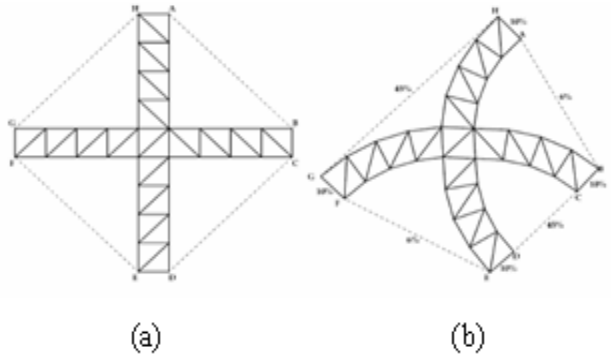

Fig. 4 Deformed Image (a) Original image (b) distorted image

Figure 4 Deformed Image (a) Original image on the left, (b) distorted image on the right with local deformation less than 10%, but consequent global deformation reaching 45%.

The reference image on the left and the test image on the right in an intermediate stage of the triangular matching is shown below.

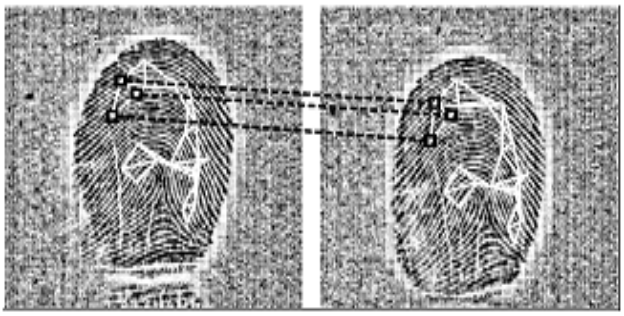

Fig. 5 Matching triangle-based graphs

The two graphs are shown in white, with the already matched minutiae at their vertices. Three matching minutiae and the connecting lines are also visible at the top of the image as dashed black lines. The upper two black squares indicate the currently extracted minutiae pair on the left image, and the corresponding pair on the right one. The third pair of black squares on the two images show the third coordinates, while this new minutiae is accepted, enlarging the already matching minutiae set. This procedure allows for matching on a local basis, where distortion is small, and can also identify two fingerprints with considerable global distortion.

Distortion can easily be measured using the two graphs, one on the reference image and the other on the test image, respectively, thanks to the already computed correspondence between single vertices and edges of the triangles that make up the graphs. A possible measure of the distortion is the average relative distortion of the corresponding edges of the triangles. When the images are distorted, translation and rotation are not uniquely defined. Translation may be defined as the movement of the mass-center of the two graphs relative to the image borders and rotation as the relative rotation of the graphs around the mass-center.

2.2.3 Matching Validation Using Hamming Distance

Let $x = (x1, x2, \ldots\ldots xn)$ $y = (y1, y2, \ldots\ldots yn)$ be bit patterns, that is, vector consisting of zeros and ones.

The Hamming distance defined as,

$$d_H(u, v) = \sum_{j=1}^{n} |x_i - y_i|$$

is equal to the number of positions where the bit patterns are different. This method requires the use of a pattern recognition scheme which can produce an ordered list of outputs ranked according to similarity to an input pattern. In our case, we use a simple nearest neighbor classification scheme and rank the outputs on the basis of Hamming distance in the case of binary images. In this post-processing algorithm, we select two parameters: k, the number of patterns from the ordered list which will participate in the shifting process (i.e., the k patterns at the top of the list), and s, the maximum path length in the shifting process. To minimize computational time, k should be chosen as small as possible, but sufficiently large so that there is a high probability that the correct image is contained in this subset of patterns. Each of the k candidate output patterns is shifted by 1 pixel in 4 possible directions: north, east, south and west. After computing a similarity measure for each of these directions, we select the direction which yields the lowest distance and move the k th pattern in that direction. This process is repeated at most s times, or until there is no improvement in the distance measure in any direction. The final distance is recorded for each of the k patterns, and the image which has the least distance after this shifting process is taken as the output of the system (the best match).

In addition, from a computational point of view, there is no need to actually shift the pixels of the image at each step. Instead, one need only to store the current corner point of the shifted image and use that as an offset index when computing the Hamming distance. Hence, the algorithm is implemented very efficiently. In fact, the computational burden of computing the optimal path consists of computing four Hamming distances at each step along with finding the minimum of those four values.

3. RESULTS

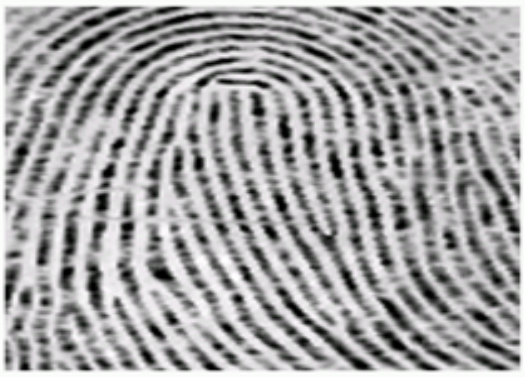

A. Original image

B. Histogram equalized image

C. Filtered image

D. Binarized image

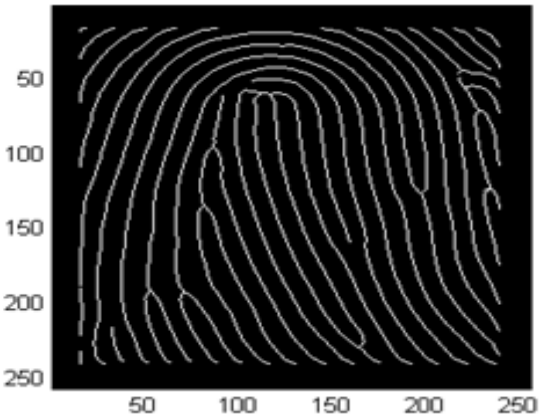

E. Thinned image

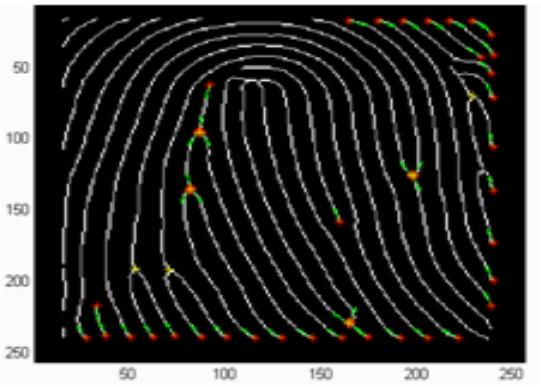

F. Minutiae extaction

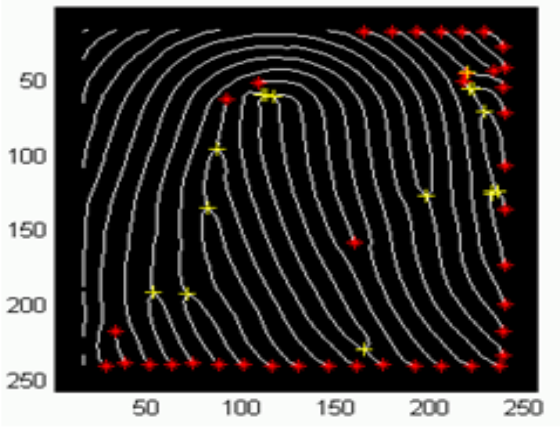

G. Removal of spurious minutiae

H. Deformed Image

In order to define an effective matching technique, a deformation model must be identified. When looking at different images containing the same fingerprint, a strong global deformation of the images can be observed. This distortion is due to static friction on a sensor surface, or paper, or rolling of the finger during ink-based registration techniques. However, small portions of the images do not take into account to exhibit manifest distortion.

Deformed image

I. Minutiae Extraction for Different Samples

For different input images, the minutiae extraction is performed as given below,

Input image 1

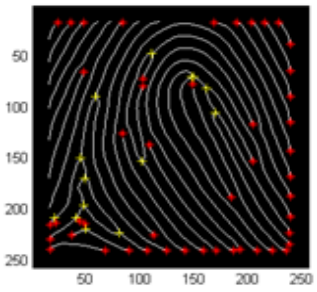

Minutiae extraction 1

Input image 2

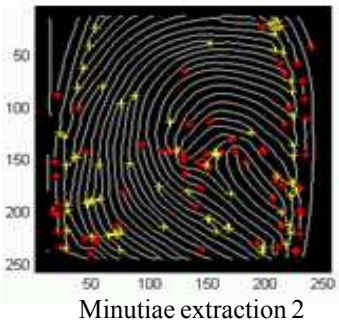

Minutiae extraction 2

Input image 3

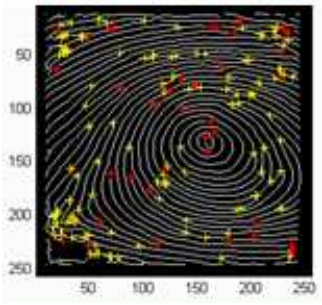

Minutiae extraction 3

Input image 4

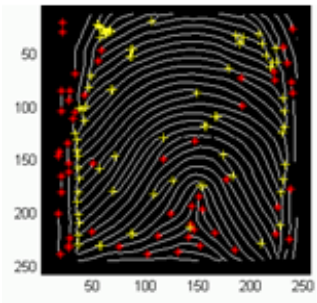

Minutiae extraction 4

J. Matching Validation

Before the validation process, the reference image is stored in the database. Here, four person's reference image taken in four different angles as a total of 16 reference images which are stored in the database. The test image is given as a deformed image. The matching validation is performed by using the hamming distance. The threshold value is set as 0.15. If the distance value is less than 0.15, then the reference image and test image is perfectly matched. If the distance value is greater than 0.15, then the reference image and test image is matched but not accurate. Here the Test1 image which is not included in the database, hence the action is denied.

Reference Image (Original Image)	Test Image (Deformed Image)	Verification (Hamming Distance)
1Per1	3Per2	0.1622
1Per2	3Per2	0.1622
1Per3	3Per2	0.1622
1Per4	3Per2	0.2125
2Per1	3Per2	0.2125
2Per2	3Per2	0.2125
2Per3	3Per2	0.2125
2Per4	3Per2	0.2125
3Per1	3Per2	0.1736
3Per2	3Per2	0(Matched)
3Per3	3Per2	0.1798
3Per4	3Per2	0.1785
4Per1	3Per2	0.1807
4Per2	3Per2	0.1810
4Per3	3Per2	0.1793
4Per4	3Per2	0.1845
1Per1	Test1	Denied
1Per2	Test1	Denied
1Per3	Test1	Denied
1Per4	Test1	Denied

4. CONCLUSIONS

In this paper, the main objective is to overcome the relative nonlinear deformation present in the fingerprint image pairs. A fingerprint verification system based on triangular matching and hamming distance is developed, in which triangular matching saves the local regularities and compensates for global deformation. The deformation model is developed by using a minutiae region rotation with a deformation angle between 0^{o}-16^{o}, and a final verification is based on hamming distance.

Hamming distance is used for matching validation and for minutiae matching between the reference and test images in which the threshold value is set as 0.15. If the distance value is less than 0.15, then the reference image and test image is perfectly matched. If the distance value is greater than 0.15, then the reference image and test image is matched but not accurate. If the test image which is not included in the database, then the action is denied Using this novel method, the accuracy of the fingerprint verification system varies between 94 -96% for 50 TIFF sample images.

REFERENCES

[1] Kovacs-vajna, "A Fingerprint Verification System Based on Triangular Matching and Dynamic Time Warping", IEEE Transaction Pattern Analysis and Machine Intelligence, Vol.22, No.11, Nov 2000, pp.1266-1276.

[2] L. Hong and A. Jain, "Integrating Faces and Fingerprints for Personal Identification", IEEE Transaction Pattern Analysis and Machine Intelligence, Vol.20, No.12, December 1998, pp.1295-1307.

[3] A. Jain, R. Bolle, and S. Pankanti, eds., and R.S. Germain, "Large Scale Systems, Biometrics: Personal Identification in Networked Soc.,", 1998, pp.311-325.

[4] A. Jain, L. Hong, and R. Bolle, "On-Line Fingerprint Verification", IEEE Transaction Pattern Analysis and Machine Intelligence, Vol.19, No.4, April 1997, pp.596-600.

[5] M. Tartagni and R. Guerrieri, "A 390dpi Live Fingerprint Imager Based on Feedback Capacitive Sensing Scheme", IEEE Int'l Solid-State Circuit Conference, 1997, pp.200-201.

[6] L. Coetzee and E.C. Botha, "Fingerprint Recognition in Low Quality Images", Pattern Recognition, Vol. 26, No.10, 1993, pp.1441-1460.

[7] NIST Special Database 4, 8-Bit Gray Scale Images of Fingerprint Image GroupsÐ(FIGS), Image Recognition Group, Advanced Systems Division, Computer Systems Laboratory (CSL), Nat'l Inst. Standards and Technology, 1992.

[8] "The Science of Fingerprints: Classification and Uses", United States Dept. Justice, Federal Bureau of Investigation, Washington, DC, rev., 1988, pp.12-84.

Mechanical Testing and Metallography of Graphite Particulate Reinforced Aluminium Metal Matrix Composite Processed By Powder Metallurgy

Thoguluva Raghavan Vijayaram
Department of Mechanical Engineering, Faculty of Engineering and Technology, Multimedia University, Malaysia
E:mail: thoguluva@mmu.edu.my, vijayaram1@gmail.com
(R)

Abstract

Metal matrix composites are engineered materials designed by a combination of a particulate or fiber reinforced in a metal or alloy matrix. This research work is concerned about the production of graphite particulate reinforced aluminum metal matrix composites and further to investigate on the physical and mechanical properties of the processed composites. Al-Graphite metal matrix composites have been processed and used for this study. In this work, the experimental study began with the mixing of aluminium powder and graphite particulate using a ball mill planetary machine at different weight fraction addition of graphite (5%, 10%, 15%, 20%, 25% and 30%). Then, the powders were compacted by using a compaction-pressing machine at 45 MPa, followed by sintering process at 550p C. The experimental result showed that density is decreased with the addition of graphite whereas porosity is increased. It was found that the hardness of the composites was also increased with the addition of graphite. From the metallographic examinations, the captured optical and SEM micrographs have shown that the graphite particulate were uniformity distributed with homogeneity. The results of XRD reveal that there were no new phases presents in this processed metal matrix composites.

Keywords: *Aluminium(Al), Graphite particulate (GP), Metal matrix composites(MMCs), Powder metallurgy (PM), Mechanical properties, Material characterization, XRD analysis.*

1. INTRODUCTION

Metal matrix composites are normally fabricated by using ductile metal as the base matrix material, and reinforced by a ceramic second phase particulate. These materials offer many advantages over monolithic materials like higher specific strength, good wear resistance, higher thermal conductivity and lower thermal expansion [1, 26]. It is beneficial to combine the metallic properties such as good ductility and toughness of the matrix with ceramic properties such as high strength and hardness in order to get higher toughness, higher specific strength and excellent wear resistance composites. Among other important materials, number of studies has been focused on the applications of aluminium graphite particulate composites. In fact, it is expected that graphite in aluminium alloys would improve friction and wear performances. This fundamental behavior is of great relevance and importance to the industries [1, 7]. Furthermore, the addition of graphite particles to aluminium alloys improves sliding wear and seizure resistance compared to monolithic aluminium alloys. Since graphite particles are lighter than matrix metallic alloys, Aluminum-Graphite composites are used to reduce the weight of the components. Aluminium and graphite are widely acceptable materials for automotive parts. Recent advances in the technology of automotive engines have generated the need to develop new materials for better antifriction and wear performance on specific materials such as pistons, connecting rods and brakes. For instance, in bearing applications, aluminium graphite composite save considerably cost, weight, and has the added benefit of being self-lubricating. Considerable efforts have been made into incorporating lubricating particles in aluminium alloys matrices to obtain reduced frictional losses. Achutha et al., have found that graphite worked as a suitable solid lubricant material. Achutha et al., have reported performance of the cylinder block of two and four stroke engines made of hypereutectic aluminium silicon alloys. An improvement in the mechanical efficiency of the engine and negligible wear loss of the cylinder block was observed because of graphite addition to the hypereutectic alloy coated with 3.5% nickel as compared to the conventional cast iron cylinder block. The powder metallurgy (PM) process is one of the most common methods for manufacturing

MMCs. One advantage is the possibility of fabricating high quality parts with complex shapes and with high tolerance standards in an inexpensive fashion. By principle, PM offers compositional flexibility, uniformity, minimum segregation effects and the possibility of producing graded microstructures with different physical and mechanical properties. Besides, PM offers economical advantages over ingot metallurgy in terms of cost, precision and productivity. The potential for expended use of aluminium-based materials produced by PM processing method is great if the improved properties can be achieved. Net shape processing routes are the key to cost reduction and represent both a significant challenge and opportunity for the aluminium powder metallurgy industry.

2. LITERATURE REVIEW

2.1 Metal Powders

There are several reasons to use powder and of course powder compaction. Some materials cannot be used in other manufacturing methods because the powder compaction method is proven to be a more economically favorable method than other manufacturing methods. One type of material used in powder compaction's are materials with a very high melting point, the so called refractory metals, where casting would not be economic because of the high melting point [1, 16]. The properties of commercial graphite are shown in Table 2.1.

Table 2.1 Properties of Commercial Graphite

Property	Commercial Graphite
Porosity (%)	0.7-53
Modulus of Elasticity (GPa)	8-15
Compressive strength (MPa)	20-200
Thermal conductivity (W/m. K)	25-470
Flexural strength (MPa)	6.9-100
Specific heat capacity (J/kg. K)	710-830

Another category of materials used in powder compaction are composite materials that cannot easily be mixed in other manufacturing methods or handled in post operation due to it constituents. The main bulk material used in powder compaction manufacturing method is ferrous metals used for structural parts. Also other materials can be summarized in this category, such as iron based metals, copper, brass, bronze, aluminium and titanium. Finally, some special high duty alloys such as nickel and cobalt alloys are used in powder compaction processes. The material powders mentioned above are manufactured in different ways depending on the mechanical behavior.

2.2 Powder Size and Shape

One of the first tasks in characterizing a powder is to obtain a small sample that represents the entire powder lot. Of all powder characteristics, probably three dominate in successful powder compactions; particle size, packing density and particle shape. Particle size is measured by determining the dimensions of a particle. The size depends on the measurement technique and particle shape. Particle size determination is possible through several techniques, but each produces a different determination due to differences in the measured parameters. Most automated particle size analyzers use one geometric parameter and make the assumption of a spherical particle shape. The basis for analysis can be surface area, projected area, maximum dimension, minimum cross sectional area, or volume. For accurate measurements, it is imperative that the powders are deagglomerated by using ultrasonic agitation before analysis. The scanning electron microscope provides a tool for visualizing the actual particle character. As the shape become less regular, the number of possible size parameters increases and the difficulty increases in assigning a single particle size.

2.3 Compaction and Sintering

In this process, custom blended metal powders are fed into a die, compacted into the desired shape, ejected from the die, and then sintered (solid state diffused) at a temperature below the melting point of the base material in a controlled atmosphere furnace. The compaction step requires the part to be removable from the die in the vertical direction with no cross movements of the toll members. The sintering step creates metallurgical bonds between the powder particles, imparting the necessary mechanical and physical properties to the part. Conventional PM offers may advantages over the other consolidation methods. It offers the lowest manufacturing cost, including modest tooling costs. It also produces the closest tolerances in the finished parts. Since it is a net shape processing technology, it yields parts requiring little or no secondary machining operations. Parts produced

through the press and sinter process are subjected to certain limitations as well. Tooling and the maximum press tonnage capabilities impose size and shape constraints on parts that can be fabricated. Finally, the presence of residual porosity in the parts will cause certain physical and mechanical properties to be lower than those of the wrought material.

3. EXPERIMENTAL

The main intention of this research work is to reinforce Aluminium MMC with graphite particulate (mixing, compaction and sintering) that influence the characteristics (strength, density and hardness) of the Aluminium metal matrix composite.

The process flow chart is shown in Figure 3.1. The first stage is the procurement of metal powders. This stage includes aluminium powder and graphite particulate preparation. The second stage is the preparation of powders for mixing, compaction, sintering and testing. Preparation is very important before the experiment. In this study, aluminium powder of 99.9% purity with a size of 75 μm (Fluka, Germany) was used as the matrix and graphite with a particulate size 50 μm (Fluka, Germany) was used as the ceramic reinforcement phase. Graphite, one of the potential oxide ceramics was chosen as reinforcement because of its higher specific strength at elevated temperature. The properties of aluminum and the physical and mechanical properties of graphite are shown in Table 3.1 and 3.2.

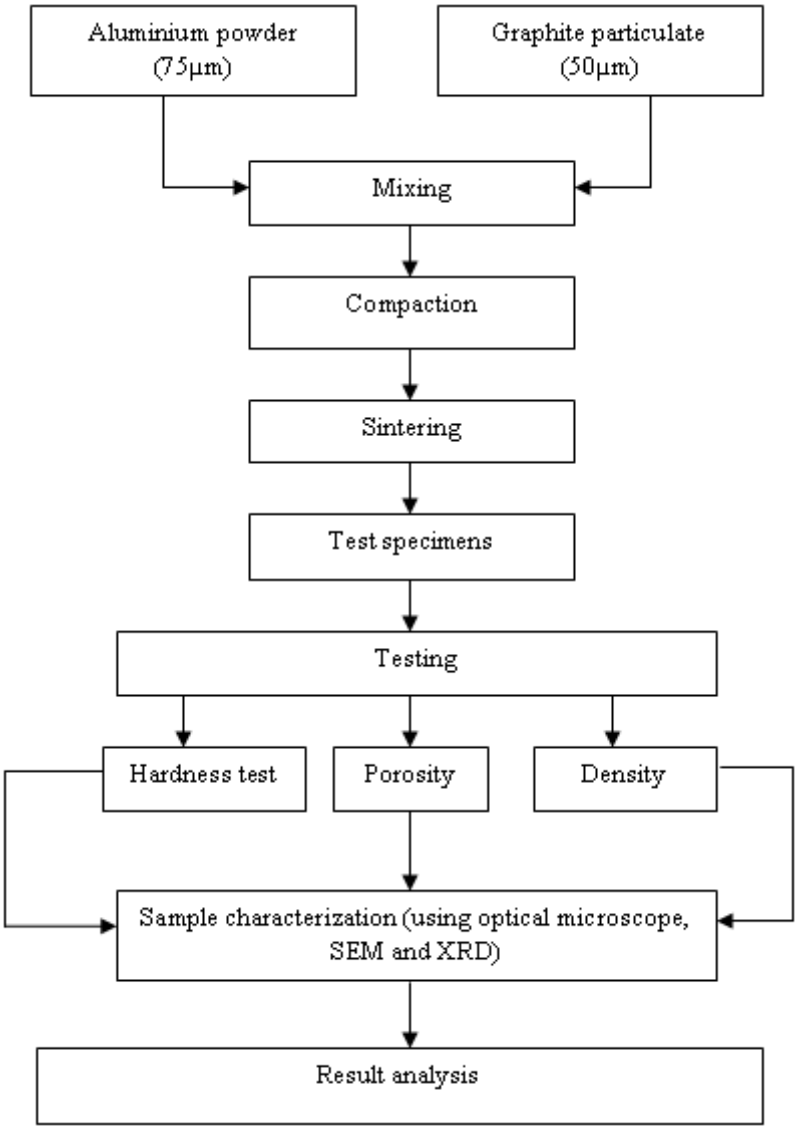

Fig. 3.1 Process flow chart

Table 3.1 Properties of Aluminium

Material	Physical Properties
Density (g/cm^3)	2.6989
Melting point (°C)	669.7
Brinell hardness (MN m^{-2})	245
Vickers Hardness (MN m^{-2})	HV15
Young Modulus (GPa)	70

Table 3.2 Physical and Mechanical Properties of Graphite

Material	Physical Properties
Density (g/cm^3)	2.25
Bulk Modulus (GPa)	34
Thermal Expansion (K)	7.8
Hardness (MNm^{-2})	10
Fusibility (°C)	800
Tensile strength (MPa)	4.8

The proportion of materials in each sample is shown in Table 3.3. Mixing process was conducted in a Ball Mill Planetary Machine (In smart system). Before mixing process, digital weight machine was used in order to weight the Aluminium and graphite. Three different sizes of balls 0.5 cm, 1.0 cm and 1.5 cm were used in the ball mill planetary machine. The mixing variables are shown in Table 3.4.

Table 3.3 Proportion of Materials in Each Sample

Experiments	Percentage of Powder by Weight Fraction (100gram)	
	Graphite Particulate	Aluminium MMC
1	5%	95%
2	10%	90%
3	15%	85%
4	20%	80%
5	25%	75%
6	30%	70%

Table 3.4 Mixing Variables

Variables	Setting condition
Mixing time	60 minutes
Mixing speed	1000 rpm

Experiments were conducted with the mixing time 60 minutes and mixing speed 1000 rpm. Compaction was performed after mixing process was done. At this stage, 45 MPa of compaction pressure was used and the compaction time was 90 seconds. After compaction has been done, the sintering furnace was used to strengthen the composites. The samples were heated for two hours to a temperature near the melting point at the Carbolite Furnace. Density of every sample was checked by using electronic densitometer. The density measurement was carried out with the Archimedes' method. Samples were weighed in air and immersed in the distilled water. An A& D ER-1824 electronic balance with an accuracy of 0.001g was used for recording the weight. The result was used to calculate the percentage of porosity in every sample. The microhardness of the composites was measured using Highwood HWMMT-X3 digital microhardness. The load applied on the indentor of the Vickers test machine was kept 200g and the indention time of 10 seconds. The morphology of the sintered composites was observed using an optical microscope. Besides that, this microscope was used to identify powder distribution of reinforcement in three differents magnifications 100X, 200X and 500X. Scanning electron microscope (SEM) was used to determine grain morphology and presence of porosity at 3500X magnification. This microscope has produced high resolution images of a sample surface and the image have a characteristics three dimensional appearance and was useful for judging the surface structure of the sample. Evo 50 Carl Zeiss Scanning Electron Microscope was used for this purpose. An X-ray diffractometer is a theta-2 theta goniometer instrument that was used for the identification of phases in powder form. An X-ray beam of known wavelength was focused on a powdered sample and x ray diffraction peaks were measured by using a germanium detector. X-ray diffraction analysis was carried out on the composite samples using automated X-Pert Pro difrractometer. The samples were exposed to CuKα radiation (λ = 1.5406) at a scanning speed of 2°/min. The Braggs angle ($n\lambda = 2d\sin\theta$) and the values of the interplanar spacing(d) obtained were subsequently matched with the standard values for aluminium, graphite and related phases.

4. RESULTS AND DISCUSSION

4.1 Analysis of True Density of Al-Graphite Composites

Results of the density tests with standard deviation are shown in Table 4.1. The values of standard deviation were 0.01 and 0.02, which means there were 1% and 2% error occurred during the experiments. Plot of density for Al-Graphite for various weight percentage of graphite reinforcement is presented in the following Figure 4.1. Density values are determined digitally by applying the Archimedes' principle, which states, "a body immersed in a fluid is buoyed up by a force equal to the weight of the displacement fluid".

Table 4.1 Density Results

Experiments	% of Powder	Density (g/cm^3)					
		Sample 1	Sample 2	Sample 3	Sample 4	Sample 5	Average
1	95 % Al 5% Gr	2.325	2.242	2.321	2.333	2.312	2.307± 0.01
2	90% Al 10% Gr	2.272	2.271	2.268	2.264	2.270	2.269 ± 0.01
3	85% Al 15% Gr	2.264	2.261	2.266	2.263	2.267	2.264 ± 0.01
4	80% Al 20% Gr	2.214	2.211	2.217	2.210	2.215	2.213 ± 0.01
5	75% Al 25% Gr	2.014	2.011	2.017	2.015	2.013	2.014 ± 0.02
6	70% Al 30% Gr	1.931	1.938	1.937	1.934	1.935	1.935 ± 0.02

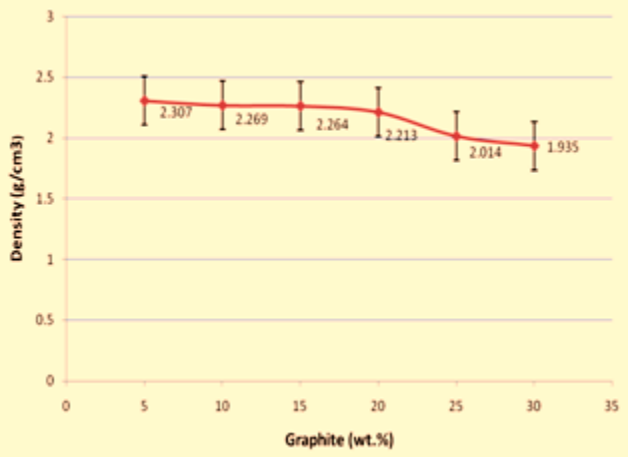

Fig. 4.1 Density versus wt%fraction of graphite

It can be seen that, an addition of graphite particulate into pure aluminium matrix caused the density of the composites decreased. It is notable that this phenomenon is unexpected because of initial prediction, whereby it is anticipated that the density values should be increased with the addition of graphite into the matrix of aluminium, however it occurred vice-versa. The decreasing pattern of density plot with the increasing amount of graphite particulate is due to the nature of the graphite.

The microstructure of graphite reinforced in the aluminium matrix provides more empty space in the fabricated composites samples molecularly. More weight percentages of graphite particulate added into aluminium matrix means more empty space is built, which later decreased the density of aluminum MMCs produced. Nevertheless, this situation provides extra advantages to the specific strength properties of the composites whereby addition of graphite into aluminium matrix itself is basically capable to increase the tensile properties and with decreasing value of density will further increase the specific properties with added advantage of weight reduction.

According to Fuentes et al., the density of Al-Graphite with 7% Carbon is about 1.86g/cm3 [1,7]. Thus, referring to the results obtained, it can be said that the densities of the composites samples with various amount of graphite is dominated by density value of virgin aluminium. Graphite reinforcement into the aluminium matrix does not gives tremendous effects to the density value due to the lower amount used. In overall, referring to the pattern of the plot as shown in the Figure 4.1, it can be said that the decreasing trend of composites density with the increasing amount of graphite particulate added, gives good indication in materials selection in design for various engineering application. Ultimate properties of Aluminium MMCs combine with specific characteristics and benefit of weight saving could gives full hopes to the automotive industries.

Table 4.2 Porosity Results

Experiments	% of Powder	Percentage of Porosity (%)					
		Sample 1	Sample 2	Sample 3	Sample 4	Sample 5	Average
1	95 % Al 5% Gr	1.38	1.69	1.40	1.35	1.43	1.45
2	90% Al 10% Gr	1.58	1.58	1.60	1.62	1.59	1.59
3	85% Al 15% Gr	1.61	1.62	1.60	1.61	1.60	1.61
4	80% Al 20% Gr	1.80	1.82	1.78	1.81	1.79	1.80
5	75% Al 25% Gr	2.54	2.55	2.52	2.53	2.54	2.54
6	70% Al 30% Gr	2.84	2.82	2.82	2.83	2.82	2.83

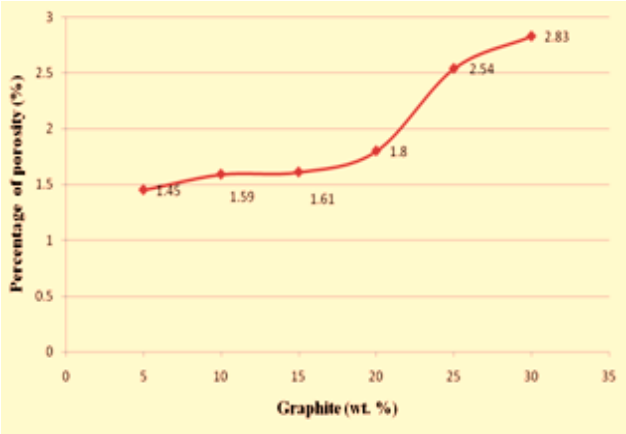

Fig. 4.2 Porosity versus wt% fraction of graphite

Porosity value determined from the sintered density of the composites. As can be seen, addition of graphite particulate into aluminium matrix caused the porosity values increased. The increasing pattern of porosity plot with the increasing amount of graphite particulate is due to pore size, pore shape and pore spacing in the aluminium metal matrix composites. According to Chawla & Deng the pores at lowest density appeared to be much larger and more irregular than pores in a highest density [1, 2]. Pores at the lowest density also appeared to be more clustered and segregated along the interstices between particles. Therefore, referring to the results in Figure 4.1, it revealed that the sample at 2.307g/cm^3 had the highest density of smaller pores, while the smallest density at 1.935g/cm^3, had a much larger pore size. The higher density with smaller pores can be attributed to the pressing and sintering process. In overall, referring to the pattern of the plot as shown in Figure 4.2, it can be observed that the increasing amount in graphite particulate had increased the porosity.

4.3 Analysis on Hardness

Result of the microhardness tests are shown in Table 4.3. In the first experiment which is 5% graphite addition, the composite had a microhardness of 26.5 HV with a standard deviation of ±1.1 HV (4.1%), while 30% of graphite addition had a microhardness of 33.1 HV with a standard deviation of ±1.2 HV (3.6%). This result shows that all the standard deviation below 5%. Due to the porosity of the matrix, there was difficulty in attaining accurate readings. Some indentations were greatly distorted because of overlapping with a pore, precipitation or grain boundary.

Figure 4.3 shows a plot of microhardness of the Al-Graphite composites with the addition of graphite particulate. It is notable that the hardness of the Al-Graphite composites increased with the addition of graphite particulate. A maximum hardness of 33.1 HV appears at 30% of graphite weight fraction. This might be associated with the changes in the microstructure with the addition of graphite.

Table 4.3 Micro Hardness Results

Experiments	% of Powder	Micro Hardness (HV)					
		Sample 1	Sample 2	Sample 3	Sample 4	Sample 5	Average
1	95 % Al 5% Gr	26.1	26.2	26.7	27.1	26.4	26.5 ± 1.1
2	90% Al 10% Gr	29.0	28.6	28.9	29.1	28.9	28.9 ± 1.1
3	85% Al 15% Gr	30.8	30.7	30.1	30.1	30.9	30.5 ± 1.1
4	80% Al 20% Gr	30.7	31.3	31.8	32.0	32.4	31.6 ± 1.1
5	75% Al 25% Gr	31.7	32.6	32.1	32.8	32.5	32.3 ± 1.2
6	70% Al 30% Gr	33.1	32.9	33.3	33.2	33.1	33.1 ± 1.2

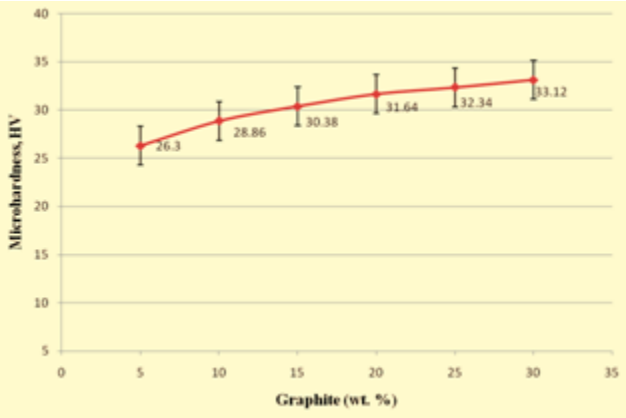

Fig. 4.3 Vickers microhardness versus wt% fraction percentage of graphite

According to Chen *et al.,* clean reinforcement matrix interfaces improve interfacial bonding strength and homogeneous dispersed reinforcing particulates result in better hardness in Aluminium metal matrix composites [1, 3]. At 550°C, graphite melts and diffuses along the interface between aluminium and graphite. Graphite grains disperse homogeneously in the boundary region or inside the grown aluminium grains. The relatively homogeneous microstructure leads to the highest hardness. Addition of graphite into the Aluminium matrix gives tremendous effects to the hardness value due to the higher amount used as shown in Figure 4.3. It can be stated that the increasing trend of composite hardness with the increasing amount of graphite added, gives better wear performance especially in automotive application.

4.4 Microstructural Evaluation and Analysis

According to the Figure 4.5(d), it is clear that the surface becomes more roughed with the increasing content of the graphite loading. Matrix of aluminium merely detached together with the pull out of graphite. Addition of graphite into aluminium matrix enhanced the stiffness of the composites and subsequently improves the strength of it. At the same time, ductility behavior was totally reduced. It is very interesting, since their morphological behavior is still comparable between each other even though the graphite used is in the extremely lower percentage. In overall, addition of graphite even at lowers percentages of loading, drastically affects the morphological behavior of Al-Graphite composites really much.

These can be seen depicted in the presented Figure 4.4 and 4.5, wherein the graphite tremendously changed the structural behavior of the fabricated Al MMCs. Certainly, this condition gives major impact to the other various properties studied, which subsequently discussed.

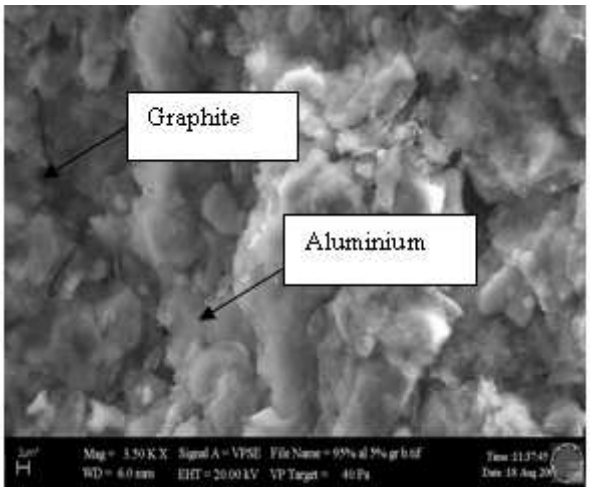

(a) Al-Graphite, magnifications 3500X (5% graphite)

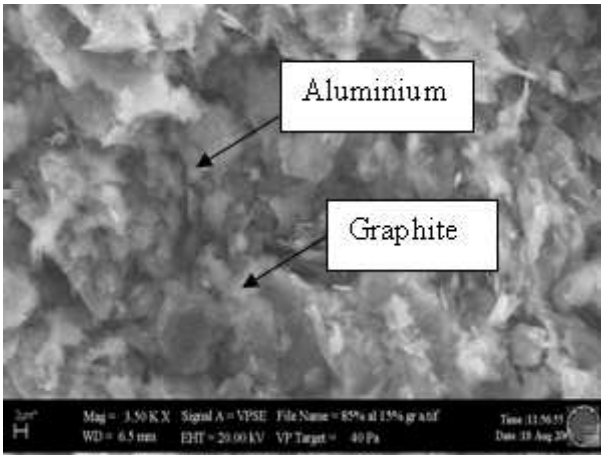

(b) Al-Graphite, magnifications 3500X (15% graphite)

Figure 4.4: Scanning electron micrographs of the Al-Graphite (a) 5% graphite, (b) 15% graphite.

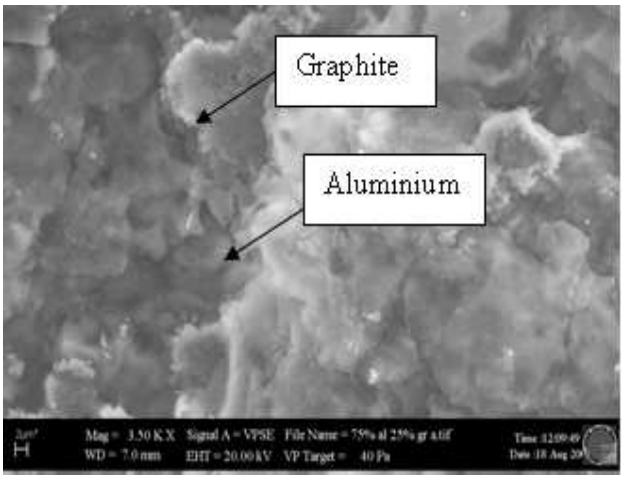

(c) Al-Graphite, magnifications 3500X(25% graphite)

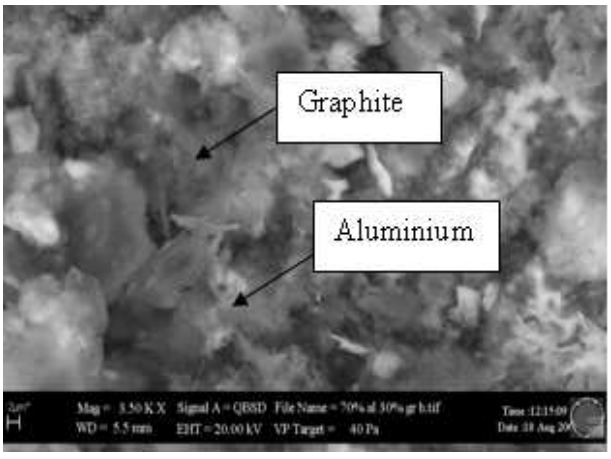

(d) Al-Graphite, magnifications 3500X (30% graphite)

Figure 4.5: Scanning electron micrographs of the Al-Graphite (c) 25% graphite, (d) 30% graphite

Optical microscope and SEM observation were done to check the particulate distribution of the composites. In addition, the dispersion and wetting state of the graphite added into aluminium matrix were examined. It is clearly can be seen that the powder is uniform in the composites. As illustrated in the Figure 4.4, SEM micrographs showed the powder distribution of the Al-Graphite at 3500X of magnification. It is clearly seen that the complete melting of graphite was achieved since there is no presence of hole and impurities are detected. Graphite particulates are properly bonded with aluminium matrix and well continuance between each other. This condition formed good initial strength to the matrix used, as confirmed by the results of the micro hardness test.

The following Figure 4.5 is the SEM micrograph for aluminium composites with 25% and 30% of graphite loading under the 3500X magnification. In general, there is no fiber clumps in every composites viewed, regardless of its fiber content. Hence, it can be stated that the blending process via planetary ball milling, which employed in this research was very effective for the dispersion of graphite particulate. As prepared, graphite particulate appeared in a quite distance between each other and can be recognized as a dark spot in the photograph taken.

Moreover, it is quite interesting to note that the presence of graphite particulate in each micrograph observed was increased with the increasing percentages of graphite added. At extremely lower graphite addition the graphite seems like embedded in the aluminium matrix. This is the indication of the good wetting behavior between the graphite and matrix used. Good dispersion and wetting conditions may creates proper stress distribution from the matrix to the graphite during the Vickers hardness test. As a result, it was enhanced the mechanical properties of the composites.

According to the Figure 4.5(d), it is clear that the surface becomes more roughed with the increasing content of the graphite loading. Matrix of aluminium merely detached together with the pull out of graphite. Addition of graphite into aluminium matrix enhanced the stiffness of the composites and subsequently improves the strength of it. At the same time, ductility behavior was totally reduced. It is very interesting, since their morphological behavior is still comparable between each other even though the graphite used is in the extremely lower percentage.

In overall, addition of graphite even at lowers percentages of loading, drastically affects the morphological behavior of Al-Graphite composites really much. These can be seen depicted in the presented Figure 4.4-4.5, wherein the graphite tremendously changed the structural behavior of the fabricated Al MMCs. Certainly, this condition gives major impact to the other various properties studied, which subsequently discussed.

4.5 XRD Analysis of Al-graphite Metal Matrix Composites

XRD characterization of Al-Graphite composites with various percentage of graphite content was conducted in order to further understand the structure of the composites. In the case of 5% of graphite, only one major peak of Al-Graphite appeared at 44.7°, corresponded to the interlayer spacing of the composites ($d_{2.02}$) reflection of the carbon atoms which indicates that the produced Al-graphite is crystalline (Chen *et al.,*2008).

Diffraction pattern of Al-Graphite composites with various percentages of graphite reinforcement within 18-45° of diffraction angle (remarkable diffraction range) is presented as in the Figure 4.6. Basically, all the identical peaks are assigned to Al-Graphite whereby six crystalline peaks at diffraction angle (2θ) of 44.77°, 44.78°, 44.82°, 44.88°, 44.89° and 44.71° were clearly detected according to lowest addition of graphite to highest addition of graphite. It can be seen that the position of the identical peaks is similar for all samples regardless different weight percentages of graphite contained in each composite.

However, the relative peak intensity for composites tested was proportionally increased with the additional amount of graphite. This condition might indicate that the addition of graphite into aluminium matrix creates crystalline. First three major peaks have shown this interesting phenomenon, even though there is inconsistency in the subsequent characteristic peaks. It is shown that the addition of graphite into the aluminium matrix even at lower percentages, capable to shift the relative intensity plot significantly.

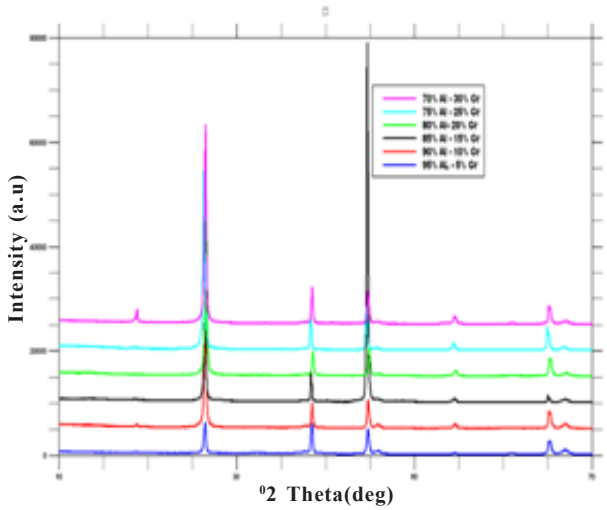

Fig. 4.6 XRD patterns of different percentage of graphite reinforced aluminium matrix composites

From the Figure 4.6, a new peak of small amount of Al-Graphite was detected at 18.79°. Concerning the formation of Al-Graphite, it seems reasonable to assume that 30% graphite is an ideal amount of graphite reinforcement in 100g weight fraction. In overall, the use of aluminium matrix even at low graphite reinforced still capable to give the identical differences in relative intensity even though it seems overlapping at several diffraction angles. Thus, the increasing shifting pattern of relative intensity is adequate to represent the affect of graphite addition into the matrix of aluminium. It can be concluded that the melt compaction process done in the Al-Graphite composites is merely physical-mechanical blending process, which may not involving any chemical interaction between the major constituents involved.

5. CONCLUSIONS

The research work reported in this paper was carried out in order to investigate the graphite particulate reinforced Aluminium metal matrix composites on density, porosity, hardness and microstructure. In the present work, Aluminium metal and graphite particulate were used in powder metallurgical processing. The processes involved mixing, compaction and sintering with the different variables included mixing time, mixing speed, compaction time, sintering time and sintering temperature. The experiment was conducted in six different weight fraction percentage of graphite particulate (5% to 30%) in order to observe the effect of graphite addition in the composites. The density was measured using densitometer and the porosity is calculated using data

from the densitometer measurement. Based on the density results, it can be concluded that the density is decreased in addition of graphite particulate. The reduction in density indicates that the graphite particulate is potential to reduce the weight of components especially in automotive industry. In the study of porosity in the composites, the result shown that the porosity increased with the addition of graphite. It was resulted a higher pore fraction, bigger average pore size, and less spherical pore shape. Increasing pore size was correlated directly with an increase in the irregularity of pore shape. The experiment for the hardness is presented and the hardness is increased with addition of graphite. It is probably as a result of carbon dissolution and increased the strength of the aluminium matrix. At sintering temperature of 550°C, graphite melts and diffuses along the interface between aluminium matrix and graphite. It is found that very thin grain boundary appears between two adjacent aluminium grains. Graphite grains disperse homogeneously in the boundary region and this condition leads to the highest hardness. The highest microhardness of 45MPa occurs at 30% graphite addition. Based on the microstructural examination, it has been shown that the molten graphite at 550°C contacts with aluminium. Due to the high surface tension, the molten graphite tends to agglomerate with aluminium grains segregating around in the grain boundary region. The rapid diffusion of the molten graphite leads to the formation of intra granular grains inside aluminium grains. This condition has increased the composites hardness and from the XRD results (Figure-4.6), there was a new peak of small amount of Al-graphite at 18.79°. It shows that 30% of graphite is an ideal amount of graphite particulate reinforcement.

REFERENCES

[1] W.D. Callister, "Material Science and Engineering: An Introduction", 5th Edition, John Wiley & sons, Inc.1999.

[2] N. Chawla and X.Deng, "Microstructure and Mechanical Behavior of Porous Sintered Steels", Vol. 390, 2005, pp.98-112.

[3] Z.C. Chen, T. Takeda and K. Ikeda, "Microstructural Evolution of Reactive-sintered Aluminium Matrix Composites", Vol. 68, 2008, pp.2245-2253.

[4] H. Choe, S. Abkowitz, S. M. Abkowitz and D.C. Dunand, "Mechanical properties of Ti-W alloys Reinforced with TiC Particles, Vol. 485, 2008, pp.703-710.

[5] K.S. Dunnett, R.M. Mueller and D.P. Bishop, "Development of Al-Hi-Mg-(Cu) Aluminium PM Alloys", Vol. 1988, 2008, pp.31-40.

[6] S. Eroglu and T. Baykara, "Effects of Powder Mixing technique and Tungsten Powder Size on the Properties of Tungsten Heavy Alloys", Vol.103, 2000, pp.288-292.

[7] R. Fuentes, E. Rubio, C. Gomez, A. Herrera and V.M.Castano, "Wear Behavior of a Self lubricating Aluminium/graphite Composite Prepared by Powder Metallurgy", 2003, Vol.55, No.4, pp.157-161.

[8] J. Garcia, P. Perez, P. Garces and P. Adeva, "Microstructure and Mechanical Properties of Ni3Al Base Alloy Reinforced with Cr Particles", Produced by Powder Metallurgy, 2006, Vol.14, pp.456-463.

[9] K.W. Huai, J.T. Guo, Q. Gao, H.T. Li and R. Yang, "Microstructure and Mechanical Behavior of NiAl-based Alloy Prepared by Powder Metallurgical Route", Vol.15, 2007, pp.749-752.

[10] O. Kolednik and K. Unterweger, "The Ductility of Metal Matrix Composites Relation to Local Deformation Behavior and Damage Evolution", Vol.75, 2008, pp.3663-3676.

[11] H.Masuda, K. Higashitani and H.Yoshida, "Powder Technology Fundamentals of Particles, Powder Beds, and Particle Generation", Taylor & Francis Group, LLC, 2007.

[12] J.M. Molina, M. Rheme, J.Carron and L.Weber, "Thermal Conductivity of Aluminium Matrix Composites Reinforced With Mixtures of Diamond and Sic Particles Thermal Conductivity of Aluminium Matrix Composites Reinforced With Mixtures of Diamond and Sic Particles", Vol. 58, 2008, pp.393-396.

[13] V. Neubert, B. Smola, I. Stulikova, A. Bakkar and J. Reuter, "Microstructure, Mechanical Properties and Corrosion Behavior of Dilute Al-Sc-Zr Alloy Prepared By Powder Metallurgy", Vol. 464, 2007, pp.358-364.

[14] B.P. Neville and A. Rabiei, "Composite Metal Foams Processed Through Powder Metallurgy", Vol. 29, 2008, pp.388-396.

[15] T.Ozben, E.Kilickap and Orhan Cakir, "Investigation of Mechanical and Machine Ability Properties of

Sic Particle Reinforced Al-MMC", Vol. 198, 2008, pp.220-225.

[16] A. Rabiei, L. Vendra and T. Kishi, "Fracture Behavior of Particle Reinforced Metal Matrix Composites", Vol.39, 2008, pp.294-300.

[17] M.E. Rodriquez, V.M.Castano and Herrera, "A Particles Distribution on Wear Behavior of an Al-Gr Composite", Vol.59, No.2, 2007, pp.77-80.

[18] D. Roy, S. Ghosh, A. Basumallick and B. Basu, "Preparation of Ti-Aluminide Reinforced in Situ Aluminium Matrix Composites by Reactive Hot Pressing", Vol.436, 2007, pp.107-111.

[19] S. Seal, T.L. Barr, N. Sobczak and S.J. Kerber, "Microscopy and Electron Spectroscopic Study of the Interfacial Chemistry in Al-Ti Alloy/Graphite Systems", Vol.33, 1998, pp.4147-4158.

[20] A.V. Tamashausky, "Surface Enhanced Flake Graphite and its Utility as A Functional Extender For Molybdenum Disulfide", Presented at the NLGI 72nd Annual Meeting.San Antonio, Texas, USA, 2005.

[21] K.S. Tun and M. Gupta, "Improving Mechanical Properties of Magnesium Using Nano-Yitra Reinforcement and Microwave Assisted Powder Metallurgy Method", Vol. 67, 2007, pp. 2567-2664.

[22] H.Wang, R. Zhang, X. Hu, C.A. Wang and Y. Huang, "Characterization of a Powder Metallurgy Sic/Cu-Al Composite", Vol. 1978, 2008, pp. 43-48.

[23] R. Weinekotter and H. Gericke, "Mixing of Solids", Kluwer Academics Publishers, Netherlands, 2000.

[24] A.A.Yousif, S.F. Moustafa, M.A. El-Zeky and F.N. El-Sabbahy, "Alumina Particulate/ Cu Matrix Composites Prepared By Powder Metallurgy", Vol.46, No.4, 2003.

[25] D. Zhao, Q. Lei, and C. Qin, "Melt Process and Performance of Multi-Walled Carbon Nanotubes Reinforced LDPE Composites", Vol.35, No.6, 2006, pp. 341-345.

[26] M.V. Achutha, B.K. Sridhara, and D. Abdul Budan, "A Reliability Based Stress-Life Evaluation of Aluminium-Graphite Particulate Composites", Vol.29, 2008, pp.769-774.

[27] M.R. German and A. Bose, "Injection Molding of Metals And Ceramics", Metal Powder Industries Federation New Jersey, United States of America, 1997.

[28] M.A. Taha, N.A. El-Mahallawy and A.M. El-Sabbagh, "Some Experimental Data on Workability of Aluminium Particulate-Reinforced Metal Matrix Composites", Vol.202, 2008, pp.380-385.

[29] Gomez-Garcia, C., Rodrigues, M.E., Castano, V.M., and Herrera, A. Particles distribution on wear Behavior of an Al-Gr composite, Vol.59, No.2, 2008, pp. 77-80.

A Novel Topology Control Algorithm for Energy Efficient Wireless Sensor Network

S.Emalda Roslin[1] and C.Gomathy[2]
[1&2]Department of Electronics & Communication Engineering, Sathyabama University, Chennai - 600 119.
E-mail: roemi_mich@yahoo.co.in
(R)

Abstract

Recent years showed a wide range of applications in Wireless Sensor Networks (WSN). For a WSN, Topology Control is crucial to obtain an energy efficient network without affecting the connectivity and other properties. In this paper the sequence of strategies carried out to obtain a better scheme for a topology control in terms of energy is discussed. The results showed the effectiveness of the different approaches proposed. The future works discussed also gives a wider vision on the p robabilities of the various for the forthcoming years.

Keywords: *Energy, Network property, Topology control, Wireless sensor network*

1. INTRODUCTION

A Network of complex sensor nodes equipped with limited sensing, computing, and radio communication capabilities is called a Wireless Sensor Network (WSN). It is classified in to two ways. One is the homogenous network and heterogeneous network. The main requirement for various applications is to prolong the lifetime of the sensor network. Each sensor node depends on small low capacity battery as energy source, and cannot expect replacement [1][2][3][4]. This makes the energy factor of the sensor node a critical one. Hence for any WSN, both energy and capacity are limited resources. The network designer should strive for reducing energy consumption of nodes but by maintaining network capacity. A suitable compromise for this is Topology Control. Topology Control (TC) refers to maintaining a topology with certain properties (e.g., connectivity) while reducing energy consumption and/or increasing network capacity. Figure 1 shows the pictorial representation of a network before and after applying TC. By implementing a TC, maximum number of communication links in the network has been reduced. This leads to minimum energy consumption and maximum network capacity [5][6]. Topology Control can be broadly categorized in to any of the two approaches. They are power Control mechanism and power management mechanism [1]. Adjusting the transmitting power of each node dynamically is termed as power control [7][8][9][10]. Power management is switching off the redundant nodes that are not involved in transmission nor reception [11][12][13][14][15]. By integrating power control and power management algorithms it is possible to increase the energy efficiency of a wireless sensor network.

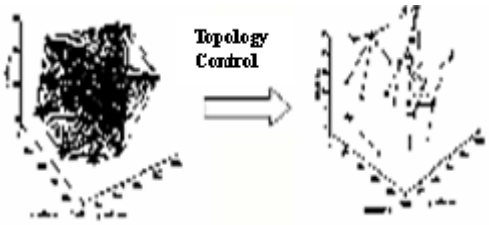

Fig.1 Network topology

The flow of this paper is as follows. The effect of using maximum transmission range is discussed in section 2. Section 3 deals with the various approaches proposed for getting an efficient network. The discussion on the results obtained using the proposed methodologies are given in section 4. Conclusion and future work are dealt in section 5.

2. IMPACT OF TRANSMISSION RANGE ON WSN PERFORMANCE

From the various literatures surveyed, it is a well known fact that reducing the maximum transmission range increases the network lifetime. To start up with the work in reaching a minimum energy consumption we first investigated the factors affected by maximum transmission range. In a dense network, increasing the transmission range is undesirable because it leads to a

higher channel interference, collision, decreased throughput and high energy consumption. So in order to increase the performance it is desirable to decrease the transmission range. It is illustrated with the following network scenario. Figure 2 shows a sample network of four nodes. When node 1 communicates using a maximum transmission range, all the adjacent nodes comes under its range. And if the adjacent nodes also start communicating, then the area of interference becomes more. On the other hand if node 1 has used minimum transmission range such that it is reachable only to node 2 interference area becomes less.

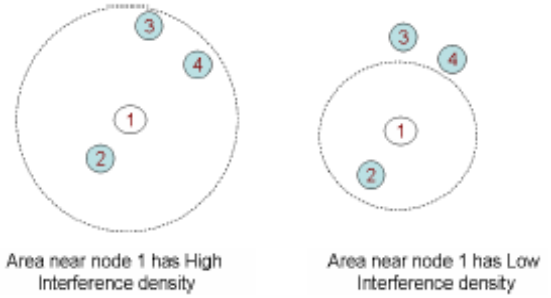

Fig. 2 Network using minimum and maximum transmission ranges

From the literatures it is understood that various transmission range reduction algorithms are done using cooperative approach [16]. However cooperative approach fails miserably, when the critical neighbors are at the same distance, as it leads to oscillation problem. Hence to overcome the oscillation problem, a Hierarchical Cooperative Technique (HCT) based on nodes usage is initially proposed.

3. HIERARCHICAL COOPERATIVE TECHNIQUE (HCT)

The mechanics of exchanging information regarding their transmission power among the nodes in the network is said to be cooperative technique. In HCT, every node maintains a best set of neighbors which leads to the desirable connected network.

3.1 HCT based on Nodes Usage

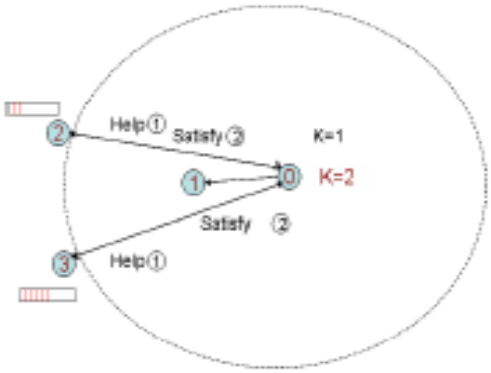

Fig.3 HCT based on nodes usage

The algorithm of HCT is discussed below.

Hierarchical Cooperative Technique (HCT) based on nodes usage

Step 1: Neighbor table is maintained
Step 2: If number of neighbors less than critical value K, HELP packet is sent
Step 3: Neighbors receiving HELP, sends back SATISFY, naming themselves as critical neighbors
Step 4: Bandwidth details of the critical neighbors is sent along with SATISFY Packet
Step 5: For critical neighbors at the same distance, priority is given for nodes with maximum unused bandwidth

The proposed algorithm is explained using Figure 3. In this sample of 4 nodes, K is assumed to be 2. Consider node 0 is with one neighbor (K=1). To satisfy the connectivity property, the transmission range is increased and exchanging of Help and Satisfy packets takes place. Since nodes 2 and 3 are at a same distance, an oscillatory behavior is encountered. To overcome this, along with the Satisfy packet, nodes 2 and 3 send their bandwidth details to node 0. Based on the hierarchy a node with lesser bandwidth is considered as neighbor. Since a node with maximum unused bandwidth is selected to avoid congestion. Average energy consumption has reduced but not significantly. Hence to further reduce the energy consumption, HCT based on Received Signal Strength Indicator (RSSI) and Residual Energy (RE) is proposed and implemented.

3.2 HCT Based on RSSI and RE

From the set of neighbors maintained using the above algorithm (HCT based on nodes usage) the best node for data forwarding is to be elected. Data forwarding through the neighboring nodes with higher RSSI is present in the literatures [8]. RSSI always depends on the distance. So when a node is at a nearer distance then the RSSI takes a higher value. And if the node with higher RSSI always gets elected for forwarding, then maximum energy drain occurs in that node. This leads to a disconnected network. To overcome this problem data forwarding node election based on RSSI and RE is proposed. The proposed algorithm is given below. Figure 4 illustrates the proposed algorithm.

Hierarchical Cooperative Technique (HCT) based on RSSI and RE

Step 1: RTS packets were sent. RSSI metric and Residual Energy were calculated and is sent back along with the CTS packet
Step 2: Neighbor table with the neighbor node id, RSSI value and RE value is maintained
Step 3: Nodes with higher RSSI and RE value is given higher priority
Step 4: Nodes not satisfying the threshold conditions were made to sleep
Step 5: Overall Energy Consumption for sleep and idle states were calculated

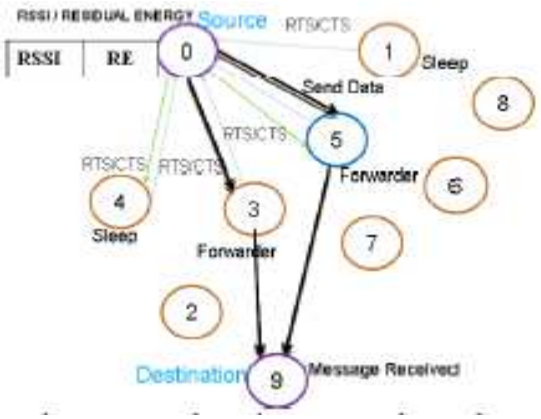

Fig.4 Sample network using HCT based RSSI and RE

In Figure 5, node 0 is the source node which tends to send packets to destination node 9. Now it's the job of the source to elect a suitable neighbor as a forwarder node. This election is based on a hierarchy formed based on the RSSI and RE of the neighbors. The other neighbors other than forwarder node are made to sleep. Thus a maximum amount of energy can be saved.

4. Results and Discussions

4.1 Relationship between Interference and Transmission Range

In order to study the impact of transmission range on Interference and Packet Delivery Ratio (PDR), a network is created with 20 nodes. There are two source nodes (green) and one sink node (yellow). Sink node has two neighbors (magenta), The simulation parameters are given in Table 1. The network for the given simulation parameters is visualized in Figure 5. Interference and PDR are calculated for four transmission ranges viz 150m , 250m, 350m and 450m and are plotted in Figure 6 and 7. The path with lesser interference is selected between the source and the sink. The intermediate nodes between them are represented by red color. The intermediate nodes keep on changing for different transmission ranges.

Table 1 The Simunation Parameters

1	Software Version	NS 2.27
2	Operating System	Fedora 7.0
3	Network Topology	Mesh
4	Number of Nodes	20
5	Transmission Ranges	150m,250m,350m,450m
6	Sink Node	Yellow Color
7	Intermediate Node	Maroon Color

The network animator of the given simulation parameters is visualized in the below screenshot

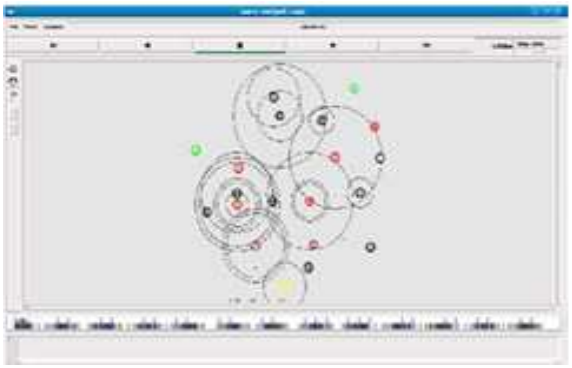

Fig. 5. Network animator screenshot

From the Figures 6 and 7, it is clear that increase in the transmission range increases the interference and decreases the packet delivery ratio.

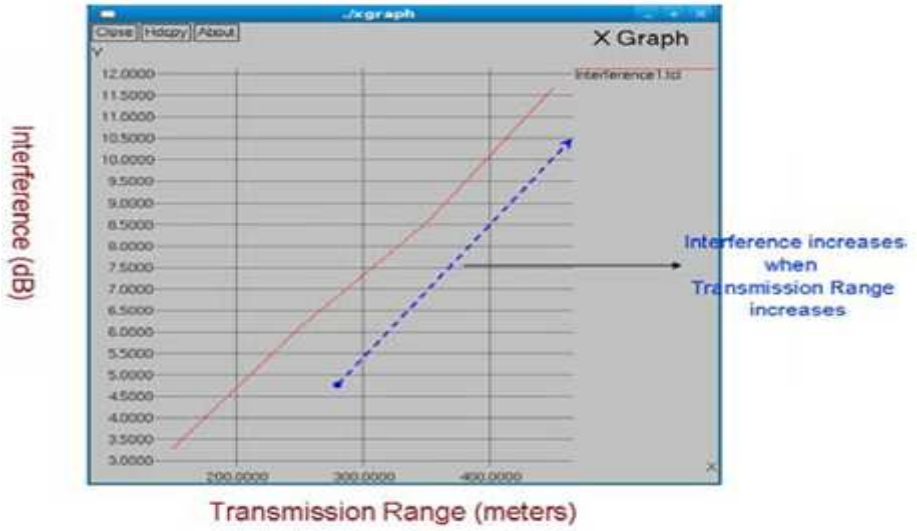

Fig.6 Transmission range Vs interference

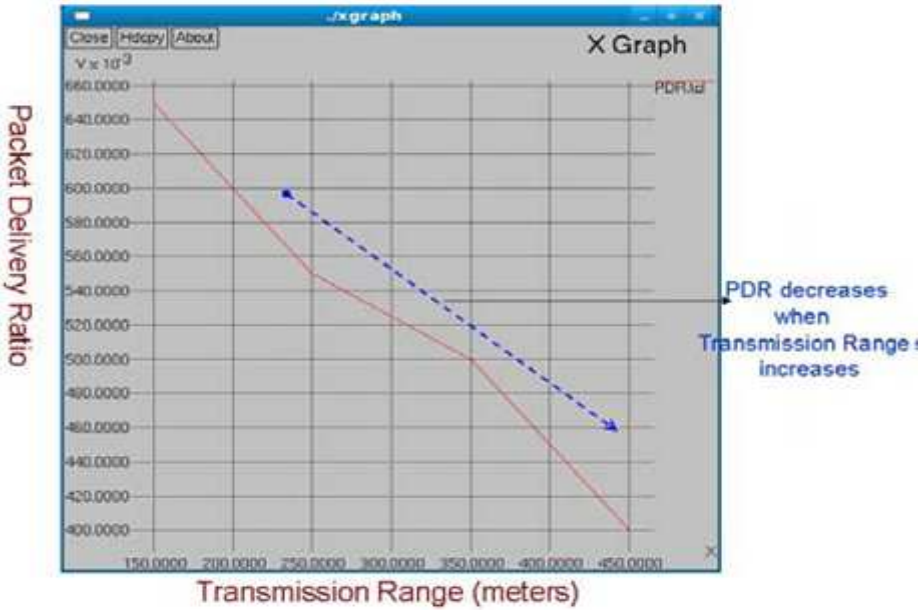

Fig. 7 Transmission range Vs PDR

4.2 HCT Based on Nodes usage

The existing cooperative approach and HCT based on nodes usage are implemented using the following simulation parameters (Table 2). A network with 10 nodes is deployed. Labels were given for source and the destination nodes. The critical nodes identified by this algorithm are circled with red color. The network animator screenshot given in Figure 8.

Table 2 Nodes Usage

1	Software Version	NS 2.27
2	Operating System	Fedora 7.0
3	Network Topology	Mesh
4	Number of Nodes	10
5	Source Node	Node 6
6	Destination Node	Node 3
7	Critical Nodes	Nodes 2 and 5

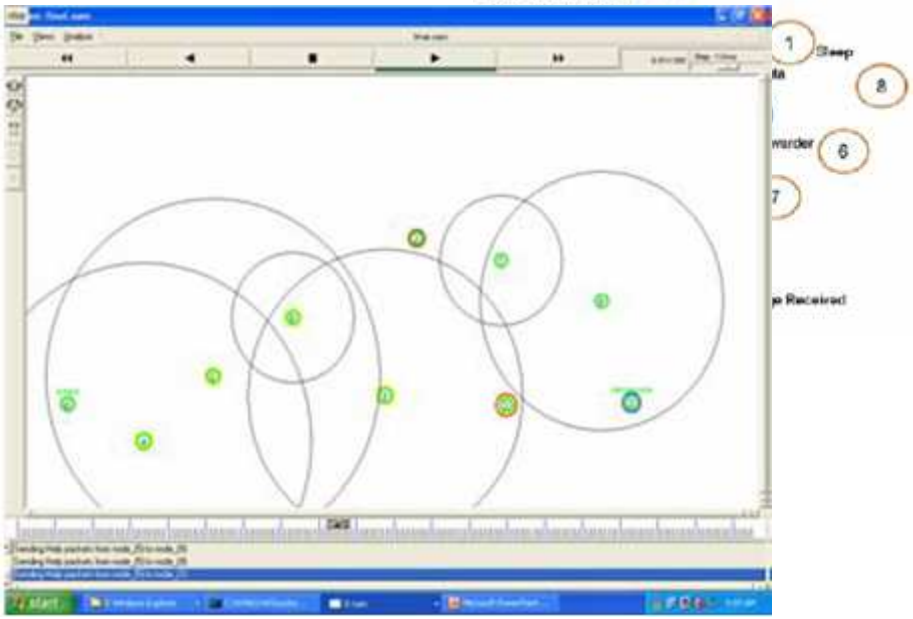

Fig. 8 Network animator screenshot for HCT based on nodes usage

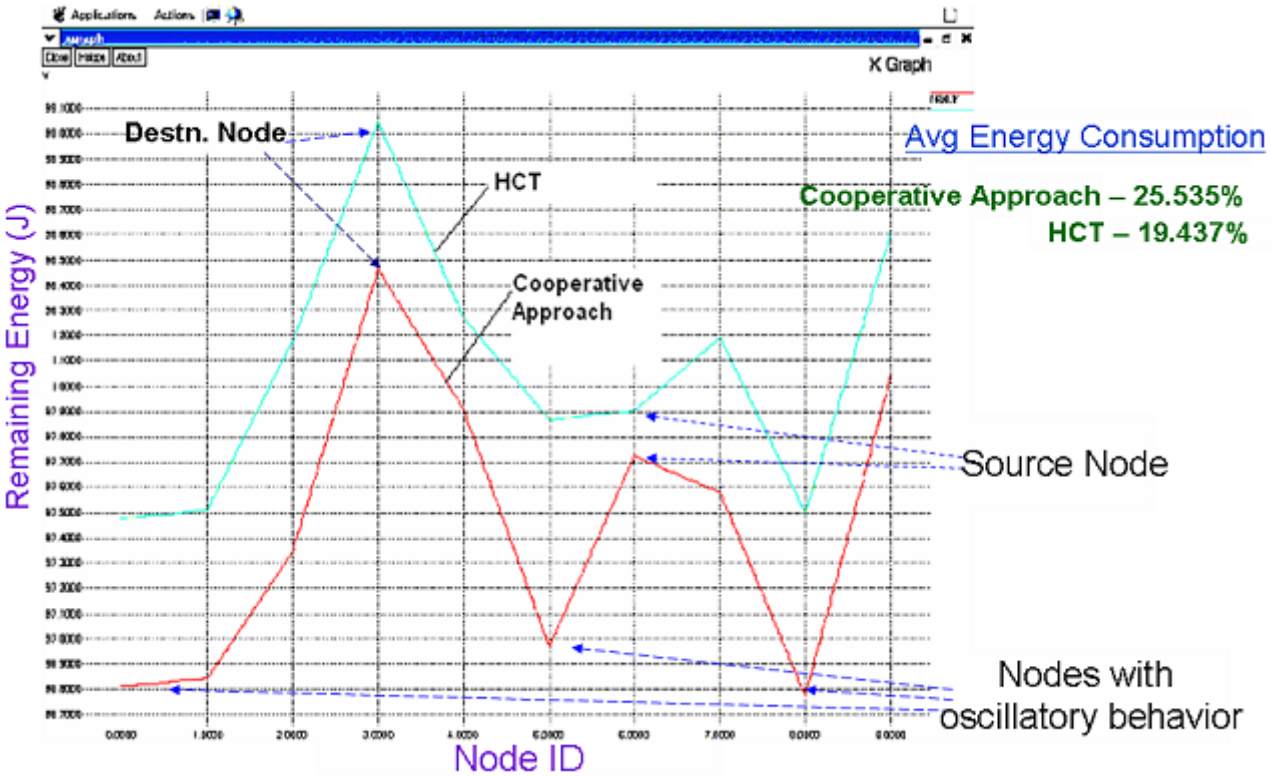

Fig.9 Energy consumption using cooperative approach and using HCT based on nodes usage

The remaining energy present in each node is calculated and is plotted for both cooperative approach and HCT based on nodes usage. The average energy consumption is also calculated and the results were compared in Figure 9. In the existing cooperative technique due to the oscillatory behavior, more amount of energy is spent by the critical nodes. This can be seen by the dip in the remaining energy calculated.

The dip occurred in the existing method gets overcame by the proposed HCT based on nodes usage. The average energy consumption calculated for a network of given parameters using cooperative approach is 25.535% and using hierarchical cooperative approach is 19.437%. Thus overall energy consumption is reduced by 6.098% using HCT based on node usage.

4.3 HCT Based on RSSI and RE

The proposed HCT based on RSSI and RE is implemented using the simulation parameters in Table 3.

Table 3 The Simulation Parameters for HCT Based on RSSI and RE

1	Software Version	NS 2.27
2	Operating System	Fedora 7.0
3	Network Topology	Mesh
4	Number of Nodes	10
5	Source Node	Node 0
6	Destination Node	Node 8
7	Critical Nodes	Node 4 and 5

A mesh topology of 10 nodes is randomly deployed in a region of 1000 x 1000 m. Nodes 0 and 8 are labeled as Source and destination. For the critical nodes 4 and 5, the proposed methodology is implemented.

Table 4 shows the sample neighbor table maintained for node 0. It shows the neighbor list for node 0 along with the RSSI and the RE values received for those neighbors. Initially all the nodes are configured with a constant RE value. So during the initialization phase, forwarder node election only depends on the RSSI value. After a defined period of time (i.e. after nodes started spending energy for forwarding) both RSSI and RE were considered for election.

Table 4 Neighbor Table of The Source CE Node

Node	Neighbor Node	RSSI	RE
0	1	-53.23	100
0	3	-42.68	100
0	4	-49.08	100
0	5	-42.76	100

The RSSI values calculated for the source node 0 with respect to all other nodes in the network is listed and is graphically shown along with its distance metric in Figure 10. As the distance increases the RSSI get decreases. From the list of all neighbors, a best set of nodes (RSSI > Threshold) were considered for forwarder node election.

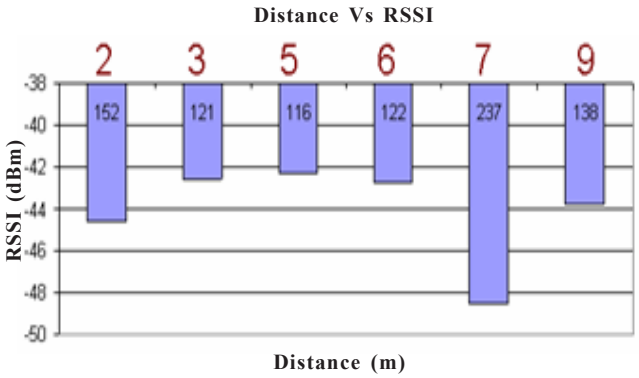

Fig.10 Inverse nonlinear graph for distance Vs RSSI

The neighbior table maintained is shown in Figure11.

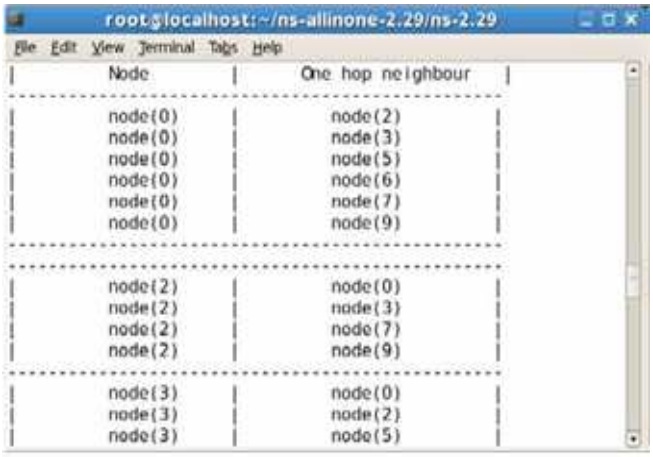

Fig.11 Neighbor table

The Figure 12 shows the RSSI calculated for node 3 with respect to all other nodes in the network.

Network Animator Screenshot For HCT Based on Nodes Usage

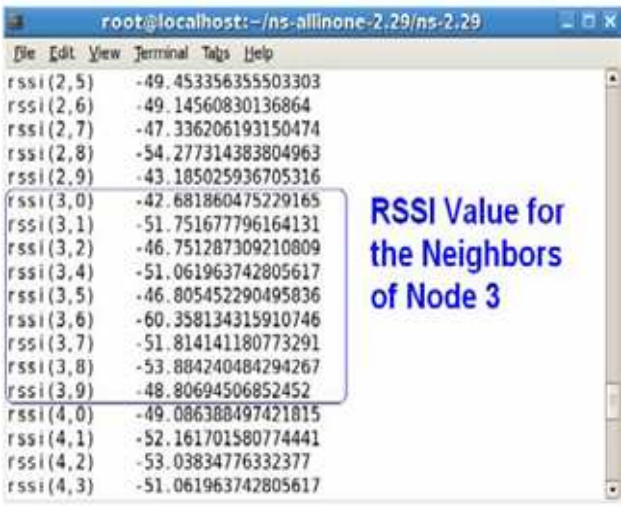

Fig. 12 RSSI calculation

The redundant nodes (not used for forwarding) can be in any one of the two states namely idle and sleep states. Energy consumption is calculated for both cases and is plotted in Figure 13. The graph proves hibernating idle nodes to sleep state gives less energy consumption. The average energy consumption calculated for a network using HCT based on RSSI and RE with idle nodes is 18.84%, and with sleep nodes it is 10.86%. Thus overall energy consumption is reduced by 7.98% using HCT based on RSSI and RE with sleep nodes.

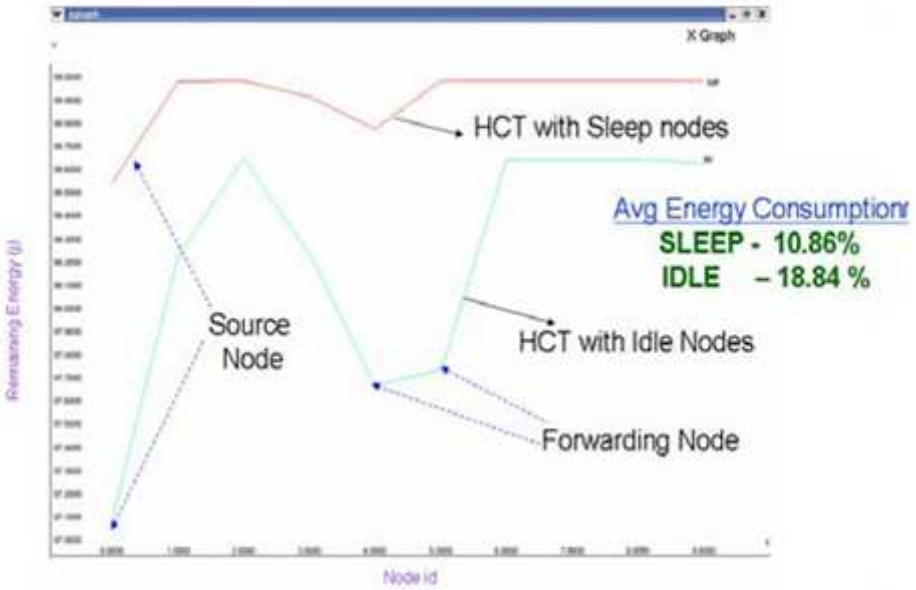

Fig. 13 Energy consumption of HCT based on RSSI and RE with idle nodes and sleep nodes

Comparisons on the average energy consumption using the different approaches proposed are done and are shown in Figure 14. The figure shows the effectiveness of the proposed methodologies compared to the existing cooperative approach. It is also proved that HCT based on RSSI and RE with sleep nodes provides a lesser energy consumption compared to the others.

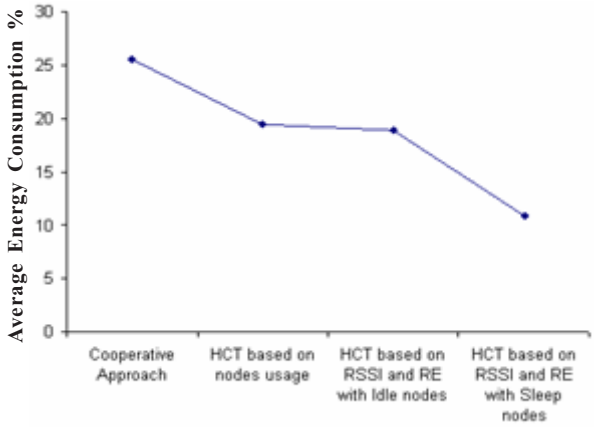

Fig. 14. Comparison on various methodologies

5. CONCLUSIONS

A new topology control algorithm called HCT is proposed and implemented. It has overcome the oscillatory behavior faced in the conventional cooperative approach.
Compared to the existing method,

i. HCT based nodes usage brings out a overall reduction in the average energy consumption by 6.098%
ii. HCT based on RSSI and RE is implemented in order to select a best forwarder out of all the selected set of neighbors
iii. The unused neighbors are put on to sleep state to further reduce the energy consumption
iv. The overall energy consumption is reduced by 7.98% by hibernating the idle nodes to sleep state using HCT based on RSSI and RE

Using genetic algorithm for the selection of best neighbors can improve the performance of the network. The proposed technique can be implementing for two tier architecture.

REFERENCES

[1] Mo Li and Baijian Yang, "A Survey on Topology Issues in Wireless Sensor Network", Citeseerx.ist.psu.edu/viewdoc/download.
[2] Holger Karl and Andreas Willig, "A Short Survey of Wireless Sensor Networks", Telecommunication Networks Group, Berlin, October 2003.
[3] Kazem Sohraby, Daniel Minoli and Taieb F. Znati, "Wireless Sensor Networks: Technology, Protocols and Applications", Textbook.
[4] John A. Stankovic, "Wireless Sensor Networks", Virginia, http://www.cs.virginia.edu/~stankovic/psfiles/wsn.pdf, June 19, 2006.
[5] Miguel A.Labrador and Pedro M. Wightman, "Topology Control in Wirless Sensor Networks: with A Companion Simulation Tool for Teaching and Research", Text book.
[6] Jianping Pany Y. Thomas Houz Lin Caiy Yi Shiz Sherman X. Shen, " Topology Control for Wireless Sensor Networks", MobiCom'03, September 14-19, 2003, pp.286-299.
[7] Dongjin Son, Bhaskar Krishnamachari and John Heidemann, "Experimental Study of the Effects of Transmission Power Control and Blacklisting in Wireless Sensor Networks", Proceedings of the First IEEE Conference on Sensor and Adhoc Communication and Networks, October, 2004, pp.289-298.
[8] Shan Lin, Jingbin Zhang, Gang Zhou, Lin Gu, Tian He and John A. Stankovic, "ATPC: Adaptive Transmission Power Control for Wireless Sensor Networks", SenSys'06, November 1-3, 2006, pp.223-236.
[9] Junseok Kim, Sookhyeon Chang and Younggoo Kwon, "ODTPC: On-demand Transmission Power Control for Wireless Sensor Networks", Information Networking, ICOIN2008, Journal of Indian Institute of Science, Vol.5, No.23-25, January 2008.
[10] B. Zurita Ares, P. G. Park, C. Fischione, A. Speranzon and K. H. Johansson, "On Power Control for Wireless Sensor Networks: System Model", Middleware Component and Experimental Evaluation citeseerx.ist.psu.edu/viewdoc/download.
[11] Amit Sinha and Anantha Chandrakasan, "Dynamic Power Management in Wireless Sensor Networks", IEEE Design & Test of Computers 2001, pp.62-74.
[12] Jonathan Hui, Zhiyuan Ren and Bruce H. Krogh, "Sentry-Based Power Management in Wireless Sensor Networks", Springer-Verlag Berlin Heidelberg 2003, pp.458-472.
[12] Ya Xu, Solomon Bien ,Yutaka Mori and John Heidemann, "Topology Control to Conserve Energy in Wireless Adhoc Networks", http://www.isi.edu/johnh/PAPERS/y004a.html January23,2003 citeseerx.ist.psu.edu/viewdoc/download.
[14] Marcel Busse and Wolfgang Efeelberg, "Conserving Energy with Topology Control in Wireless Sensor Networks", http://www.informatick.uni-mannheim.de.
[15] Safwan Al-Omari and Weisong Shi, "Redundancy-Aware Topology Management in Wireless Sensor Networks", http://www.cs.wayne.edu/~weisong/papers/omari06-topology-management.pdf.
[16] P. Costa, M. Cesana, S. Brambilla, L. Casartelli and L.Pizziniaco, "A Cooperative Approach for Topology Control in Wireless Sensor Networks: Experimental and Simulation Analysis", World of Wireless, Mobile and Multimedia Networks, 23-26 June 2008, pp.1-10.

Indian Journal of Engineering, Science, and Technology (IJEST)

(ISSN: 0973-6255)
(A half-yearly refereed research journal)

Information for Authors

1. All papers should be addressed to The Editor-in-Chief, Indian Journal of Engineering, Science, and Technology (IJEST), Bannari Amman Institute of Technology, Sathyamangalam - 638 401, Erode District, Tamil Nadu, India.
2. Two copies of manuscript along with soft copy are to be sent.
3. A CD-ROM containing the text, figures and tables should separately be sent along with the hard copies.
4. Submission of a manuscript implies that : (i) The work described has not been published before; (ii) It is not under consideration for publication elsewhere.
5. Manuscript will be reviewed by experts in the corresponding research area, and their recommendations will be communicated to the authors.

Guidelines for submission

Manuscript Formats

The manuscript should be about 8 pages in length, typed in double space with Times New Roman font, size 12, Double column on A4 size paper with one inch margin on all sides and should include 75-200 words abstract, 5-10 relevant key words, and a short (50-100 words) biography statement. The pages should be consecutively numbered, starting with the title page and through the text, references, tables, figure and legends. The title should be brief, specific and amenable to indexing. The article should include an abstract, introduction, body of paper containing headings, sub-headings, illustrations and conclusions.

References

A numbered list of references must be provided at the end of the paper. The list should be arranged in the order of citation in text, not in alphabetical order. List only one reference per reference number. Each reference number should be enclosed by square brackets.

In text, citations of references may be given simply as "[1]". Similarly, it is not necessary to mention the authors of a reference unless the mention is relevant to the text.

Example

[1] M.Demic, "Optimization of Characteristics of the Elasto-Damping Elements of Cars from the Aspect of Comfort and Handling", International Journal of Vehicle Design, Vol.13, No.1, 1992, pp. 29-46.

[2] S.A.Austin, "The Vibration Damping Effect of an Electro-Rheological Fluid", ASME Journal of Vibration and Acoustics, Vol.115, No.1, 1993, pp. 136-140.

SUBSCRIPTION

The annual subscription for IJEST is Rs.600/- which includes postal charges. To subscribe for IJEST a Demand Draft may be sent in favour of IJEST, payable at Sathyamangalam and addressed to IJEST. Subscription order form can be downloaded from the following link http:// www.bitsathy.ac.in./ ijest.html.

For subscription / further details please contact:

IJEST
Bannari Amman Institute of Technology
Sathyamangalam - 638 401, Erode District, Tamil Nadu Ph: 04295 - 226340 - 44
Fax: 04295 - 226666 E-mail: ijest@bitsathy.ac.in Web:www.bitsathy.ac.in

Indian Journal of Engineering, Science, and Technology

Volume 5, Number 1, January - June 2011

CONTENTS